UNIVERSIDAD NACIONAL DE COLOMBIA

UMONS Université de Mons

Contribution to the computation of regions of attraction of nonlinear systems based on the extended dynamic mode decomposition - Application to the anaerobic digestion

Camilo García Tenorio

Universidad Nacional de Colombia
Facultad de Ingeniería
Departamento de Mecánica y Mecatrónica
Bogotá, Colombia

Université de Mons
Faculté Polytechnique
SECO lab
Mons, Belgique

2021

Contribution to the computation of regions of attraction of nonlinear systems based on the extended dynamic mode decomposition - Application to the anaerobic digestion

Camilo García Tenorio

In partial fulfillment of the requirements for the degree of
Docteur en Sciences de l'Ingénieur et Technologie and
Doctorado en Ingeniería Mecánica y Mecatrónica

Supervisors
Prof. Eduardo Mojica Nava
Prof. Alain Vande Wouwer

Universidad Nacional de Colombia
Facultad de Ingeniería
Departamento de Mecánica y Mecatrónica
Bogotá, Colombia

Université de Mons
Faculté Polytechnique
SECO lab
Mons, Belgique

2021

Members of the Jury

Prof. John Cortes (UNAL), president
Dr. Laurent Dewasme (UMONS), secretary
Prof. Christine Renotte (UMONS)
Prof. Alexandre Mauroy (UNAMUR)
Prof. Denis Efimov (INRIA-Lille)
Prof. Iván Gil (UNAL)
Prof. Eduardo Mojica Nava (UNAL), supervisor
Prof. Alain Vande Wouwer (UMONS), supervisor

To Andrea and Julian

Acknowledgments

First I would like to offer my sincere gratitude to my esteemed advisors, Prof. Eduardo Mojica and Prof. Alain Vande Wouwer, whose support, encouragement and patience led to the satisfactory completion of this thesis. Their courage and willingness to explore and learn new topics in control systems analysis made this thesis possible.

Apart from my advisors I want to express my gratitude to Duvan Tellez for encouraging the exploration of new techniques that ended up being the core of this thesis. All the hours in front of a whiteboard dissecting books and papers where not only entertaining, but crucial for the development of the thesis.

I am also pleased to thank the peers and colleagues from the decision systems & network control lab (DESYNC) at Universidad Nacional de Colombia, Catalina, Wladimir and David as well as the members of the research group programa de investigación análisis de señales (PAAS). In addition I would like the members of the systems, estimation, control and optimization lab (SECO) at Université de Mons, Vincent, William, Christine, Carlos, Valentin, Jesus, Laurent, Gilles, Maxime, Alejandra, Perla, Federico, Ivan and Merouane.

Special gratitude to the members of the jury of my thesis, Prof. John Cortes, president of the jury, and Prof. Iván Gil (Universidad Nacional de Colombia), to Dr. Laurent Dewasme, secretary and Prof. Christine Renotte (Université de Mons), Prof Denis Efimov (Inria - Lille) and Prof. Alexandre Mauroy (Université de Namur). I would like to give special thanks to Prof. Mauroy for the insightful discussions and comments regarding the Koopman operator and the thesis manuscript.

Additionally, I would like to thank Minciencias, Colciencias and Col-

futuro for the support provided by the grant: “Doctorado Nacional - 647/2015”

I also want to express my deepest gratitude to my parents and my sister, Luis, Berta and Andrea, whose love and support where paramount for the development of the thesis. Finally, this thesis is dedicated to my lovely wife Andrea and my son Julián, who had the courage to undertake this experience together. They encouraged me with love and made this journey possible.

Abstract

The main topic of the thesis is the data-driven identification of the region of attraction (ROA) of asymptotically stable equilibrium points. Although this is the main computational contribution, satisfying the underlying conditions to make this possible constitutes most of the work of the thesis. To achieve an accurate data-driven approximation of the ROA in systems with multiple fixed or equilibrium points it is necessary to properly complete a series of steps parting from some trajectories of the system, i.e., assuming there is no access to the differential or difference model equation. The main condition is an accurate approximation of the Koopman operator because it provides a set of eigenfunctions where a particular composition of them gives another non-trivial eigenfunction with an associated eigenvalue that is unitary. The main property of this eigenfunction is that it gives the stable manifold of saddle points in the boundary of the ROA, where this stable manifold is in fact, the actual boundary of the ROA. Therefore, for this whole procedure to work, it also necessary to have an approximation of the location and stability of the fixed points of the system, recalling that the only input to the algorithm is a set of trajectories of the system. Consequently, the algorithm must be an appropriate approximation of the dynamics of the system and be able to provide a difference equation able to give the location and stability of fixed points upon further traditional non-linear system analysis. The algorithm that has the potential to achieve these requisites is the extended dynamics mode decomposition (EDMD) algorithm, where most of the work of this thesis focuses in transforming the potential into actual. For the most part, the development focus is on the numerical stability of the algorithm, reducing the computational effort and necessary steps to perform the approximation. Techniques such as the p-q-quasi norm

reduction of orthogonal polynomials and polynomial element elimination according to its error, ensures that smaller bases perform the approximations while guaranteeing the existence of solutions because of the orthogonality property. Improvements such as the recovery of the state via the inverse of univariate order-one polynomials reduce the number of necessary matrix inversions. Finally, a priori expansions of the state with arbitrary trigonometric functions or any other kind of elemental functions, expand the possible types of systems that the algorithm can handle. As a consequence of these improvements, the thesis achieves the original objectives of analyzing systems and controlling sets of interconnected systems in a data-driven context. Finally, the main application of the thesis is the analysis of the ROA to the anaerobic digestion process, where the analysis of multi-stability phenomena that guarantees the proper operation of the reactor is of paramount importance.

Keywords: Region of Attraction, Koopman Operator, Extended Dynamic Mode Decomposition, Anaerobic Digestion

Resumen

Contribución al cálculo de regiones de atracción de sistemas no lineales basado en la descomposición dinámica extendida - Aplicación a la digestión anaeróbica

El tema principal de la tesis es la identificación basada en datos de la región de atracción (ROA por sus siglas en ingles) de puntos de equilibrio asintóticamente estables. Aunque esta es la principal contribución computacional, la mayoría del trabajo de la tesis constituye en satisfacer las condiciones subyacentes para lograr aproximar la ROA. Para obtener una aproximación precisa basada en datos del ROA en sistemas con múltiples puntos fijos o de equilibrio es necesario completar apropiadamente una serie de pasos partiendo de algunas trayectorias del sistema, i.e., asumiendo que no hay ningún acceso al modelo de ecuaciones diferenciales. La condición principal es una aproximación precisa del operador de Koopman ya que proporciona un grupo de eigenfunciones donde una composición particular de las mismas proporciona otra eingenfunción no trivial con eigenvalor asociado unitario. La principal propiedad de esta eingenfunción es que proporciona el "manifold" estable de los puntos de silla en el perímetro de la ROA. Por esta razón, para todo este procedimiento de trabajo, también es necesario tener una aproximación de la ubicación y estabilidad de los puntos fijos del sistema, recordando que la única entrada al algoritmo es un conjunto de trayectorias del sistema. Por consiguiente, el algoritmo debe ser una aproximación apropiada de las dinámicas del sistema y ser capaz de proporcionar una ecuación de diferencia que pueda proporcionar la ubicación y estabilidad de puntos fijos basándose en el análisis tradicional de sistemas no lineales. El algoritmo que tiene el potencial de alcanzar estos requisitos es el "extended dynamics mode decomposition" (EDMD), en donde la mayor parte del

trabajo de esta tesis se enfoca en transformar el potencial que tiene este algoritmo en una realidad. En su mayor parte, el enfoque del desarrollo es sobre la estabilidad numérica del algoritmo, reduciendo el esfuerzo computacional y pasos necesarios para llevar a cabo la aproximación. Técnicos como la reducción de los polinomios ortogonales basándose en las casi normas p-q y la eliminación de elementos polinomiales segur su error, aseguran que bases mas pequeños realicen las aproximaciones garantizando la existencia de soluciones debido a la propiedad de ortogonalidad. Mejoras como la recuperaron del estado a troves de la función inversa de los polinomios de una sola variable reducen el numero necesario de inversiones de matrices. Finalmente, las expansiones a priori del estado con funciones trigonométricas arbitrarias o cualquier otro tipo de funciones elementales, expanden los tipos posibles de sistemas que el algoritmo puede manejar. Como consecuencia de estas mejoras, la tesis logra los objetivos originales de analizar sistemas y controlar conjuntos de sistemas interconectados en un contexto basado en datos. Finalmente, la aplicación principal de la tesis es el análisis de la ROA en el proceso de digestión anaerobia, donde el análisis del fenómeno de multi-estabilidad que garantiza la operación correcta del reactor es de suma importancia.

Palabras clave: Región de Atración, Operador de Koopman, Extended Dynamic Mode Decomposition, Digestión Anaerobia

Résumé

Contribution au calcul des régions d'attraction des systèmes non linéaires basé sur la décomposition en modes dynamiques étendus - Application à la digestion anaérobie

Le sujet principal de cette thèse de doctorat est la détermination de la région d'attraction des points d'équilibre asymptotiquement stables d'un système dynamique non linéaire. Cette détermination est réalisée numériquement sans avoir recours à la connaissance explicite d'un modèle mathématique du système, mais sur base d'un ensemble de trajectoires de celui-ci. Ces trajectoires peuvent être soit collectées expérimentalement au départ du système physique, soit obtenues par simulation numérique d'un modèle de forme arbitraire qui serait déjà disponible mais dont la structure ne doit pas être connue. A cette fin, le système dynamique non linéaire est représenté par un opérateur de Koopman. Cet opérateur est linéaire mais de dimension infinie et en pratique il est nécessaire de procéder à une approximation en dimension finie. Celle-ci est fournie par la méthode "extended dynamic mode decomposition" (EDMD), qui permet de construire une matrice de Koopman et de calculer les fonctions propres et les valeurs propres associées à celle-ci. En particulier, les fonctions propres associées à la valeur propre unitaire apparaissent comme étant particulièrement utiles. Ces fonctions propres permettent en effet de déterminer les "manifolds" stables des points selle qui se trouvent à la frontière de la région d'attraction. Outre cette détermination des points d'équilibre et de leur région d'attraction, ce travaille de thèse s'intéresse aux aspects numériques de la méthode EDMD, notamment le choix de bases polynomiales performantes et la réduction de l'ordre de l'approximation en utilisant des techniques telles que les quasi-normes p-q. Le choix des bases polynomiales est aussi important pour la représen-

tation des entrées de commande des systèmes ou de leur couplages, dans le contexte de l'interconnexion de plusieurs systèmes dynamiques. Les dernières considérations théoriques de ce travail concernent donc les systèmes avec des entrées de commande et la possibilité de développer une commande prédictive en relation avec la représentation de Koopman. Enfin ce travail contient plusieurs illustrations dont une application à la détermination des points d'équilibre et des régions d'attraction du processus de digestion anaérobie, ainsi qu'un pendule inversé approximé par la méthode EDMD utilisant des fonctions de base trigonométriques, ainsi que des oscillateurs de Duffing couplés.

Mots-clés: Région d'attraction, Opérateur de Koopman, Extended Dynamic Mode Decomposition, Digestion Anaérobie

Contents

List of Figures

List of Tables

Chapter 1

Introduction

The concept of stability is ubiquitous in the world, just by riding a bicycle, a person experiences the act of maintaining stability. It is a concept that pervades any type of systems, physical, social, economical, ecological, or biochemical among others. A possible definition of stability is the property of a system that causes it to return to its original condition when it experiences a disturbance from the equilibrium state. Being these equilibria states the main concept of system analysis and the synthesis of forces or moments that drive them to a desired equilibrium, understanding equilibrium as a condition where a system remains unchanged in the absence of external influences. Within the analysis of these equilibrium states, it is important to determine if they are unstable or stable, and if they are the latter, the analysis turns toward its robustness; the ability of the system to return to its equilibrium state after small disturbances. As a consequence of not having just one stable point, i.e., the multi-stability phenomena, there is a limit to the disturbance such that the system does not converge to another (possibly undesired) stable point. How big is this disturbance limit, gives a measure of the stability of the point, and this measure is related to the concept of region of attraction (ROA). A simple example of the concept of stability and equilibrium points is a ball that can move between two wells, depicted in Figure 1.1. The system has three equilibrium points, the bottom of the two wells and the top of the hill where the wells are stable points and the hill is unstable. Assuming that the objective is to keep the ball in the well on the left, any distur-

bance is bounded such that the ball does not pass through the unstable point at the hill. Otherwise, it will converge to the undesired well on the right. Meaning that the ROA of the desired state is the area to the left of the unstable point at the hill. These unstable points and the analysis of certain invariant subspaces that they possess are the foundation for the identification of the ROA of stable points.

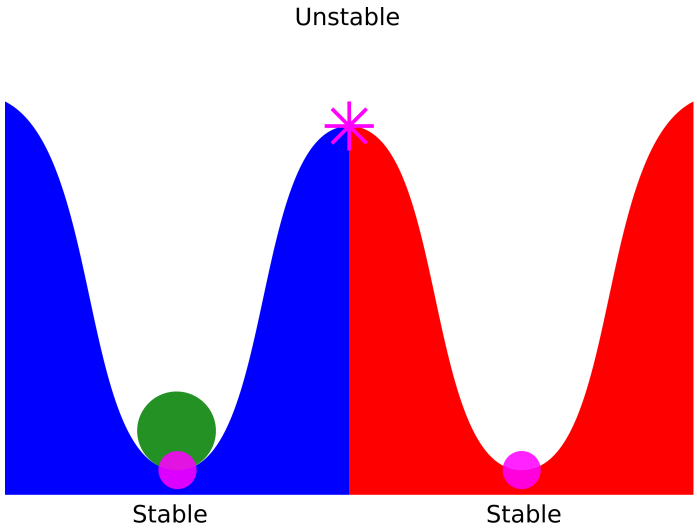

Figure 1.1: Ball between two valleys where there are three equilibrium or fixed points: the left one is the desired stable point, in the center there is an unstable point, and the right is the undesired stable point.

The subject of *control systems* deals with the analysis and synthesis algorithms for these equilibrium states, called equilibrium points in the continuous-time analysis, and fixed points when the system is in discrete-time. Given that the results of this thesis are in discrete-time, the remainder of this thesis will refer to these equilibrium states as fixed points.

When dealing with the analysis of fixed points, systems with unique equilibrium states are rare, in general, for non-linear systems it is common to find sets of equations that deal with the multi-stability phenomena. Conversely, the analysis of non-linear systems often focuses on the stability and especially, the global stability of systems with unique fixed

points. Whereas in systems with multiple stable points, the concept of the ROA is as important as their stability. Questions such as: how far a disturbance can drive the system away from an equilibrium point without leaving the region where it can converge back to it? Or, from which initial conditions does the system converge to the desired point? Are as important as determining the local stability of fixed points.

Traditional model-based methods such as Lyapunov, dissipativity, passivity (Energy-based) or input-output based techniques for non-linear systems [Haddad and Chellaboina, 2008, Khalil, 2002, Garcia-Tenorio et al., 2016] are suitable for low dimensional dynamical systems or low-order systems, but they cannot get a handle on complexity [Ahmadi and Parrilo, 2011, Majumdar et al., 2014, Anderson and Papachristodoulou, 2010, Giesl and Hafstein, 2015, Budišić et al., 2012, Skar et al., 1981, Cuesta et al., 1999], not only for the difficulty of the analysis but also because modeling complex systems is a difficult task. Therefore, complex dynamic systems require tools for their analysis that transcend beyond the current knowledge in control theory [Dimirovski, 2016]. The escalating behavior in the number of equilibria, and the modeling difficulties do not allow for a simple and straightforward approach. Still, the overall performance has to be guaranteed.

In order to solve this issue, instead of approaching it with the traditional model based techniques, data-driven frameworks are a suitable alternative to get a solution. Within these data-driven strategies, that include artificial intelligence, machine learning and the whole plethora of algorithms encapsulated by these techniques, the extended dynamic mode decomposition (EDMD) that under certain conditions gives an approximation of the Koopman operator is a promising alternative that makes possible the use of a modern approach where traditional analysis methods still apply.

The Koopman operator framework provides a way of having eigenfunctions ϕ of a linear operator U be observables or measures of a particular dynamical system, i.e., the evolution of eigenfunctions relate to the evolution of the states of the system [Koopman, 1931]. For discrete-time systems, the application of U on ϕ gives the same function scaled by its corresponding eigenvalue μ as in

$$U\phi = \mu\phi. \tag{1.1}$$

This approach is suitable for an analysis of the evolution of eigenfunctions rather than the analysis of state evolution [Budišić et al., 2012, Mezić, 2017]. The trade-off with this approach concerns linearity and dimensionality, finite-dimensional nonlinear systems described by an infinite-dimensional linear system.

Given that this operator is linear, it has a spectral decomposition that contains information about the underlying non-linear dynamical system. Furthermore, the analysis of eigenfunctions allows the identification of invariant subspaces that capture specific characteristics of the dynamical system. If an eigenfunction has an eigenvalue equal to one, the value of this function is invariant along the trajectories of the dynamical system. Coupled with the fact that finding the ROA of a stable fixed point relies on the ability to approximate some invariant subspaces of the system state space, for a specific type of system, these unitary eigenfunctions give the solution to the multi-stability phenomena.

An advantage of using the Koopman operator is that there are several methods to have a finite-dimensional approximation of this infinite-dimensional operator via snapshot data of the system with the application of, among others, the EDMD algorithm [Williams et al., 2015]. A solution that is closely related to modern data-driven and machine learning techniques, where the analysis comes solely from information gathered either from the numerical integration of a nonlinear differential equation, or from the measurements of a real system. In contrast with traditional techniques that rely upon the explicit knowledge of the differential equation that comes from modeling and identification methods [Garnier and Wang, 2008, Augusiak et al., 2014, ElKalaawy and Wassal, 2015], where the identification also relies on the available data of the system, the EDMD avoids the modeling and identification tasks. Moreover, it also gives an approximation of the system dynamics with the additional benefit of having an expanded linear approximation of some measurements or observables of a system, opening up the possibility of adapting traditional linear system analysis techniques to these approximations.

Juxtaposing the analysis of eigenfunctions and the linear evolution

of observables provides a set of tools for accurately handling nonlinear dynamical systems. Giving the possibility to find the fixed points, their stability, and finally, analyze the spectral decomposition to determine the ROA of asymptotically stable points. Additionally, the linear evolution of observables allows for the application of linear control techniques such as model predictive control (MPC) for the synthesis of controllers that drive the system into the desired equilibrium [Korda and Mezić, 2018b].

In order to take advantage of these benefits; eigenfunctions and linear predictors, it is necessary to have an accurate approximation of the Koopman operator from the available data. Although, there are several methods to compute the approximation [Williams et al., 2015, 2016, Kaiser et al., 2018, Li et al., 2017], all of those have some inherent difficulties that hinder the fulfillment of the objectives of this thesis. Accordingly, most of the development of this thesis focuses on the refinement of the EDMD algorithm using orthogonal polynomial basis as a means to overcome those difficulties. The main contribution in this regard is in the amount of necessary data to calculate the approximation of the discrete-time Koopman operator. In contrast to the available methods, the algorithm developed in this thesis achieves an accurate representation with one order of magnitude reduction in the amount of data. Another reason for the improvement of the algorithm is according to the dimension of the basis; for the regular formulations, the dimension of the observables grows exponentially with the addition of state variables. Increasing the number of state variables or the maximum order of the polynomials hinders the possibility of calculating the discrete time approximation of the operator because of the course of dimensionality problem; the computational complexity of the algorithm is prohibited for a standard computer. Therefore, the use of p-q-quasi norm reduction methods, based on the proposed ideas for reliability analysis in polynomial chaos expansion [Konakli and Sudret, 2016a,b] gives a truncation scheme on the polynomial basis that serve as the observables for the discrete-time approximation of the EDMD. Moreover, the accuracy of the linear predictors and eigenfunctions is directly related to the contribution of each of the observables on the approximation. Hence, an error criterion on the contribution of these individual elements, in conjunction with an error threshold based on the error of the individual elements of the basis that must remain, serves to eliminate those elements that

contribute to the inaccuracies in the approximation.

Indeed, there are some polynomial elements that must remain in the basis since the use of orthogonal polynomials is sufficient to easily recover the state. Some available methods include elements in the set of observables that capture directly each of the states, with the risk of breaking the orthogonality of the basis, and making the problem impossible to solve or numerically unstable. Whereas machine learning techniques, such as radially basis functions and Kernel methods need to solve a second minimization problem to recover the state as a linear combination of the observables, at the risk of having inaccurate solutions, or no solution at all.

The solution to this dilemma, of including or not elements that directly capture the state, is the selection of univariate and order one injective polynomial elements for the recovery of the state [Garcia-Tenorio et al., 2020]. There is no need to break the orthogonality of the set while still being able to recover the state as a linear function of the observables, without a second optimization solution. In addition to the recovery of the state, the exponential growth of the maximum order and dimension of the set of observables based on orthogonal polynomial has a solution via p-q-quasi norms, and polynomial accuracy methods.

In summary, the methods and algorithms achieve the following analysis objectives:

1. Approximate the discrete-time Koopman operator with the least amount of data, and with a reduced set of observables, both in dimension and maximum order of the polynomials.

2. Approximate the location of the system fixed points, which is made possible by the linear predictors of the observables that can easily recover the state.

3. Accurately determine their stability (asymptotically stable, unstable or saddle points) because the approximation also provides a nonlinear evolution map of the state. This mapping can be linearized and evaluated at the fixed points to assess stability.

4. Identify the saddle points in the boundary of the ROA.

5. Generate an eigenfunction with unitary associated eigenvalue or in the ideal case, have this eigenfunction present in the original approximation.

6. Find an algebraic criterion that accurately classifies an arbitrary initial condition in the state space to its corresponding attractor, with the benefit that the criterion is a comparison between real numbers, therefore suitable to handle higher dimensional systems.

It is important to emphasize that the analysis is solely data-driven, and although this thesis makes use of the differential model equations, it is only to produce the data for the analysis. This data-driven presupposition also restricts the analysis to hyperbolic systems because we are not able to characterize a limit cycle or chaotic behavior without the differential equation. Without this restriction, the results of this thesis still apply, with the caveat that there are better alternatives for two-dimensional systems, or slices of three-dimensional ones using time averages [Mezić, 2005], or for a higher dimensional system, finding the isostables of a dynamical system by the Laplace averages of the differential equation forward integration [Mauroy et al., 2013, Mauroy and Mezic, 2016].

Production

1. Journal: Garcia-Tenorio Camilo, Gilles Delansney, Mojica-Nava Eduardo, Vande Wouwer Alain, "Trigonometric Embeddings in Polynomial EDMD and Linear Representations of Interconnected Oscillators" in "Mathematics", 2021, vol. 9, pp. 1119.

   Journal paper presenting the results of applying trigonometric, or in general any functional embeddings into the set of state variables of the system. These embeddings serve to improve the accuracy of the EDMD algorithm by incorporating a priori knowledge of the differential equation in to the set of observables while preserving the benefits of the p-q and polynomial accuracy reduction methods.

2. Journal: Garcia-Tenorio Camilo, Tellez-Castro Duvan, Mojica-Nava Eduardo, Vande Wouwer Alain, "Hyperbolic Systems Region of Attraction via EDMD Koopman Operator" in "Submitted".

Journal paper covering an in depth analysis of the data driven algorithm for obtaining the ROA of asymptotically stable fixed points. The method covers the key aspects in dynamical system analysis for the estimation of the ROA: Finding the fixed points of the system, giving their stability, and estimating the boundary of the ROA for the stable points.

3. Journal: Garcia-Tenorio Camilo, Sbarciog Mihaela, Mojica-Nava Eduardo, Vande Wouwer Alain, "Analysis of the ROA for the Anaerobic Digestion Process via Data-Driven Koopman Operator" in "Nonlinear Engineering", vol. 10, no. 1, 2021, pp. 109-131.

   Journal paper covering an in depth analysis of the multi-stability problem for the Anaerobic digestion process. This work also presents in detail the reduction methods for the observables based on orthogonal polynomials.

4. Colloquium/Abstract: Garcia Tenorio Camilo, Mojica-Nava Eduardo, Vande Wouwer Alain, "Linear Predictors for Interconnected Systems: a Koopman Operator Approach" in "39th Benelux Meeting on Systems and Control", 128, Elspeet, The Netherlands, 2020.

   Abstract that shows the general idea for the linear predictors when dealing with external forcing signals and interconnection inputs.

5. Conference: Garcia-Tenorio Camilo, Tellez-Castro Duvan, Mojica-Nava Eduardo, Vande Wouwer Alain, "Analysis of a Class of Hyperbolic Systems via Data-Driven Koopman Operator" in "23rd International Conference on System Theory, Control and Computing (ICSTCC)", Sinaia, Romania, 2019.

   Conference paper that describes some of the methods that achieve the approximation of the ROA for the multi-stability problem. Specializes in the study of polynomial systems under the MAK modeling paradigm for biochemical reaction networks. Precedes the ROA Journal paper submission.

6. Colloquium/Abstract: Garcia-Tenorio Camilo, Vande Wouwer Alain, Mojica-Nava Eduardo, "Biochemical Reaction Networks, Dynamics and Regions of Attraction: A Koopman Operator Based

Approach" in "38th Benelux meeting on Systems and Control", Lommel, Belgique, 2019.

Abstract that presents the preliminary concepts for the formulation of the solutions based on the Koopman operator for the ROA problem.

7. Colloquium/Abstract: Garcia-Tenorio Camilo, Vande Wouwer Alain, Mojica-Nava Eduardo, "Order reduction for EDMD based on observable error: Application to the anaerobic digestion model" in "Cape Forum", Liege, Belgique, 2019.

   Abstract that contains the first approach for the order and dimensionality reduction of orthogonal polynomials as an observable basis for the approximation of the Koopman operator. Exemplified via the two-dimensional representation of the AD process. Precedes the Journal submission with the complete analysis of the AD process and observables reduction methods.

8. Colloquium/Abstract: Garcia-Tenorio Camilo, Sbarciog Mihaela, Mojica-Nava Eduardo, Vande Wouwer Alain, "Anaerobic Digestion, Dynamics and Regions of Attraction: A Koopman Operator Based Approach" in "9th IWA Specialized Conference on Sustainable Viticulture, Winery Wastes &; Agri-industrial Wastewater Management", Mons, Belgium, 2019.

   Abstract preceding the Journal paper on the analysis of the ROA for the AD process. The abstract shows the feasibility of using the operator based techniques to analyze the process.

9. Conference: Garcia-Tenorio Camilo, Quijano Nicanor, Mojica-Nava Eduardo, Sofrony Jorge, "Bond-Graph model-based for IDA-PBC" in "2016 IEEE Conference on Control Applications (CCA)", Buenos Aires, Argentina, 2016.

   Conference paper with preliminary research concerning the use of Bond-Graph models to systematically solve the interconnection and damping assignment problem under passivity based control techniques.

This thesis is organized as follows: Chapter 2 is a literature review that covers some history and important references for the development

of the thesis. Chapter 3 contains the main theoretical concepts necessary for the development of the thesis. Section 3.1 contains the theoretical aspects from discrete-time nonlinear dynamical systems. Under this discrete-time framework, section 3.2 shows how to perform the analysis under the multi-stability phenomena to determine the ROA of stable points. Next, Section 3.3 presents the Koopman operator, introduces its spectrum, and gives an example of a particular type of discrete-time dynamical systems that accepts a closed analytical form. Given that this operator is more often approximated than calculated, Section 3.4 shows how to perform the approximation of the discrete part of the operator based on the EDMD algorithm. In addition to the EDMD algorithm, the aforementioned section shows the developed improvements to the algorithm that allow the calculation of more accurate approximation with a reduction of the necessary data. These improvements are the reduction by p-q-quasi norms, polynomial accuracy and trigonometric embeddings. For the latter, Section 3.5 shows a detailed description of how to perform the embeddings along with the algorithmic concepts to handle systems with forcing inputs. In the context of the EDMD algorithm, for input signals and interconnected systems, Section 3.6 shows how to handle the linear predictors coming from the EDMD to handle such combination of signals to synthesize controllers for the interconnected systems. For closing this Chapter, Section 4.6.1 presents the method of mass action systems for dealing with reaction and their corresponding differential equations. Next, Chapter 4 shows the main results of the thesis regarding the data-driven approximation of the ROA using the tools from the previous chapter, describing how to handle the fixed points in Section 4.1, and their stability in Section 4.2 and the method to analyze the fixed points of the state space via the approximation of the Koopman operator to get the ROA of the stable points. The remaining of the Chapter shows several examples to demonstrate the effectiveness of the algorithm. Chapter 5 shows a detailed analysis of the anaerobic digestion process using the EDMD-Koopman based approach for the estimation of the ROA, giving a detailed description on the different methods proposed by the thesis. Finally, Chapter 6 gives some additional discussion and conclusions regarding the subject matter of the thesis and its development.

Notation $\mathbb{C}$ denotes the field of complex numbers. $\mathbb{R}$ and $\mathbb{R}_+$ denote the field of real and nonnegative real numbers, respectively. For any matrix $A \in \mathbb{R}^{n\times n}$, $A^\top$ denotes transpose, A^+ denotes its pseudoinverse, and $||x||$ represents the Euclidean norm. For a complex number λ, $|\lambda|$ represents its absolute value. For any set A, $\bar{A}$ denotes its closure. For a set of eigenspaces E^i, $\oplus$ represents their direct sum. The vector exponentiation $M^{\pm\eta}$ is defined term by term. A level set of an arbitrary function $h(x)$ for any constant c is $\Gamma(h(x)) = \{x \in \mathbb{R}^n \colon h(x) = c\}$.

Chapter 2

Literature Review

The main focus of the thesis concerns the approximation of the ROA, more specifically, its boundary via the analysis of eigenfunctions from the Koopman operator. Additionally, some of the most important contributions in this subject matter are in the refinement of the EDMD algorithm that is a suitable data-driven technique for the approximation of the discrete part of the Koopman operator i.e., the point spectrum of the operator. Finally, the thesis contributes some techniques for handling control synthesis algorithms for interconnected systems, again by improving on the current algorithmic techniques of the EDMD algorithm. Therefore, this literature review will cover the relevant topics in order of importance, that is, regions of attraction, the Koopman operator and EDMD, and finally, interconnected systems.

2.1 Regions of Attraction

The analysis of dynamical systems with multiple equilibrium points cover their location, the local stability characteristics and for Asymptotically Stable (AS) equilibrium points, the ROA that describes the set of initial conditions that converge to a specific AS point. The concept of ROA is crucial for the analysis of a dynamical system, as it is often necessary to maintain the system in one of the AS equilibrium points, and guarantee that any perturbation does not make the system converge

into an undesired equilibrium or diverge.

Traditionally, the ROA in the multi-stability problem comes from the maximal Lyapunov set. This is a domain that contains the equilibrium point where the local Lyapunov function is positive definite and its derivative along the trajectories is negative definite. Meaning, that the estimate of the ROA is the largest level set of the Lyapunov function where the aforementioned conditions hold [Khalil, 2002], where the constant value for this largest level set is often called the critical level value.

Even though there are several optimization methods to find local Lyapunov functions from linear programming or linear matrix inequalities [Peter Giesl, 2015], this is not an easy task, especially when the dimensionality of the system grows. Additionally, the level sets of the Lyapunov function are a conservative approach, given that the Lyapunov function is not unique, and it is a great challenge to find a function whose level sets maximize the estimate of the ROA.

In addition to the Lyapunov methods, energy function methods give a less conservative approximation of the ROA. These methods are restricted to dynamical systems that admits a global or a local energy function, and the process for either case is similar, the difference between them is in the method to find the critical level values. If the system admits a global function, the theory is equivalent to the Lyapunov function, that is, to find the critical level value of the energy function where the energy function is non-negative, and its derivative along the trajectories is decreasing. The critical level value comes from evaluating this global energy function in the saddle points of the system and selecting the point with the lowest value after evaluation. If the system admits a local energy function, the critical level value comes from the evaluation of the closest saddle point with the local energy function. The difference between energy and Lyapunov functions, is that for the latter, the largest level set does not necessarily intercept with a saddle point in the boundary as it is the case with either form of energy functions. Assume there is an arbitrary system where the origin is stable and around this point are several unstable and saddle points. Additionally, assume that there is an arbitrary Lyapunov and energy function. Figure 2.1 shows such a system with the potential outcome of the approximation of the ROA via either

method. The derivatives of Lyapunov (left) function along the trajectories of the system are no longer decreasing when outside the square, while the energy function (right) is less conservative because its critical value corresponds to the function evaluated at the nearest saddles (that are equidistant to the origin). This is a depiction of the difference between the selection of the critical value for the two methods, the results for either case are dependent on the system under analysis, and the available Lyapunov and energy functions.

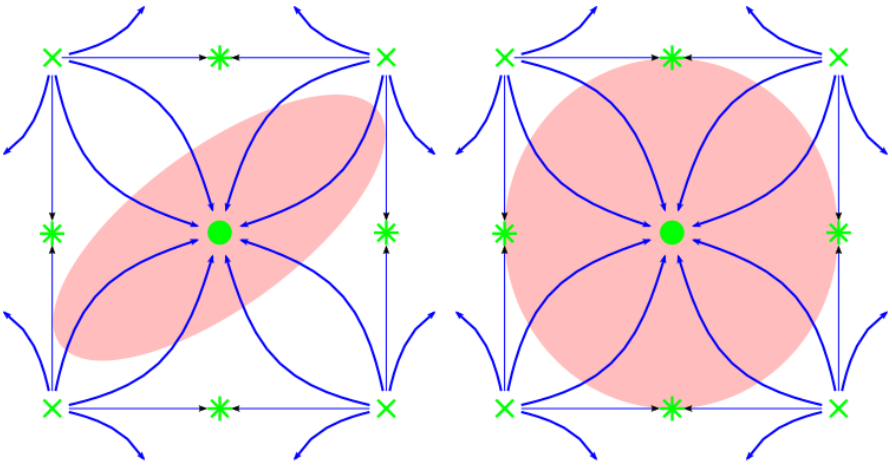

Figure 2.1: Lyapunov vs. Energy function ROA.

The feasibility of getting a solution with either of these methods is questionable. Starting from the difficulties in getting a function that satisfies the conditions, coupled with the difficulties of calculating level sets, those level sets are points of an $n-1$ dimensional hyper-surface of the state space, where the classification of an arbitrary initial condition on higher than three-dimensional systems is not trivial. This classification depends on the geometry of the stable manifold, and the ability to interpolate between the identified points to perform the comparison.

Along with the traditional analysis of the differential equation via Lyapunov or energy functions, there are some methods that rely on the numerical integration of the differential equation in reverse time. This process is summarized as follows: First, locate all the equilibrium points of the system and determine their local stability by the Jacobian matrix.

Then, find the stable eigenvectors of the saddle points, next, find the intersection of these eigenvectors with a ϵ-*ball* of the saddle point, i.e., a small n-dimensional hyper-sphere around the saddle point, and integrate numerically to check which of the asymptotically stable points ROA is under analysis. Finally, perform the backward integration, or a trajectory reversing algorithm from several initial conditions close enough to the intersection point between the stable eigenvectors and the ϵ-*ball* to get the boundary of the ROA. In conclusion, the method gives a set of trajectories that converge to the saddle point in the boundary. Although this method can yield an accurate approximation of the boundary of the ROA, it is computationally intensive, and has the same geometry and interpolation problems of the Lyapunov and energy function methods. Figure 2.2 shows a summary of this process: from the fixed points (green: stable dot, unstable crosses, saddle asterisks) there is an ϵ-*ball* from the saddles. In the intersection of the stable manifold (red lines) and the ϵ-*ball* (yellow dots) the forward integration of the system gives the stable point under analysis. Finally, The backward integration from initial conditions near the intersection (green dotted lines) gives an approximation of the boundary of the ROA.

In summary, the method gives a set of trajectories that converge to the saddle point in the boundary. This method shares the computational and geometric problems as the Although this method can yield an accurate approximation of the boundary, it is computationally intensive, and has the same geometry and interpolation problems of the Lyapunov and energy function methods. For a detailed approximation of the ROA in the problem at hand using backward integration we refer to [Sbarciog et al., 2010b].

2.2 Koopman Operator & EDMD

The theoretical framework of the Koopman operator (1.1) for control has its origins in the work of Koopman [1931], where he extends the linear transformations of the Hilbert space given in harmonic equations and ergodic theory to Hamiltonian systems. Up until the 2000s, the theory had applications in ergodic theory, chaos, and measure theory analysis via the adjoint Perron-Frobenius operator [Lasota and Yorke, 1982]. In

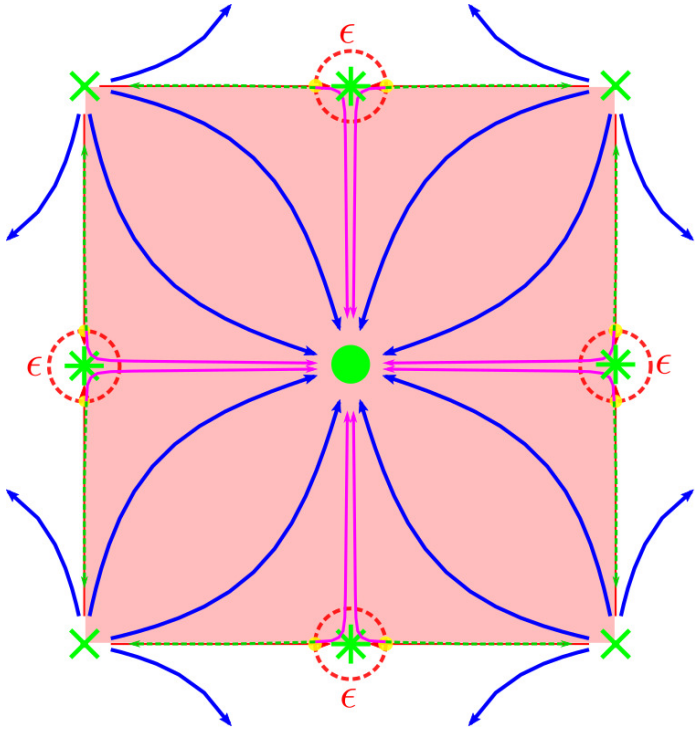

Figure 2.2: Backward evolution for the ROA.

the mid-2000s Mezić [2005] established the relation that the Koopman operator has with linear decompositions such as Karhunen-Loeve, singular value, proper orthogonal, and dynamic mode decomposition (DMD). From this relation, the Koopman mode decomposition (KMD) was able to exploit the spectral characteristics of the operator to analyze nonlinear systems, where KMD is a means to reduce complex flow models and analyze the properties of the system near the attractors.

The possibility to get the spectrum of nonlinear systems for analysis gave rise to the extended dynamic mode decomposition (EDMD) [Williams et al., 2015]. The objective then shifted, from the reduced analysis near the attractor to a higher dimensional representation. This representation results in the exchange of dimensionality with complexity, where low-dimensional nonlinear systems have a high-dimensional representation with the advantage of the spectral analysis.

There are several variants of the EDMD algorithm, from norm-based

expansions, radial-basis functions, kernel-based [Williams et al., 2016], orthogonal polynomials, and their variations [Kaiser et al., 2018, Li et al., 2017]. These representations give tools for analyzing nonlinear systems via the spectral decomposition and are the fundamentals for developing synthesis algorithms such as the EDMD for control [Proctor et al., 2016].

Within the theoretical framework under consideration, that is, the use of an approximation of the Koopman operator to analyze the system, there are some recent studies [Mezić, 2005, Lan and Mezić, 2013, Mauroy et al., 2013, Mauroy and Mezic, 2016] that lead to our theoretical framework and algorithm. Most notably, in [Mezić, 2005] the authors propose a visual method where the time average of an observable (i.e., an arbitrary function of the state space) approximates the eigenfunction of the Koopman operator whose eigenvalue is approximately unitary. Although this method provides visual information in two-dimensional systems or slices of three-dimensional ones, the method does not give a criterion to determine the convergence of an arbitrary point, and is not feasible to analyze higher dimensional systems. Another notable approach is [Mauroy et al., 2013], where the authors calculate isostables of the system. An isostable of a stable equilibrium point is a set of points, or initial conditions that converge synchronously to the attractor, that is, they simultaneously intersect subsequent isostables along the trajectory to the stable point. The definition of an isostable comes from the magnitude of the Koopman operator slowest eigenfunction, whose level sets give the isostables. Similar to the Lyapunov and energy function based methods, this approach requires the calculation of the level sets of a particular function, which yields the same problems related to those methods regarding the classification of an arbitrary initial condition in higher dimensional systems. The last important contribution is Mauroy and Mezic [2016], where the authors present a global stability analysis and the approximation of the region of attraction based on the spectral analysis of the Koopman eigenfunctions. The global stability analysis comes from the zero level sets of the Koopman eigenfunctions related to Koopman eigenvalues whose real part is less than zero. The approximation of the region of attraction comes from the traditional analysis of Lyapunov function built upon the same Koopman eigenfunctions and eigenvalues from the global stability analysis. To get these eigenfunctions and eigenvalues, the authors use a numerical method based on Taylor and Berstein polynomi-

als where it is necessary to know the analytic vector field of the system. Again, for the approximation of the region of attraction, the calculation of level sets hinders the possibility of performing the approximation on higher dimensional systems, and it is impossible without the knowledge of the vector field.

2.3 Interconnected Systems

The concept of interconnected dynamical systems has been a topic of research since the early '70s [Siljak, 1972, Grujic and Siljak, 1973, Sezer and Hüseyin, 1978], where the main focus was on large-scale and multilevel nonlinear dynamical systems interconnected by a function of their output variables. The analysis consists of the way of attaining the system stability conditions based on the local stability conditions and the analysis of the interconnection functions of the system. The basis for the analysis of the system is Lyapunov vector functions (LVF) [Bellman, 1962], in which a vector of distinct Lyapunov functions is defined based on the functions of the different subsystems. A simple algebraic condition on the interconnection matrix gives the interconnection's overall stability. The local dynamics of the local state variables, the interconnection functions, and a comparison vector function give the interconnection matrix. These methods rely on the ability to find suitable Lyapunov and comparison functions, which can be a difficult task. Furthermore, they rely on having the subsystem's dynamics identified.

Also, in the '70s, and with a different approach, Willems [Willems, 1972b] set the bases for the energetic analysis of dynamical systems and the energetic characteristics of the subsystem's interconnection. Willem's stability analysis consists of the identification of the overall storage function of the system, all of these subject to the condition of the system having a "Neutral" interconnection constraint (i.e., the interconnecting system must be lossless). Another approach for linear systems from Shih-Ho Wang and Davison [1973] consists of the decentralization of large scale system's controllers, with the system considered as a whole, and each subsystem stabilized via local output feedback with segregated controllers. Controllable and observable modes introduce the notion of "fixed modes" that prove stability when they are in the left-hand part of the complex

plane.

In the '80s, two approaches emerged, Ioannou [Ioannou, 1986] considers the subsystems as linear with a low relative degree of interconnection to other systems. For the synthesis of controllers, he designs local controllers assuming there is no noise in the output of the system and sets the interconnection input to zero. He handles the interconnection with a stability analysis that assumes that the noise in the system and the interconnection inputs are bounded signals. The second approach is from Linnemann [1984] that considers the stabilizability and reachability conditions of the linear subsystems and the stability conditions of the dynamics of the linear interconnections. He concludes that a system is stabilizable by decentralized output feedback if the subsystems are stabilizable by centralized output feedback, and the interaction system is stable.

The prevalent ideas in the '90s are by Siljak [1991], where large-scale systems are interconnections of physical entities or pure mathematical artifices. These descriptions are partitioned suitably in order to take advantage of the structural features that reduce the dimensionality of the analysis and synthesis methods via graph-theoretical methods. The approach considers the overall system as a collection of individual subsystems whose individual Lyapunov functions are combined to perform the analysis.

Another interesting approach comes from Maschke and van der Schaft [1996], where the notion of large-scale is not present; instead, they develop the paradigm of network interconnection, where the different interconnection structures appearing in the network models are analyzed presenting interconnections as energy exchanging components in some geometric space in correspondence with Dirac structures. This analysis is an extension of Willems [1972a,b] energetic analysis, where the Dirac structures represent the energetic exchange in the interconnection of Lagrangian and Hamiltonian dynamical formalisms.

More recently, an interesting approach to interconnected systems is in terms of decentralized control as population games, and evolutionary dynamics [Quijano et al., 2017]. The main idea of this approach is to use a multi-agent system method where the interactions between agents come from a game-theoretical approach. The local controller problem is

a game where the available control inputs are associated with strategies and the control objective as a pay-off function.

For the analysis of interconnected systems via the Koopman operator, there are two recent developments. Mauroy and Hendrickx [2017a] propose a method in which the application of the EDMD algorithm on some sparse measurements of some nodes of the network, and possibly from measurements of just one node of the network gives a spectral decomposition. From the graph-theoretical properties of the EDMD spectral decomposition, they deduce the topology of the network, i.e., the arrangement of the different edges and nodes. Meaning that the algorithm is a graph identification tool when the topology of the network is unknown. More recently Mauroy and Hendrickx [2017b] extended their previous theory for forced linear systems in the edges of the network.

2.4 Summary

The current literature covers several aspects that give the starting point for the development of the thesis. A key aspect in all the previous developments is the availability of a differential equation model to perform all the calculations. Given that it is not always possible to satisfy this assumption and when possible, several identification techniques rely on numerical and optimization methods to parametrize the models, the use of algorithmic techniques such as the EDMD is a promising approach that relies on the same data, yet bypasses the nonlinear models to give linear predictors of the state in an extended space of functions. Therefore, improving the algorithm such that it gives more accurate approximations with less amount of data is a valuable line of research.

On the subject of linear approximations in an extended space of functions, there is the Koopman operator, an infinite transformation of the state space into a function space where the evolution of a set of so-called eigenfunctions, relate to the evolution of the original state space. The availability of Koopman operator and the EDMD algorithm, and the fact that under some assumptions on the amount of data and the size of the extended space of functions, the EDMD converges to the point spectrum of the Koopman operator, continuing with the line of research of

the that combines the Koopman operator paradigm with its approximation methods is an interesting and promising line of research. Specifically concerning the Koopman operator, a deeper characterization of the properties of the available eigenfunctions and their relation to the analysis of nonlinear systems is an interesting line of research.

An interesting property of the eigenfunctions of the discrete-time Koopman operator is that their eigenvalues determine their evolution (1.1). From this property a nontrivial eigenfunction that has a unitary eigenvalue must be invariant, its value must not change along the trajectories of the states of the system. Matching these phenomena with the fact that the analysis of attraction regions, or domains of attractions is based on the ability to find invariant sets of these kind, shows that it is worth pursuing the line of research that combines these two concepts for the analysis of non-linear systems.

For the dual aspect of analysis in the subject of *control systems* theory, i.e., synthesis algorithms, the EDMD and the Koopman operator are also an alluring approach. The world of linear systems control has a plethora of techniques for driving systems into a desired state. These techniques are available for driving non-linear systems in a vicinity of the equilibrium points where the linearization of the system is valid. Then again, it is clear the advantageous use of linearization techniques such as the EDMD that provide linear approximations of the non-linear dynamical system. Coupled with the availability of the point spectrum of the Koopman operator, it is reasonable that there is an opportunity to bring and adapt linear systems techniques into the expanded linearization from the EDMD approximation of the Koopman operator.

Exploiting the linear predictors from the EDMD algorithm gives the possibility to adapt linear systems techniques, these approximations are versatile in the use of different forms of observables for the state variables, and the inputs. The EDMD algorithm can be set such that the observables of the inputs are either linear constant functions, or non-linear observables like the ones for the state variables. Notably, in the context of interconnected systems, some inputs are not driven by a controller, although their action affects the dynamics of the system, for these inputs, it is not necessary to have linear observables, instead, polynomial non-linear observables have the possibility to provide more accurate ap-

proximations according to these interconnection inputs, while keeping the linear effect on the driven inputs. This paradigm is specially useful for synthesizing model predictive control algorithms that require linear driven inputs. The combination of all these methods has the potential of providing a tool for decentralized control of interconnected systems.

Chapter 3

Dynamical Systems, ROA & EDMD

In order to present the methods based on the discrete time approximation of the Koopman operator via the EDMD algorithm, this section will cover preliminary concepts of dynamical systems theory that are necessary to understand the subsequent development. As any traditional control systems analysis, this section starts with the definition of fixed points and presents the concept of stability based on the classical Lyapunov analysis. Along with these definitions, this chapter presents the Hartman-Grobman theorem that defines what is a hyperbolic fixed point. Finally, this chapter presents the multi-stability problem along with the theoretical aspects that define the region of attraction.

Given that all of the theoretical preamble is developed for nonlinear system with explicit knowledge of the differential model equations, the next development of this theoretical chapter is the basic theory of the Koopman operator and the EDMD algorithm. Besides the theoretical foundation for the subsequent developments, this chapter also includes the algorithmic improvements to the calculation of the EDMD. Those improvements are the reduction methods by p-q-quasi norms and polynomial accuracy, the expansion of the state of the system by trigonometric embeddings and the production of bi-linear predictors with mixed affine and non-affine inputs for handling interconnected systems. Furthermore, this chapter presents the synthesis of controllers for these interconnected

systems making use of these linear predictors.

To conclude the chapter, and in line with the general topic of this work, the last section shows how to get polynomial models from reaction networks that serve to illustrate the different developments of the thesis due to their geometrical properties.

3.1 Discrete Nonlinear Systems

Consider the autonomous nonlinear system $(\mathcal{M}; T(x); k)$ in discrete-time, with state variables $x \in \mathcal{M}$ where $\mathcal{M} \subseteq \mathbb{R}^n$ is the nonempty compact state space, $k \in \mathbb{Z}_0^+$ is the discrete time, and $T \colon \mathcal{M} \to \mathcal{M}$ is the differentiable vector-valued evolution map, i.e.,

$$x(k+1) = T(x(k)), \quad x_0 = x(0). \tag{3.1}$$

The solution to (3.1) is the successive application of T from an initial condition $x_0 \in \mathcal{M}$ at $k = 0$, i.e., $x_k = T^k(x_0) \in \mathcal{M}$, which is an infinite sequence called a trajectory of the system.

As an example, consider an arbitrary non-linear system in discrete-time with two states [Chiang and Alberto, 2015], depicted in Figure 3.1 with evolution map

$$x_1(k+1) = x_1(k)^3 + \frac{3}{4}x_1(k) \tag{3.2}$$

$$x_2(k+1) = x_2(k)^3 + \frac{3}{4}x_2(k) \tag{3.3}$$

Suppose $x^* \in \mathcal{M}$ is a fixed point of (3.1); i.e.,

Definition 3.1.1 (Fixed Point)**.** *Let x^* be a fixed point of the dynamical system $(\mathcal{M}; T(x); k)$, then the flow map $T^k(x^*)$ maps into itself, i.e.,*

$$T^k(x^*) = x^*. \tag{3.4}$$

To obtain the fixed points in the Example (3.2-3.3), it is necessary to solve

$$x = x^3 + \frac{3}{4}x, \tag{3.5}$$

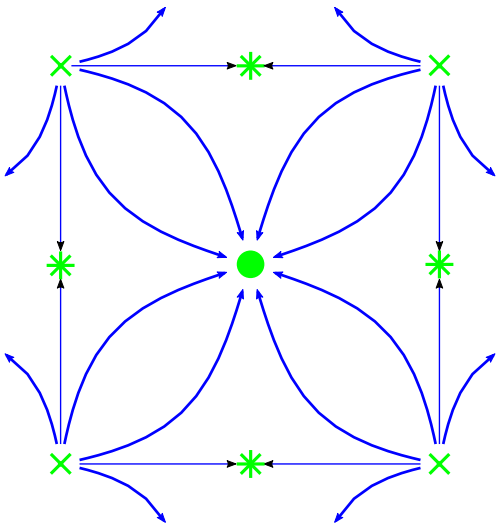

Figure 3.1: Discrete-time system with an AS point at the origin, unstable points at the corners and unstable-saddles at the edges.

whose solution is $x = 0$ or $x = \pm 0.5$, i.e., there are nine fixed points, one at the origin, two at $(0, \pm 0.5)$, two at $(\pm 0.5, 0)$ and four at $(\pm 0.5, \pm 0.5)$.

Definition 3.1.2 (Stability)**.** *The fixed point x^* of $x(k+1) = T(x(k))$ is*

a. *Stable if, for each $\epsilon(x^*) > 0$, there is a $\delta = \delta(\epsilon) > 0$ such that*

$$\|x_0 - x^*\| < \delta \Rightarrow \left\|T^k(x) - x^*\right\| < \epsilon. \tag{3.6}$$

b. *Unstable if it is not stable.*

c. *Asymptotically stable if, δ can be chosen such that*

$$\|x_0 - x^*\| < \delta \Rightarrow \lim_{k\to\infty} T^k(x) = x^* \tag{3.7}$$

d. *Globally asymptotically stable if, x^* is unique and δ can be chosen arbitrarily large.*

Returning to the example at hand, the origin satisfies condition a and condition c of Definition 3.1.2 making it an asymptotically stable (AS) point while other fixed points are unstable.

In order to determine the stability of an equilibrium point it is very useful to understand the qualitative behavior near the equilibrium point. The linearization principle around an equilibrium point states that the analysis of eigenvalues of the linear state transition matrix gives the stability of the point. The analysis of eigenvalues and eigenvectors under consideration comes from systems that satisfy the Hartman-Grobman theorem [Khalil, 2002, Coayla-Teran et al., 2007, Giesl and Hafstein, 2015].

Theorem 3.1.1 (Hartman-Grobman)**.** *Consider system* (3.1) *with a fixed point* x^* *and consider the linear system* $x(k+1) = Ax(k)$ *where* A *is the Jacobian* $DT(x^*)|_{x^\star}$*. If the modulus of all the eigenvalues of* A *are different from one (i.e., Hyperbolic), then there exists a homomorphism* H*, defined on a neighborhood of* x^**such that, for all initial points* x_0 *along the flows of the system* $T^k(x)$

$$H \circ T^k(x_0) = A^k H(x_0) \tag{3.8}$$

is satisfied. This means that the homeomorphism preserves the sense of the flows of the nonlinear system and is chosen to preserve parametrization by time.

A hyperbolic fixed point of a non-linear discrete time system is a point where all the eigenvalues of the linearization at the point have a modulus different from one. According to the Hartman-Grobman theorem in discrete-time a hyperbolic fixed point admits a local linearization that preserves the behavior of the non-linear system. Evaluating this

condition on the current example gives,

$$DT(x) = \begin{bmatrix} 3x_1^2 + \frac{3}{4} & 0 \\ 0 & 3x_2^2 + \frac{3}{4} \end{bmatrix}$$

$$DT(x)|_{(0,0)} = \begin{bmatrix} \frac{3}{4} & 0 \\ 0 & \frac{3}{4} \end{bmatrix} \tag{3.9}$$

$$DT(x)|_{(0,\pm 0.5)} = \begin{bmatrix} \frac{3}{4} & 0 \\ 0 & \frac{3}{2} \end{bmatrix} \tag{3.10}$$

$$DT(x)|_{(\pm 0.5,0)} = \begin{bmatrix} \frac{3}{2} & 0 \\ 0 & \frac{3}{4} \end{bmatrix} \tag{3.11}$$

$$DT(x)|_{(\pm 0.5,\pm 0.5)} = \begin{bmatrix} \frac{3}{2} & 0 \\ 0 & \frac{3}{2} \end{bmatrix}, \tag{3.12}$$

given that all the eigenvalues of the different fixed points are real and different from one, they are all hyperbolic. Furthermore, the modulus of the eigenvalues of a particular hyperbolic fixed point gives its corresponding local stability.

Theorem 3.1.2 (Local stability)**.** *The local stability of a hyperbolic fixed point x^* of a linear discrete time system with respect to its eigenvalues μ_i is:*

a. *The equilibrium point x^* is asymptotically stable if $|\mu_i| < 1$ for all eigenvalues of its state transition matrix.*

b. *The equilibrium point x^* is unstable if $|\mu_i| > 1$ for one or more eigenvalues of its state transition matrix.*

c. *The equilibrium point x^* is a saddle point if some but not all $|\mu_i| < 1$, which means that the equilibrium has some modal components that converge to it.*

Remark 1. *In general, if the eigenvalues are distinct and their modulus is equal to one, the fixed point is not unstable. Theorem 3.1.2 does not consider this case because the fixed point is not hyperbolic in that case (refer to theorem 3.1.1).*

The linearization principle, along with the local stability of fixed points states that a fixed point x_s^* is AS if the modulus of all the eigenvalues of the Jacobian matrix evaluated at the fixed point are less than one, and unstable otherwise with an index k equal to the number of eigenvalues with modulus greater than one. A hyperbolic fixed point is of *type-k* if k eigenvalues of the Jacobian matrix have modulus greater than one. If only one eigenvalue has modulus greater than one x^* is a *type-one* fixed point. When the index k of unstable fixed points is equal or greater than one, and less than n, the fixed point is called a saddle; denoted by $\hat{x}^*$. The *type-one* saddle points play an important role in the approximation of the ROA.

Returning to the discrete-time Example (3.2-3.3), and analyzing the nine fixed points of the system based on Theorem 3.1.2 gives as a result that the origin is asymptotically stable, the edges of the "square" are saddle points of *type-one* and the corners are unstable. Table 3.1 summarizes these results.

Table 3.1: Fixed points, stability and *type-k* for the arbitrary non-linear system (3.2)

Equilibrium point	Stability	*type-k*
$(0, 0)$	AS	*type-0*
$(0, \pm 0.5)$	Saddle	*type-one*
$(\pm 0.5, 0)$	Saddle	*type-one*
$(\pm 0.5, \pm 0.5)$	Unstable	*type-2*

When the AS fixed point is not unique, the concept of attraction regions of the AS fixed points defines the subset of the state space where an arbitrary initial condition converges to one of them.

3.2 Regions of Attraction

The central question is: how far can an initial condition be from the AS equilibrium point in order that the discrete-time nonlinear evolution map (3.1) converges to it? Or, how big can a disturbance from an AS

be such that state converges to another AS point or diverges? These questions are especially relevant for the case when the equilibrium point is not unique, and there are several AS points. For that case the ROA is the open set from which every initial condition converges to a particular AS point x_s^*, defined as

$$R_A(x_s^*) \equiv \left\{ x \in \mathbb{R}^n : \lim_{k\to\infty} T^k(x) = x_s^* \right\}. \tag{3.13}$$

The least conservative approach is to characterize the stability boundary of the attraction region, defined as the closure of the set (3.13) without its interior

$$\partial R_A(x_s^*) = \overline{R_A(x_s^*)} \backslash \text{int}(R_A(x_s^*)). \tag{3.14}$$

For the particular case of dynamical systems, this boundary comes from the analysis of saddle fixed points, which have stable eigenvalues that provide modes that converge to the saddle point, and unstable eigenvalues that provide modes that diverge from them. The method consists of finding the stable manifolds of the saddle points, where the union of the stable manifolds of saddle points in the stability boundary of an AS gives the entire boundary. The objective is to approximate these stable manifolds.

From the linearization principle it is known that eigenvalues λ with modulus less than one are stable eigenvalues with stable eigenvectors and generalized eigenspace E_λ that spans the stable eigenspace E^s of the fixed point; i.e., $E^s = \oplus E_{|\lambda|<1}$. Conversely, eigenvalues greater than one are unstable eigenvalues with unstable eigenvectors and generalized eigenspace that spans the unstable eigenspace E^u of the fixed point; i.e., $E^u = \oplus E_{|\lambda|>1}$. The type of the hyperbolic fixed point defines the dimension of the corresponding eigenspaces, $E^u \in \mathbb{R}^k$ and $E^s \in \mathbb{R}^{n-k}$. The space state $\mathbb{R}^n$ is the direct sum of the two invariant stable and unstable eigenspaces $\mathbb{R}^n = E^s \oplus E^u$.

As the Hartman-Grobman theorem establishes a one-to-one correspondence between the nonlinear system and its linearization, locally, the stable and unstable eigenspaces are tangent to the stable and unstable manifolds of the hyperbolic fixed point. The definitions of these

manifolds are

$$W^s(x^*) = \{x \in \mathbb{R}^n : \lim_{k\to\infty} T^k(x) = x^*\}, \tag{3.15}$$

$$W^u(x^*) = \{x \in \mathbb{R}^n : \lim_{k\to-\infty} T^k(x) = x^*\}, \tag{3.16}$$

for the stable and unstable manifold respectively, assuming there is an inverse for $T^k(x)$.

The theorem characterizing the ROA for asymptotically stable fixed points, with stability boundary $\partial R_A(x_s^*)$, is taken from [Chiang and Alberto, 2015, Th. 9-(10,11)], where the system satisfies the following assumptions:

Assumption 1. *All the fixed points on the stability boundary are saddle points.*

Assumption 2. *The stable and unstable manifolds of the fixed points on the stability boundary satisfy the transversality condition*[1].

Assumption 3. *Every trajectory on the stability boundary approaches one of the saddle points as* $k \to \infty$.

Theorem 3.2.1. *Consider an autonomous nonlinear discrete-time dynamical system* (3.1)*, satisfying Assumptions 1-3. Let* $\{\hat{x}_i^*\}_{i=1}^P$ *be the* P *saddle points on the stability boundary of an asymptotically stable fixed point. Then,*

a. $\hat{x}_i^* \in \partial R_A(x_s)$ *if and only if* $W^u(\hat{x}_i^*) \cap R_A(x_s^*) \neq \varnothing$

b. $\partial R_A(x_s^*) = \cup W^s(\hat{x}_i^*)$.

Hence, the stability boundary is the union of the stable manifolds of the hyperbolic fixed points on the stability boundary.

To illustrate the role of the stable manifolds of saddle points in the boundary, recall the non-linear example from Section 3.1 equation (3.2).

[1] For manifolds A and B in $\mathcal{M}$, the transversality condition is satisfied if the tangent spaces of the intersection between A and B span the tangent space of $\mathcal{M}$.

This system has four *type-one* saddle points at $(0, \pm 0.5)$ and $(\pm 0.5, 0)$, where their corresponding stable and unstable eigenspaces are

$$E^s(0, 0.5) = \{x \in \mathbb{R}^2 \colon x_2 = 0.5\} \tag{3.17}$$
$$E^u(0, 0.5) = \{x \in \mathbb{R}^2 \colon x_1 = 0\} \tag{3.18}$$
$$E^s(0, -0.5) = \{x \in \mathbb{R}^2 \colon x_2 = -0.5\} \tag{3.19}$$
$$E^u(0, -0.5) = \{x \in \mathbb{R}^2 \colon x_1 = 0\} \tag{3.20}$$
$$E^s(0.5, 0) = \{x \in \mathbb{R}^2 \colon x_1 = 0.5\} \tag{3.21}$$
$$E^u(0.5, 0) = \{x \in \mathbb{R}^2 \colon x_2 = 0\} \tag{3.22}$$
$$E^s(-0.5, 0) = \{x \in \mathbb{R}^2 \colon x_1 = -0.5\} \tag{3.23}$$
$$E^u(-0.5, 0) = \{x \in \mathbb{R}^2 \colon x_2 = 0\}. \tag{3.24}$$

Figure 3.2 depicts the stable eigenspaces of these *type-one* saddle points with solid black lines, and highlights the ROA of the AS point in the origin as the union of these sets.

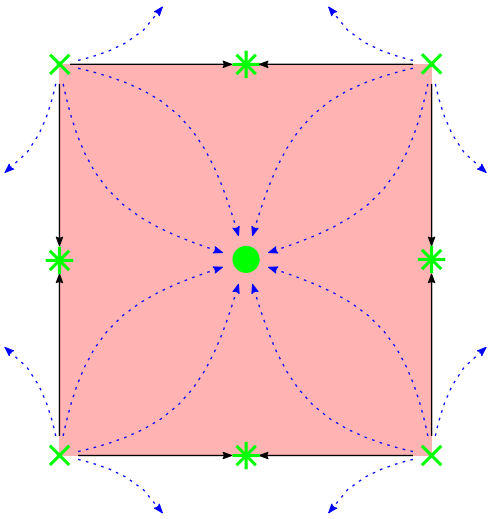

Figure 3.2: Region of attraction as the union of the stable manifolds (solid black lines) of the saddle fixed points.

Remark 2. *Assumption 1 is a generic property of differentiable dynamical systems, while Assumptions 2 and 3 must be verified. Figure 3.3 shows the importance of Assumption 2, where a part of the stable manifold of* $\hat{x}_A^*$

does not intercept with the stability boundary. For this particular case, the transversality condition is not satisfied because part of the tangent space of the unstable manifold of $\hat{x}_A^*$ is equal to a part of the tangent space of the stable manifold of $\hat{x}_B^*$.

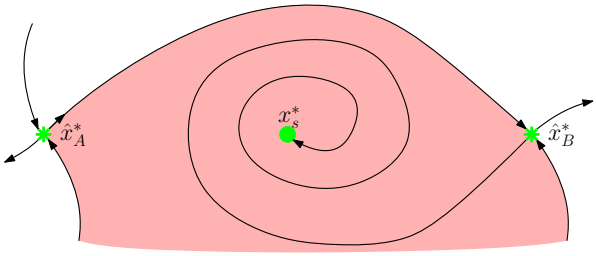

Figure 3.3: Transversality condition violation by the stable and unstable manifold of saddle points.

3.3 The Koopman Operator

This section contains the basic theory of the Koopman operator for systems that admits a discrete-time point spectrum. The main quality of this operator, related to the underlying dynamical system is the linear evolution of a set of observables (later defined as eigenfunctions) that capture the nonlinear evolution of the system.

Consider the autonomous nonlinear discrete-time system (3.1), and a set of observation functions

$$f(x)\colon \mathcal{M} \to \mathbb{C}$$

that belong to some function space, i.e., $f(x) \in \mathcal{F}$. For these functions there is a discrete operator U^k, where the action of this operator on observables defines their evolution. This is the Koopman operator, and its relationship with the observables (i.e., arbitrary functions of the states) and the states of the system is

$$\left[U^k f\right](x) = f\left(T^k(x)\right). \tag{3.25}$$

In other words, the time-evolution of observations is the observations of the time-evolution of states. The trade-off with this approach concerns linearity and dimensionality, a finite-dimensional nonlinear system being described by an infinite-dimensional linear one. The linearity of the operator allows it to have a spectral decomposition of tuples $\{(\mu_i, \phi_i(x), v_i)\}_{i=1}^{\infty}$ of eigenvalues, eigenfunctions and modes that contain information on the underlying dynamical system. The eigenvalues and eigenfunctions satisfy the condition that the corresponding eigenvalue determines the dynamics associated with a specific eigenfunction as

$$[U^k \phi_i](x) = \mu_i^k \phi_i(x), \tag{3.26}$$

and the Koopman modes serve to recover the observation functions $f(x)$, i.e., they map the linear evolution of eigenfunctions (3.26) into the original observables by weighting the eigenfunctions as

$$f(x) = \sum_{i=1}^{\infty} v_i \phi_i(x). \tag{3.27}$$

The importance and advantages of the Koopman operator and the diagonalization provided by the spectral decomposition are highlighted by (3.26) and (3.27), which show that the eigenvalue associated to an eigenfunction defines its time evolution and that the modes recover the value of the defined set of observables $f(x)$. Therefore, the evolution of observables with respect to the spectral decomposition of the Koopman operator is

$$f\left(T^k(x)\right) = \left[U^k f\right](x) = \sum_{i=1}^{\infty} v_i \mu_i^k \phi_i(x). \tag{3.28}$$

3.3.1 Koopman Operator Example

The exact solution to the Koopman operator of a dynamical system is available for a family of polynomial difference equations [Brunton et al., 2016a]. This closed form solution is only possible for systems with a unique fixed point. Therefore, there is no exact solution for the problem of approximating the ROA. Consider the following autonomous nonlinear

discrete-time dynamical system

$$\begin{aligned} x_1(k+1) &= \gamma x_1(k) \\ x_2(k+1) &= \delta x_2(k) + (\gamma^2 - \delta) x_1^2(k). \end{aligned} \tag{3.29}$$

The solution of the system under the Koopman operator requires the definition of a set of observable functions whose evolution is defined by the operator as in (3.25). For this particular case (see [Brunton et al., 2016a] for the deduction of the set of observables), the set of observables and the Koopman system are

$$f(x) = \begin{bmatrix} x_1 \\ x_2 \\ x_1^2 \end{bmatrix} \;\Rightarrow\; f\left(x(k+1)\right) = \begin{bmatrix} \gamma & 0 & 0 \\ 0 & \delta & (\gamma^2 - \delta) \\ 0 & 0 & \gamma^2 \end{bmatrix} \begin{bmatrix} x_1 \\ x_2 \\ x_1^2 \end{bmatrix}. \tag{3.30}$$

The spectral decomposition of the operator gives the set of eigenvalues $\mu_1 = \gamma$, $\mu_2 = \gamma^2$ and $\mu_3 = \delta$, and the sets of left and right eigenvectors, defined as $W^\star$ and Ξ respectively and given by

$$W^\star = \begin{bmatrix} 1 & 0 & 0 \\ 0 & 0 & 1 \\ 0 & 1 & -1 \end{bmatrix} \qquad \Xi = \begin{bmatrix} 1 & 0 & 0 \\ 0 & 1 & 1 \\ 0 & 1 & 0 \end{bmatrix}. \tag{3.31}$$

From the left eigenvectors and the set of observables $f(x)$, the definition of the set of eigenfunctions $\Phi(x)$ of the Koopman operator is the observables weighted by the left eigenvector, i.e,. $\Phi(x) = \left(f(x)^\top W^\star\right)^\top$, which gives

$$\begin{aligned} \Phi(x) = \begin{bmatrix} \phi_1(x) \\ \phi_2(x) \\ \phi_3(x) \end{bmatrix} &= \left(\begin{bmatrix} x_1 & x_2 & x_1^2 \end{bmatrix} \begin{bmatrix} 1 & 0 & 0 \\ 0 & 0 & 1 \\ 0 & 1 & -1 \end{bmatrix} \right)^\top \\ &= \begin{bmatrix} x_1 \\ x_1^2 \\ x_2 - x_1^2 \end{bmatrix}. \end{aligned} \tag{3.32}$$

With the complete spectral decomposition of the Koopman operator for system 3.29, with right eigenvectors Ξ, eigenvalues

$$M = \mathrm{diag}(\gamma,\, \gamma^2,\, \delta),$$

and using (3.28), the evolution of observables in matrix form is

$$\begin{aligned} f\left(x(k+1)\right) &= \Xi M \Phi(x(k)) \\ &= \begin{bmatrix} 1 & 0 & 0 \\ 0 & 1 & 1 \\ 0 & 1 & 0 \end{bmatrix} \begin{bmatrix} \gamma & 0 & 0 \\ 0 & \gamma^2 & 0 \\ 0 & 0 & \delta \end{bmatrix} \begin{bmatrix} x_1(k) \\ x_1^2(k) \\ x_2(k) - x_1^2(k) \end{bmatrix}, \end{aligned} \tag{3.33}$$

and the evolution of states $[x_1,\, x_2]^\top = B^\top f(x)$ is

$$\begin{aligned} x(k+1) &= B^\top \Xi M \Phi(x(k)) \\ &= \begin{bmatrix} 1 & 0 \\ 0 & 1 \\ 0 & 0 \end{bmatrix}^\top \begin{bmatrix} 1 & 0 & 0 \\ 0 & 1 & 1 \\ 0 & 1 & 0 \end{bmatrix} \begin{bmatrix} \gamma & 0 & 0 \\ 0 & \gamma^2 & 0 \\ 0 & 0 & \delta \end{bmatrix} \begin{bmatrix} x_1(k) \\ x_1^2(k) \\ x_2(k) - x_1^2(k) \end{bmatrix} \\ &= \begin{bmatrix} \gamma x_1 \\ \delta x_2 + (\gamma^2 - \delta) x_1^2 \end{bmatrix}, \end{aligned} \tag{3.34}$$

where $B \in \mathbb{R}^{3\times 2}$ is a selection matrix with a unitary value per column in the index of the observables that capture every one of the states. In this particular case, the set of observables contains the functions that capture every one of the states, i.e., $f_1(x) = x_1$ and $f_2(x) = x_2$. Note that (3.34) circles back to the original dynamical system (3.29).

It is often difficult to obtain a closed analytical form for the Koopman operator, and due to the fact that for the multiple stability problem at hand, there is no known closed analytical form of the discrete-time Koopman operator it is necessary to use approximation techniques to circumvent this difficulty. Algorithms such as the EDMD approximate a truncated version of the Koopman operator with data from the dynamical system [Korda and Mezić, 2018a]. Furthermore, complementing the algorithm with order and dimension reduction methods, coupled with the retention of order one polynomial elements in the basis, provides a way to have accurate approximations of polynomial systems that provide all the necessary components to perform the analysis.

3.4 The EDMD Algorithm

The objective of the EDMD algorithm [Williams et al., 2015] is to get a truncated approximation of the discrete-time Koopman operator based

on sampled data of the underlying system [Klus et al., 2016, Korda and Mezić, 2018a]. Consider the autonomous nonlinear discrete dynamical system (3.1), the EDMD algorithm to approximate the Koopman operator in discrete-time requires N pairs of data snapshots, either from a real system or a numerical simulation at a specific sampling Δt. The snapshot pairs, $\{(x_i, y_i)\}_{i=1}^{N}$, where $y_i = T(x_i)$, are organized in data sets

$$X = \begin{bmatrix} x_1 & x_2 & \dots & x_N \end{bmatrix}, \; Y = \begin{bmatrix} y_1 & y_2 & \dots & y_N \end{bmatrix}. \tag{3.35}$$

The "extended" part of the EDMD algorithm consists in the approximation of the Koopman operator in a "lifted" space of the state variables, rather than approximating the state space as in the DMD algorithm [Schmid, 2010]. The "lifting" procedure consists in evaluating the state space of the system on a vector-valued function of observables $\Psi = [\psi_1 \cdots \psi_d]^T : \mathcal{M} \to \mathbb{C}^{1\times d}$ [Williams et al., 2015]. The approximation of the Koopman operator will be of dimension d. This operator has to satisfy the condition

$$\Psi(y) = U_d \Psi(x) + r(x), \tag{3.36}$$

where $r(x) \in \mathcal{F}$ is the residual term to minimize in order to find U_d. This problem is closely related to the least mean squares problem, polynomial chaos expansion [Sudret, 2008], statistical estimation [Walter and Pronzato, 1997], and machine learning [Neumaier, 2003] problems. Considering that the best approximation is the solution that minimizes the residual term, a solution of the objective function

$$\|r(x)\|^2 = \frac{1}{N} \sum_{i=1}^{N} \frac{1}{2} \left\| \Psi(y_i) - U_d \Psi(x_i) \right\|_2^2, \tag{3.37}$$

gives an accurate approximation of U_d. The solution corresponds with the ordinary least-squares [Williams et al., 2015], which has a closed analytical form given by,

$$U_d \triangleq A G^{+}, \tag{3.38}$$

with matrices $G, A \in \mathbb{C}^{d\times d}$ defined by

$$G = \frac{1}{N}\sum_{i=1}^{N} \Psi(x_i)\Psi(x_i)^\top, \tag{3.39}$$

$$A = \frac{1}{N}\sum_{i=1}^{N} \Psi(x_i)\Psi(y_i)^\top. \tag{3.40}$$

Remark 3. *A critical factor for the effectiveness of the solutions to* (3.37) *is the choice of observables* Ψ*. Although there are several proposed procedures, the choice of the so-called dictionary elements is still an open problem.*

For a formal deduction of solution (3.38), consider the problem (3.37) in matrix form.

$$\min_{U_d} J = \min_{U_d} \frac{1}{2}\|\Psi(Y) - U_d\Psi(X)\|_2^2. \tag{3.41}$$

The solution to the minimization problem is

$$J = \frac{1}{2}(\Psi(Y) - U_d\Psi(X))(\Psi(Y) - U_d\Psi(X))^\top \tag{3.42}$$

$$= \frac{1}{2}(\Psi(Y) - U_d\Psi(X))(\Psi(Y)^\top - \Psi(X)^\top U_d^\top) \tag{3.43}$$

$$= \frac{1}{2}(U_d\Psi(X)\Psi(X)^\top U_d^\top - \Psi(Y)\Psi(X)^\top U_d^\top + \Psi(Y)\Psi(Y)^\top) \tag{3.44}$$

$$\frac{\mathrm{d}}{\mathrm{d}U_d} J = \frac{1}{2}(2U_d\Psi(X)\Psi(X)^\top - 2\Psi(Y)\Psi(X)^\top) \tag{3.45}$$

$$0 = U_d\Psi(X)\Psi(X)^\top - \Psi(Y)\Psi(X)^\top \tag{3.46}$$

$$U_d = (\Psi(Y)\Psi(X)^\top)(\Psi(X)\Psi(X)^\top)^+ \tag{3.47}$$

$$= AG^+. \tag{3.48}$$

Solution (3.38) is suitable when matrix G is not ill-conditioned. Otherwise, solutions based on the Moore-Penrose pseudoinverse or regularized least-squares give a more accurate result. The former being the most accurate, and the latter being computationally efficient and able to

provide sparse approximations of U_d. For the regularized least-squares case, the objective is to find a set of d linear fitting functions, i.e., one linear regression for each row of matrix U_d. The set of fitting functions is $\{h_j(x) = U_{d_j}\Psi(x)^T\}_{j=1}^{d}$ of the 'lifted" space, where j indexes the rows of the operator that minimize the error function for each of the rows. The error function in the regularized least squares sense is

$$E(U_{d_j}) = \frac{1}{N}\sum_{i=1}^{N} L(\psi_j(y_i), h_j(x_i)) + \alpha R(U_{d_j}), \tag{3.49}$$

where L is the loss function that measures the model fit, R is the regularization term, and $\alpha \in \mathbb{R}_+$ is a nonnegative parameter. The choice of L gives different types of classifiers [Rosasco et al., 2004], while different regularization terms R provide various solutions to the over fitting problem that arises from ill-conditioned problems.

The common choices for the loss function are the Ridge regression, absolute value loss, and support vector machines (epsilon-intensive) functions [Rosasco et al., 2004]. For the regularization term, the common choices are l_1, l_2, and a linear combination of the two (elastic net) norms.

With the solution to (3.36), and the spectral decomposition M, Ξ, W^*, where $M = \text{diag}(\mu_1, \ldots, \mu_d)$ is the diagonal matrix of eigenvalues, $\Xi = [\xi_1, \ldots, \xi_d]$ is the aforementioned matrix of right eigenvectors, and $W^\star = \Xi^{-1}$ is the matrix of left eigenvectors. The definition of the eigenfunctions of the Koopman operator according to EDMD algorithm (according to Williams et al. [2015]) $\Phi = [\phi_1, \ldots, \phi_d]^\top$ are

$$\Phi^\top(x) = \Psi(x)^\top W^\star, \tag{3.50}$$

from (3.26) that describes the evolution of eigenfunctions according to their eigenvalue, the evolution of eigenfunctions from the EDMD algorithm is

$$\Phi(x(k)) = M^k\Phi(x_0), \tag{3.51}$$

with the evolution of eigenfunctions, the right eigenvectors or modes serve to recover the original set of observables

$$\Psi(x) = \Xi\Phi(x), \tag{3.52}$$

and the time evolution of observables according to the spectrum of the Koopman operator [Williams et al., 2015] is

$$\Psi(T^k(x)) = \Xi M^k \Phi(x). \tag{3.53}$$

To recover the state, we define a matrix $B \in \mathbb{R}^{(d\times n)}$ with a unitary value per column in the index of an injective observable-function and zeros otherwise. This matrix selects the functions whose inverse gives the value of the state. If we define this set of functions selected by B as $\Psi_B(x)$, then, with (3.53), the approximation of the state evolution map $T^k(x) = x_k$ from the initial condition x_0 in terms of the approximation of the Koopman decomposition $\{(\mu_i, \phi_i(x), v_i)\}_{i=1}^d$ is

$$\bar{x}(k) = \bar{T}^k(x_0) = \Psi_B^{-1}\left(B^\top \Xi M^k \Phi(x_0)\right). \tag{3.54}$$

Note that the Koopman representation of the system also allows for a clean representation of the backward evolution of the states given by

$$\bar{x}(-k) = \Psi_B^{-1}\left(B^\top \Xi M^{-k} \Phi(x_0)\right). \tag{3.55}$$

Given that the approximation of the discrete-time Koopman operator comes from a set of orbits of the system, the comparison between these theoretical orbits against the evolution map of the Koopman operator gives a measure for the algorithms accuracy. The empirical error for a number of N_s trajectories, where each has a number of N_k data points is

$$e = \frac{1}{N_s}\sum_{i=1}^{N_s}\frac{1}{N_k}\sum_{k=1}^{N_k}\frac{|T^k(x_i) - \bar{T}^k(x_i)|}{|T^k(x_i)|}. \tag{3.56}$$

A low error over a set of test trajectories of the Koopman state evolution map, gives a Koopman operator approximation whose eigenfunctions are accurate enough for the subsequent calculations related to them.

3.4.1 Observables

A critical part of the approximation via the EDMD algorithm is the choice of observables. These functions of the state $\psi_l(x)$ usually consists of an orthogonal basis of polynomials [Koekoek et al., 2010], radial basis

functions, or an arbitrarily constructed set with polynomial elements, and trigonometric functions, among others [Brunton et al., 2016b].

The choice of orthogonal polynomials for the approximation of the Koopman operator has the advantage that the rank and dimension of the vector-valued function of observables Ψ can be reduced [Konakli and Sudret, 2016a,b], and the state can be recovered by the inverse of injective observable-functions. A sequence of orthogonal polynomials $\{\pi_\alpha(x)\}_{\alpha=0}^{p}$ where $\pi_\alpha(x)$ is a univariate (i.e., $x \in \mathbb{R}$) polynomial of degree $\alpha \in \mathbb{N}_+$ up to order p. This sequence is defined over a range $[a, b]$ where some inner product between distinct elements is zero, i.e., $\langle \pi_i(x), \pi_j(x) \rangle = 0$ for $i \neq j$, and satisfies a particular ordinary differential equation. For example, the set of Laguerre polynomials, which is defined over the range $[0, \infty]$ satisfies the ordinary differential equation

$$x\frac{\mathrm{d}^2 y(x)}{\mathrm{d}x^2} + (1 - x_1)\frac{\mathrm{d}y(x)}{\mathrm{d}x} + \alpha y(x) = 0, \qquad \alpha = 1, 2, \ldots. \tag{3.57}$$

Consider an autonomous nonlinear discrete-time dynamical system such as (3.29), where the number of state variables $n = 2$, and the selected polynomial basis consists of Laguerre polynomials. Table 3.2 shows the set of univariate polynomials on the first component of the state space vector (i.e., $j = 1$) for a choice of maximum polynomial degree $p = 3$, and a set of indices $\alpha_1 = \{0, 1, 2, 3\}$.

Table 3.2: Basis for the first state variable x_1. Solution to the Laguerre ODE: $x_1\ddot{y} + (1 - x_1)\dot{y} + \alpha_1 y = 0$ where $\dot{y} = \frac{dy}{dx_1}$.

$J(\alpha_1)$	ODE	$\pi_{\alpha_1}(x_1) = y(x_1)$
$J(0_1)$	$x_1\ddot{y} + (1 - x_1)\dot{y} = 0$	1
$J(1_1)$	$x_1\ddot{y} + (1 - x_1)\dot{y} + y = 0$	$-x_1 + 1$
$J(2_1)$	$x_1\ddot{y} + (1 - x_1)\dot{y} + 2y = 0$	$\frac{1}{2}x_1^2 - 2x_1 + 1$
$J(3_1)$	$x_1\ddot{y} + (1 - x_1)\dot{y} + 3y = 0$	$-\frac{1}{6}x_1^3 + \frac{3}{2}x_1^2 - 3x_1 + 1$

With these univariate polynomials, every element of the vector-valued function of observables is the tensor product of n univariate polynomials, that is,

$$\psi_l(x) = \prod_{j=1}^{n} \pi_{\alpha_j}(x_j), \qquad l = 1, \ldots, d. \tag{3.58}$$

If we consider a full degree p and full dimension vector-valued function of observables, the order and dimension grows exponentially with the number of state variables n. The maximum degree of the polynomials in $\Psi(x)$ is p^n and the dimension of the whole set is

$$d = \dim\Psi(x) = \binom{n+p+1}{p+1} = \frac{(n+p+1)!}{(p+1)!n!}. \tag{3.59}$$

The exponential growth of the order produces an over-fitting problem in the discrete approximation of the Koopman operator via the EDMD algorithm, and the growth in the dimension has the course of dimensionality problem, especially in the definition of the discrete Koopman matrix from (3.38) that needs the inverse of matrix G. To avoid these problems it is necessary to restrict the maximum order of the polynomial basis and its dimension.

3.4.2 Reduction by p-q-quasi Norms

The proposed reduction of the order and dimension of the polynomial basis is via a p-q-quasi norm[2] reduction first introduced in the solution of polynomial chaos problems [Konakli and Sudret, 2016a]. Define the q-quasi norm as,

$$\|\alpha\|_q = \left(\sum_{i=1}^{n} \alpha_i^q\right)^{\frac{1}{q}}, \tag{3.60}$$

for a polynomial element $\psi_l(x)$ consider a maximum degree $p \in \mathbb{N}$, a quasi norm $q \in \mathbb{R}_+$ and define the set of indexes α_l as

$$\alpha_l = \{\alpha \in \mathbb{N}^n \colon \|\alpha\|_q \leq p\}. \tag{3.61}$$

Given that each element of the polynomial basis is the tensor product of the univariate polynomials (3.58) in the retained indexes given by (3.61), this approach reduces the maximum order, and the overall dimension of the vector-valued function of observables.

Figure 3.4 shows the effect of the truncation scheme for the previous example on Laguerre polynomials (3.57) for the case where the maximum

[2]The quantity $\|\cdot\|_q$ is not a norm because it does not satisfy the triangle inequality.

polynomial order is $p = 3$, and the number of state variables is $n = 2$. Certainly, reducing the value of the quasi norm q, reduces the maximum order and dimension of the vector valued function of observables.

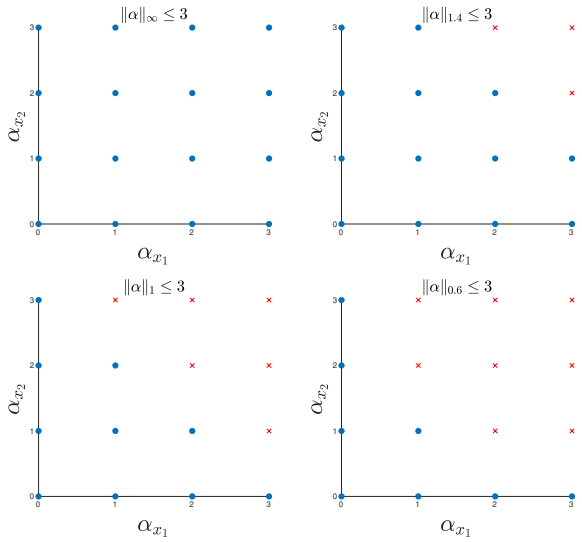

Figure 3.4: Retained basis terms for the low-rank polynomial basis.

Every element of the polynomial basis comes from the tensor product in (3.58), and a full basis, i.e., with $q = \infty$, has 16 elements resulting from all the available combinations of indices in two state variables with a univariate order less or equal to $p = 3$. The available combinations for this example are

$$\alpha = \begin{Bmatrix} 0 & 1 & 2 & 3 & 0 & 1 & 2 & 3 & 0 & 1 & 2 & 3 & 0 & 1 & 2 & 3 \\ 0 & 0 & 0 & 0 & 1 & 1 & 1 & 1 & 2 & 2 & 2 & 2 & 3 & 3 & 3 & 3 \end{Bmatrix}. \tag{3.62}$$

This selection gives the following set of orthogonal polynomials as the vector-valued function of observables for the approximation of the

discrete-time Koopman operator.

$$\Psi(x) = \begin{bmatrix} J(0_1)J(0_2) \\ J(1_1)J(0_2) \\ J(2_1)J(0_2) \\ \vdots \\ J(0_1)J(1_2) \\ J(1_1)J(1_2) \\ \vdots \\ J(3_1)J(3_2) \end{bmatrix} = \begin{bmatrix} 1 \\ -x_1 + 1 \\ \frac{1}{2}x_1^2 - 2x_1 + 1 \\ \vdots \\ -x_2 + 1 \\ (-x_1 + 1)(-x_2 + 1) \\ \vdots \\ (-\frac{1}{6}x_1^3 + \frac{3}{2}x_1^2 - 3x_1 + 1)(-\frac{1}{6}x_2^3 + \frac{3}{2}x_2^2 - 3x_2 + 1) \end{bmatrix} \tag{3.63}$$

If the selection of truncation scheme is a value $q = 0.6$, the set of retained indices reduces the polynomial basis dimension from 16 elements to 8, and the maximum order from 6 to 3. That is, the remaining indices to perform the tensor product on univariate polynomials are,

$$\alpha = \begin{Bmatrix} 0 & 1 & 2 & 3 & 0 & 1 & 0 & 0 \\ 0 & 0 & 0 & 0 & 1 & 1 & 2 & 3 \end{Bmatrix}, \tag{3.64}$$

This new set of indices redefines the vector valued function of observables

$$\Psi(x) = \begin{bmatrix} J(0_1)J(0_2) \\ J(1_1)J(0_2) \\ J(2_1)J(0_2) \\ J(3_1)J(0_2) \\ J(0_1)J(1_2) \\ J(1_1)J(1_2) \\ J(0_1)J(2_2) \\ J(0_1)J(3_2) \end{bmatrix} = \begin{bmatrix} 1 \\ -x_1 + 1 \\ \frac{1}{2}x_1^2 - 2x_1 + 1 \\ -\frac{1}{6}x_1^3 + \frac{3}{2}x_1^2 - 3x_1 + 1 \\ -x_2 + 1 \\ (-x_1 + 1)(-x_2 + 1) \\ \frac{1}{2}x_2^2 - 2x_2 + 1 \\ -\frac{1}{6}x_2^3 + \frac{3}{2}x_2^2 - 3x_2 + 1 \end{bmatrix} \tag{3.65}$$

Even though this reduction method eliminates most of the higher order polynomial elements in the vector valued function of observables, it does not guarantee that the remaining elements give an accurate approximation of the Koopman operator. Some polynomial elements in the basis rather than reducing the error of the approximation, will increase it. Therefore, a second reduction method based on the individual error of each element of the basis reduces the dimension even further, and gives a more accurate approximation.

3.4.3 Reduction by Polynomial Accuracy

The idea of the reduction is to calculate the error of the individual multivariate polynomials and eliminate the elements whose error is greater than a specified threshold. The approximation of the Koopman operator from the EDMD algorithm comes from a set of the system orbits. This set of orbits comes from one of two distinct sets, one for solving the least-squares problem (9) and one for testing the accuracy of the solution. Evaluating the posterior time event Y in every element of the vector-valued function, and comparing it with the effect of the operator on the evaluation of the anterior time event X, gives a metric of the contribution of the individual multivariate elements to the accuracy of the solution. Every element of this error criterion, $\epsilon = (\epsilon_1, \cdots, \epsilon_d)$ is

$$\epsilon_l = \frac{1}{N} \sum_{i=1}^{N} \frac{|\psi_l(y_i) - U_{d_l} \psi_l(x_i)|}{|\psi_l(y_i)|} \tag{3.66}$$

where U_{d_l} is the l-th row of the Koopman operator matrix.

Recall that for the case of orthogonal polynomials, the way to recover the state is by the inverse of n injective multivariate elements, if these elements are the ones with index one in each of the state variables, the recovery is a linear vector-valued function of the observed values. Therefore, the threshold $\bar{\epsilon}$ for the elimination of elements is the maximum of the errors with an index equal to one,

$$\bar{\epsilon} = \max(\epsilon \colon \|\alpha_l\|_1 = 1) \tag{3.67}$$

and the multivariate polynomial elements that stay as a part of the reduced vector-valued function of observables $\Psi_R(x)$ are

$$\Psi_R(x) = \{\Psi(x) \colon \epsilon \leq \bar{\epsilon}\}. \tag{3.68}$$

The application of the p-q-quasi norms and polynomial error reductions allow for the approximation of the Koopman operator of the underlying systems with significant fewer basis elements than the current methods and increases the accuracy of the operator. This increase in accuracy allows for the training of the operator with less training trajectories.

3.4.4 EDMD Example

The proposed method for obtaining the low-order polynomials based on the p-q-quasi norms and the error of the multivariate elements is by applying a greedy approach for the calculation of a suboptimal p-q parametrization, and a second calculation of the operator based on the elimination of the multivariate elements.

The greedy approach to find the suboptimal approximation of the Koopman operator relies on the error from the comparison on the test set of orbits, and the predicted orbits of the operator. Consider (3.36), where the k-th application of the operator U_d gives the evolution of the observables $\Psi(x)$ up to that time. From this evolved state, consider a matrix $B \in \mathbb{R}^{d\times n}$ with a unitary value per column in the position where an element of the vector-valued function has an index equal to one, i.e., every column of matrix B is defined as

$$B_l = \{e_l \colon \|\alpha_l\|_1 = 1\}. \tag{3.69}$$

Consider the set of indices from the reduced p-q-quasi norm reduction of Laguerre polynomials with $p = 3$ and $q = 0.6$ in (3.64). The indices that satisfy the condition $\|\alpha\| = 1$ are the second and fifth polynomial elements. Hence, the B matrix for that particular case is

$$B = \begin{bmatrix} 0 & 1 & 0 & 0 & 0 & 0 & 0 & 0 \\ 0 & 0 & 0 & 0 & 1 & 0 & 0 & 0 \end{bmatrix}^\top, \tag{3.70}$$

These two polynomial elements are the vector valued function whose inverse recovers the state from the values of $\Psi(x)$. For this particular case of Hermite polynomials with the selected truncation scheme

$$\Psi_B^{-1}(x) = \begin{bmatrix} -\psi_2 + 1 & -\psi_5 + 1 \end{bmatrix}^\top. \tag{3.71}$$

This serves to define the state evolution map in terms of the discrete approximation of the Koopman decomposition $\{(\mu_i, \phi_i(x), v_i)\}_{i=1}^d$ (for the aforementioned example, $d = 8$). The k-th application of the state evolution map $T^k(x) = x_k$ from the initial condition x_0 is

$$\hat{x}(k) = \Psi_B^{-1}\left(B^\top U_d^k \Psi(x(0))\right). \tag{3.72}$$

Remark 4. *Note that this approximation of the evolution of states is different from* (3.54)*, that describes the evolution as a function of eigenfunctions and their corresponding eigenvalues, while for this case, the approximation is a function of observables evolution weighted by the Koopman matrix* Ud*. This is an important distinction because the evolution of observables is less prone to error because it only depends on the inverse of* G*. Conversely, the evolution of eigenfunctions not only depends on the inverse of* G*, it also depends on the spectral decomposition of* U_d*, where additional numerical calculation increments the empirical error* (3.56)*.*

The first step of the process is to select a set of training and testing trajectories, and to generate the N pairs of data snapshots. All throughout this thesis, these sets come from the integration of ordinary differential equations from different initial conditions. For an accurate approximation of the discrete-time Koopman operator, there are two important aspects to consider. First, if an orbit reaches steady state, the integration must stop in order to avoid redundant data at steady state that causes the condition number of matrix G to increase making the matrix ill-conditioned and very sensitive to approximation errors. This is the reason why the solution (3.38) is in terms of the Moore-Penrose pseudo inverse. If G has a condition number sufficiently small, the accuracy of the solution increases with the use of the inverse, i.e.,

$$U_d = AG^{-1}. \tag{3.73}$$

The second aspect to consider is that in the construction of the N pairs of data snapshots, the last value of each trajectory must be discarded. Given that the integration must stop at steady state, usually, the last value of the trajectory is less than one Δt away from the penultimate, and this small difference decreases the accuracy of the approximation.

For an illustrative example, consider the Duffing equation, a benchmark case in the literature for analyzing the accuracy of Koopman-based methods. The system has different types of behavior depending on the parametrization. This example will consider the case with damping and two basins of attraction. The general form of the duffing equation is

$$\dot{x}_1 = x_2 \tag{3.74}$$

$$\dot{x}_2 = -\delta x_2 - x_1(\beta + \alpha x_1^2). \tag{3.75}$$

The parametrization to have two basins of attraction is $\delta = 0.5$, $\beta = -1$, $\alpha = 1$. This parametrization describes a system with two stable focus points at $(\pm 1, 0)$ and a saddle point at $(0, 0)$. The samples for the system come from 4 uniformly distributed initial conditions over $x_1, x_2 \in \begin{bmatrix} -2 & 2 \end{bmatrix}$ and are obtained by numerical integration with a $\Delta t = 0.1$ until they reach one of the steady states. This means that the number of points per trajectory is not the same. Along with the samples, the training and test sets are 50% of the total samples each. Figure 3.5 shows the testing and training trajectories. Note that for each set, there is one trajectory that converges to each of the asymptotically stable equilibrium points. For the case depicted, the total amount of points in the training set is 404.

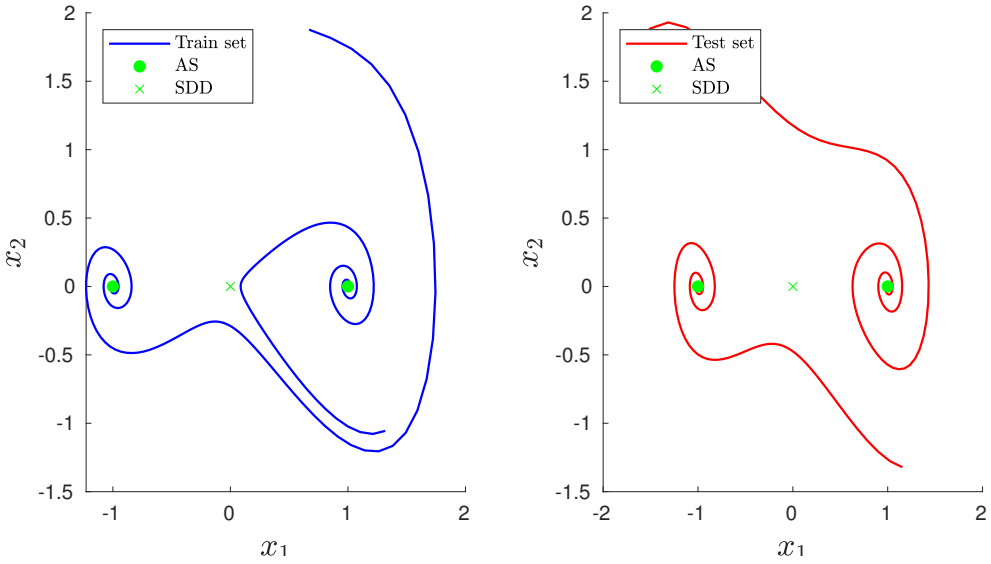

Figure 3.5: Training and testing sets for the discrete-time approximation of the Koopman operator via the EDMD algorithm with reduced basis.

From the trajectories of the training set, the next step is to generate the X and Y snapshots sets. Recall that excluding the last element of the orbits increases the accuracy. Furthermore, given that an (x, y) snapshot pair is the value at a time instant, and the value at the next one, it is possible to concatenate all the available pairs in two sets for the evaluation of the A and G matrices. Consider a set of Tn_r training

trajectories, each with an N_k number of points, i.e., $Tn_r \in \mathbb{R}^{N_k \times n}$. The X and Y set are:

$$X = \begin{bmatrix} Tn_1(1:N_{k_1}-2)^\top & Tn_2(1:N_{k_2}-2)^\top & \cdots & Tn_r(1:N_{k_r}-2)^\top \end{bmatrix}^\top \tag{3.76}$$

$$Y = \begin{bmatrix} Tn_1(2:N_{k_1}-1)^\top & Tn_2(2:N_{k_2}-1)^\top & \cdots & Tn_r(2:N_{k_r}-1)^\top \end{bmatrix}^\top \tag{3.77}$$

The third step of the process is to select a set of q norms and a set of maximum multivariate order p. For each p, sweep along the parameter q calculating the error (3.56), then select the suboptimal parameters from the approximation that gives the least one. For the Duffing equation under consideration, the selection of orthogonal polynomials is the same Laguerre basis as for the illustration of the p-q-quasi norm reduction methods with a parameter sweep of $p = 3$ and $q = \begin{bmatrix} 0.4 & 0.5 & 0.7 & \infty \end{bmatrix}$, that includes the infinity norm for illustration purposes of the effect of the reduction. Figure 3.7 shows the polynomial elements for each of the q values in the sweep, where it is clear that for the case where there is no truncation, the error increases compared to $q = 0.7$. Additionally, it is important to remark that the proposed algorithm makes an accurate approximation of the system with just one trajectory that converges to each of the asymptotically stable equilibrium points in the training set.

With the first approximation of the discrete-time Koopman operator, the next step is to compute the error (3.66) for the individual multivariate elements and select the elements that will stay on the polynomial basis according to (3.68). Figure 3.6 shows how the second reduction has an effect on the polynomial basis for the different choices of q. The "best" value $q = 0.7$ does not lead to a polynomial reduction, and to illustrate the procedure, we will focus on $q = 0.5$ (which is the "worst" value). In this case,

$$\epsilon = \begin{bmatrix} 0.0000 & 0.0017 & 0.0019 & 0.0132 & 0.0165 & 1.1708 & 0.0192 & 0.0637 \end{bmatrix}, \tag{3.78}$$

where the error threshold is the maximum between the second and fifth elements because these correspond to the order-one and single-variable

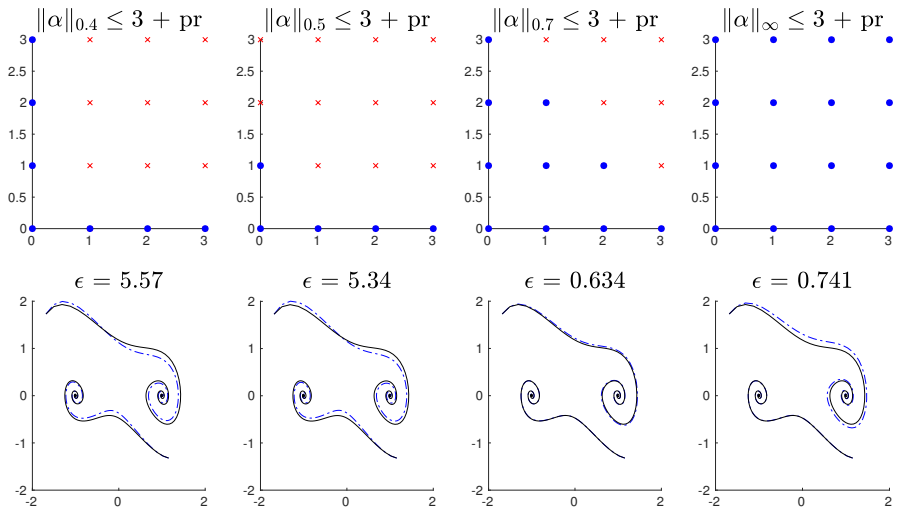

Figure 3.6: Test orbits from the EDMD algorithm with polynomial accuracy truncation scheme for a Laguerre Polynomial basis. Solid lines are the theoretical trajectories and dashed lines are the approximation by the Koopman operator.

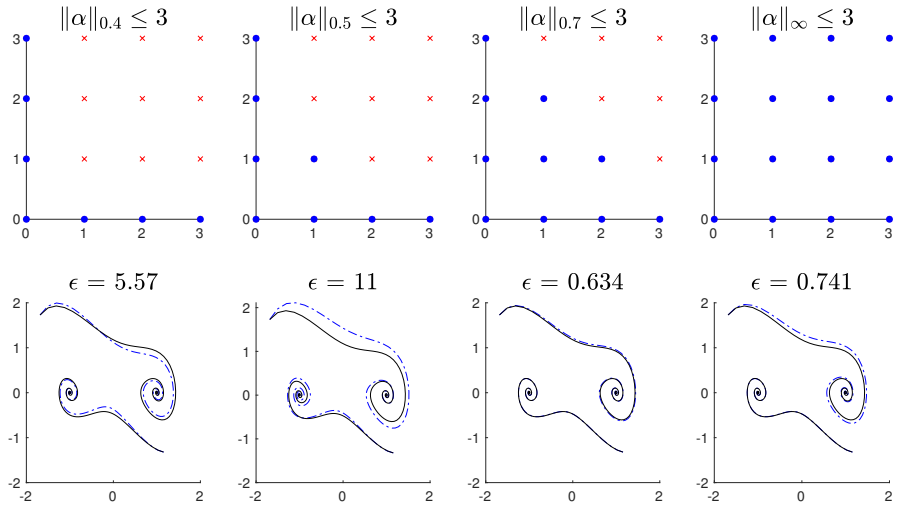

Figure 3.7: Test orbits from the EDMD algorithm with different p-q truncation schemes for a Laguerre Polynomial basis. Solid lines are the theoretical trajectories and dashed lines are the approximation by the Koopman operator

observables from (3.65). As the last three elements in the error vector are larger than the fifth, they must be discarded from the basis where the reduced polynomial basis has indices

$$\alpha = \begin{Bmatrix} 0 & 1 & 2 & 3 & 0 \\ 0 & 0 & 0 & 0 & 1 \end{Bmatrix}, \tag{3.79}$$

as a consequence, this polynomial basis is of reduced dimension with an error less than the previous approximation that only had a p-q-quasi norm reduction.

$$\Psi(x) = \begin{bmatrix} J(0_1)J(0_2) \\ J(1_1)J(0_2) \\ J(2_1)J(0_2) \\ J(3_1)J(0_2) \\ J(0_1)J(1_2) \end{bmatrix} = \begin{bmatrix} 1 \\ -x_1 + 1 \\ \frac{1}{2}x_1^2 - 2x_1 + 1 \\ -\frac{1}{6}x_1^3 + \frac{3}{2}x_1^2 - 3x_1 + 1 \\ -x_2 + 1 \end{bmatrix} \tag{3.80}$$

Note that the polynomial reduction improves the error ϵ from 11 to 5.34, which is better but still not as good as the basis corresponding to $q = 0.7$ with $\epsilon = 0.634$. However, the second reduction does give an accurate approximation of five elements that can be enough for control purposes reducing the computational complexity of any synthesis algorithm that makes use of it. Along with this line of thought, and continuing with the example, the approximation of the dynamical system evolution, from (3.38) and (3.72) is,

$$\Psi(k+1) = \begin{bmatrix} 1.0000 & 0.0000 & -0.0000 & 0.0000 & 0.0000 \\ -0.0723 & 0.9171 & 0.0880 & -0.0294 & 0.0967 \\ -0.0448 & -0.2259 & 1.2794 & -0.1041 & 0.1129 \\ 0.0401 & -0.4680 & 0.6016 & 0.7709 & 0.1009 \\ 0.5446 & -1.6488 & 1.7501 & -0.5846 & 0.9407 \end{bmatrix} \Psi(k) \tag{3.81}$$

$$\hat{x} = \begin{bmatrix} -\psi_2 + 1 \\ -\psi_5 + 1 \end{bmatrix}, \tag{3.82}$$

giving a linear system of the observables Ψ and a nonlinear system according to the state x.

3.4.5 Approximating the Koopman Operator

Recall that from the solution of either (3.38) or (3.73) depending on the condition number of G, the spectral decomposition of eigenvalues M and the left eigenvectors $W^\star$ give the set of eigenfunctions of the discrete-time approximation of the Koopman operator according to (3.50). As the left eigenvectors come from the inverse of the right ones, this extra computational step hinders the accuracy of eigenfunctions for subsequent analysis. Therefore, in practice, the algorithm calculates the transpose of U_d as

$$U_d^\top = G \backslash A, \tag{3.83}$$

and proceeds to calculate the spectral decomposition $[W^\star, M] = \text{eig}(U_d^\top)$, where both functions are presented in the Matlab® notation that gives the best results. Applying this functions to the example of the Duffing equation gives a spectral decomposition,

$$M = \begin{bmatrix} 1.0 + 0.0i & 0.0000 + 0.0000i & 0.0000 + 0.0000i & 0.0000 + 0.0000i & 0.0000 + 0.0000i \\ 0.0 + 0.0i & 0.9565 + 0.1450i & 0.0000 + 0.0000i & 0.0000 + 0.0000i & 0.0000 + 0.0000i \\ 0.0 + 0.0i & 0.0000 + 0.0000i & 0.9565 - 0.1450i & 0.0000 + 0.0000i & 0.0000 + 0.0000i \\ 0.0 + 0.0i & 0.0000 + 0.0000i & 0.0000 + 0.0000i & 0.9976 + 0.0087i & 0.0000 + 0.0000i \\ 0.0 + 0.0i & 0.0000 + 0.0000i & 0.0000 + 0.0000i & 0.0000 + 0.0000i & 0.9976 - 0.0087i \end{bmatrix} \tag{3.84}$$

$$W^\star = \begin{bmatrix} -1.0 + 0.0i & 0.206 - 0.051i & 0.206 + 0.051i & -0.159 + 0.024i & -0.159 - 0.024i \\ 0.0 + 0.0i & -0.650 - 0.020i & -0.650 + 0.020i & 0.573 + 0.011i & 0.573 - 0.011i \\ -0.0 + 0.0i & 0.688 + 0.000i & 0.688 + 0.000i & -0.750 + 0.000i & -0.750 + 0.000i \\ -0.0 + 0.0i & -0.229 + 0.006i & -0.229 - 0.006i & 0.286 - 0.012i & 0.286 + 0.012i \\ -0.0 + 0.0i & -0.015 + 0.055i & -0.015 - 0.055i & -0.006 - 0.000i & -0.006 + 0.000i \end{bmatrix}. \tag{3.85}$$

The application of (3.50) gives a set of five eigenfunctions of the truncated approximation of the Koopman operator. Figure 3.8 shows the respective real and imaginary parts of the evaluation of the eigenfunction in the set from which the initial conditions come, i.e., $x_1, x_2 \in \begin{bmatrix} -2 & 2 \end{bmatrix}$. The surface colors show the different values of the evaluated function, where the yellow (lighter) regions are the bigger values and the blue (darker) regions the smaller. As previously stated, this representation is not suitable for analysis, only for control, because the eigenvalues of the eigenfunctions are near unitary and the surface should reflect an approximation to the two basins of the original system.

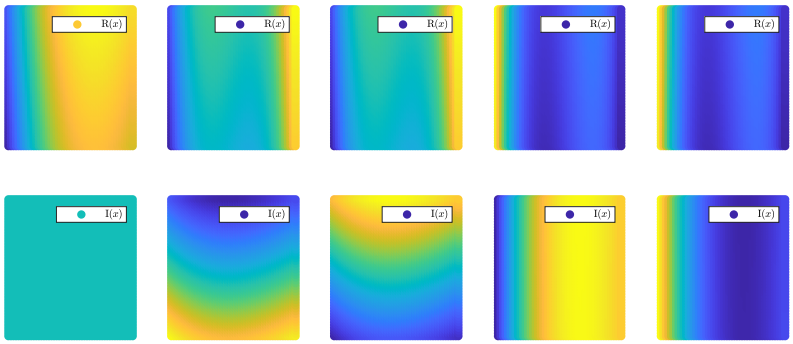

Figure 3.8: Eigenfunction of the discrete-time approximation of the Koopman operator for the Duffing equation with a reduced Laguerre polynomial basis.

3.5 EDMD for Control

This section presents a description of the traditional algorithm for dealing with forced systems, along with its improvements via embedding trigonometric functions into the state of the system. These embeddings are an a priori expansion before the application of the EDMD. It also shows via simulations and real experiments, the advantages of modeling a pendulum on a cart over the current alternative methods. So far the EDMD algorithm deals with unforced or autonomous systems, and given that for synthesizing controllers there is a manipulation of the different forces that inject energy into the system, the EDMD algorithm needs to be modified such that it can capture the dynamics according to the inputs. The relation of the inputs and the algorithm is established by Korda and Mezić [2018b], where they conclude for the synthesis of controllers, especially in the model predictive control framework, the driven inputs of the system must be affine. Although these approximations for control come from modifying the EDMD algorithm, the relation that they have with the Koopman operator has not been established yet. Therefore, the remaining of this sections will refer to these as linear predictors, and not the approximation of the Koopman operator.

Consider the non-autonomous nonlinear system $(\mathcal{M}, \mathcal{U}, T(x,u), k)$ in discrete time, with state variables $x \in \mathcal{M}$ where $\mathcal{M} \subseteq \mathbb{R}^n$ is the nonempty compact state space, forcing signals $u \in \mathcal{U}$ where $\mathcal{U} \subseteq \mathbb{R}^r$ is the nonempty

compact input space, $k \in \mathbb{Z}_0^+$ is the discrete time, and $T\colon \mathcal{M} \times \mathcal{U} \to \mathcal{M}$ is the differentiable vector-valued evolution map, i.e.,

$$x(k+1) = T(x(k), u(k)), \tag{3.86}$$

where a trajectory, or an orbit of the system is the sequence of states $(x_i)_{i=0}^{k}$ that come from the solution of (3.86), which is the successive application of the non-linear mapping T from an initial condition $x_0 \in \mathcal{M}$ at $k = 0$ and a specific sequence of forcing signals $u \triangleq (u_i)_{i=0}^{k-1}$.

For example, consider a pendulum and a moving cart attached by a swivel that allows the pendulum to rotate freely. The cart wheels rotate on a rail and a DC motor drives the whole system. The available information from two encoders are the displacement of the cart and the angular rotation of the pendulum. Figure 3.9 depicts the experimental set-up where x is the horizontal displacement of the cart and θ is the angle of the pendulum with respect to the vertical axis. Mass and energy balances give a set of ordinary differential equations that describe the dynamics of the system.

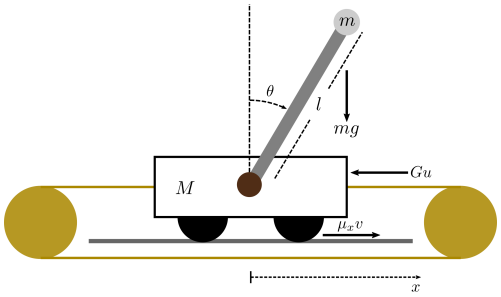

Figure 3.9: Pendulum on a cart

The system equations, which depend on the masses of the cart (M) and pendulum (m), the length of the pendulum rod (l), the linear damping (μ_x) of the cart wheels with the rails and the gravitational constant (g), are given by

$$
\begin{aligned}
\dot{x} &= v \\
\dot{v} &= \frac{Gu - \mu_x v - ml\theta_v^2 \sin(\theta)}{M + m\sin^2(\theta)} \\
\dot{\theta} &= \theta_v \\
\dot{\theta}_v &= \frac{Gu - \mu_x v - ml\theta_v^2 \sin(\theta))\cos(\theta) + (M+m)g\sin(\theta)}{l - ml\cos^2(\theta)},
\end{aligned} \tag{3.87}
$$

where the states are the cart displacement x, the cart velocity v, the rod angle θ and the angular velocity θ_v. The model also considers a gain G between the voltage of the motor u and the resulting force on the cart. The parameter values come either from the available data of the manufacturer (Feedback Instruments Ltd) or from an identification of the parameters from a set of data collected in preliminary experiments with the system. Table 3.3 lists the value of these parameters.

Table 3.3: Parameters of the inverted pendulum on a cart.

	Description	Value	Units
M	Cart Mass	1.12	[kg]
m	Pendulum Mass	0.0905	[kg]
g	Gravity	9.81	$[\mathrm{m} \cdot \mathrm{s}^{-2}]$
l	Pendulum length	0.365	[m]
μ_x	Cart Friction	6.65	$[\cdot]$
G	Tension-Force Gain	7.5	$[\cdot]$

Let us now consider a set of seven orbits or trajectories obtained by numerical integration of (3.87) with the assumption that all the state variables of the system are available. For the accuracy of the algorithm, it is necessary that the trajectory samples are collected at a constant rate, which is chosen equal to 0.01 seconds, both in the numerical simulation and the experimental study. This set of orbits sampled at a constant Δt corresponds to the solution of the non-linear discrete-time mapping (3.86).

Figure 3.10 depicts the discrete-time evolution of some of these trajectories with their respective forcing signals. These trajectories serve

as the available data to approximate the non-linear dynamics via the EDMD algorithm.

As EDMD is a data-driven approach, the set of trajectories is divided into training and testing sets for the approximation and validation of the algorithm. In our case study, the selection is five orbits for training the linear predictor, and two for testing (Figure 3.10). Finally, the snapshot data is defined as a set of tuples $\{(x_i, y_i, u_i)\}$, where $y_i = T(x_i, u_i)$. From these tuples, the snapshot matrices are given by:

$$X = \begin{bmatrix} x_1 & \dots & x_N \end{bmatrix}, \; Y = \begin{bmatrix} y_1 & \dots & y_N \end{bmatrix}, \; U = \begin{bmatrix} u_1 & \dots & u_N \end{bmatrix}, \quad (3.88)$$

according to the traditional EDMD algorithm [Williams et al., 2015] and the extension for including the inputs of the system [Korda and Mezić, 2018b]. The rationale behind the approach is to get linear predictors of the state evaluated on a vector-valued function of observables $\Psi(x) = [\psi_1(x), \cdots, \psi_d]^\top : \mathcal{M} \to \mathbb{C}^{d \times 1}$ where d is the dimension of the set of observables that must satisfy the condition

$$\Psi(y) = U_{d,x}\Psi(x) + U_{d,u}u + r(x, u) \quad (3.89)$$

$r(x, u) \in \mathcal{F}$ is the residual term that has to be minimized in order to find matrices $U_{d,x}$ and $U_{d,u}$. This leads to the least squares problem

$$\|r(x, u)\|^2 = \frac{1}{N}\sum_{i=1}^{N} \frac{1}{2} \left\| \Psi(y_i) - U_{d,x}\Psi(x_i) - U_{d,u}u \right\|_2^2, \quad (3.90)$$

which as a closed-form solution

$$\begin{bmatrix} U_{d,x} & U_{d,u} \end{bmatrix} = \Psi(Y) \begin{bmatrix} \Psi(X) \\ U \end{bmatrix} \left(\begin{bmatrix} \Psi(X) \\ U \end{bmatrix} \begin{bmatrix} \Psi(X) \\ U \end{bmatrix}^\top \right)^{-1}. \quad (3.91)$$

As the purpose of these predictors is the synthesis of controllers, it is necessary to recover the state from the observable functions. Thus, an additional least squares problem for the best projection matrix of x onto the span of Ψ has to be solved. The projection must satisfy the condition

$$\bar{x} = U_{d,c}\Psi(x) + r_c(x), \quad (3.92)$$

where $r_c(x)$ is the residual term to be minimized to find $U_{d,c}$, that admits a pseudo-inverse based least squares solution

$$U_{d,c} = X\Psi(X)^{+}. \tag{3.93}$$

Instead of solving (3.93) to recover the state, a common practice is to include the state in the set of observables, so that matrix $U_{d,c} = [I_n,\ 0_{n\times(d-n)}]$ after reordering the observables such that the state vector form the first n elements.

The EDMD formulation (3.91) and (3.93) can be used with a basis of Jacobi type monomials for the approximation of the pendulum dynamics (3.87), i.e., a sequence of orthogonal polynomials $\{\pi_\alpha(x)\}_{\alpha=0}^{p}$ where $\pi_\alpha(x)$ is a univariate polynomial (i.e., a polynomial in only one of the state variables x_i, $i = 1, ..., n$) of degree $\alpha \in \mathbb{N}_+$ up to order p according to Equation (3.58).

For the approximation of the pendulum dynamics, the order $p = 1$ can be chosen, giving a set of observables of dimension $d = 17$ with maximum order 4, i.e., the product of all the univariate monomials, e.g., $\psi_{17} = \prod_{i=1}^{4} 5x_i + 1$ for parameters $a = 5$ and $b = 3$ of a Jacobi type monomial $J(1, a, b, x) = a/2-b/2+x(a/2+b/2+1)$. The five trajectories of the training set sum 1110 data points, and the two trajectories of the testing set sum 490 data points. Figure 3.11 shows the trajectories produced by the EDMD, where the empirical error $\epsilon = 1/N \sum_i^N |x_i - \bar{x}_i|$ is 1.31. While it is possible to perform the approximation with higher p values, the results do not necessarily improve. For $p = 2$ as the maximum order of the univariate polynomials, the basis has dimension $d = 81$ with a maximum order of eight, which shows that these two numbers grow exponentially with the maximum univariate order p. Moreover, the empirical error increases to 1.77 in this particular case, which is also the sign of numerical issues.

There are some inherent numerical instabilities with the method. First, the EDMD algorithm is a linear map on the function space that the set of observables span, and the accuracy of the solution depends on the characteristics of this set. Choosing an orthogonal basis with an observable that corresponds to a constant generally improves the performance of the approximation. In contrast, adding the state to the set of observables is prone to break the orthogonality of the observables,

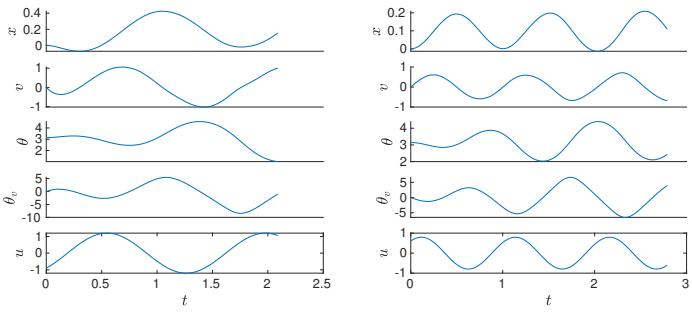

Figure 3.10: Pendulum trajectories with sinusoidal input.

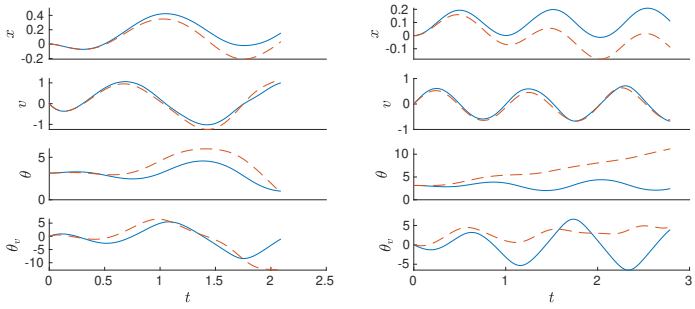

Figure 3.11: Testing trajectories of the traditional computation of the EDMD algorithm with a Jacobi orthogonal polynomial basis up to order four. Solid lines are the orbits from the numerical integration of the ODE and dashed lines the approximation by the EDMD algorithm.

depending on their actual choice. As a consequence, the square matrix $[\Psi(X),\ U]^\top[\Psi(X),\ U]$ in (3.91) becomes singular or close to singular, and while replacing the inverse by a Moore-Penrose pseudo inverse can partly alleviate this issue, the result can still be inaccurate. Second, preserving an orthogonal basis, without explicitly including the states as observables poses a similar matrix inversion problem, when there is no solution to the projection of the state space onto the set of observables.

The way out of this dilemma is the selection of order-one, univariate, injective, polynomial elements for the recovery of the state, which implies that there is no need of breaking the orthogonality of the set while still being able to recover the state as a linear function of the observables,

completely avoiding the burden of a matrix inversion as described in Section 3.4.1. Besides, the exponential growth of the maximum order and dimension of the set of observables based on orthogonal polynomial has a solution via p-q-quasi norms and polynomial accuracy methods as described in Section 3.4.3.

In our case study of the inverted pendulum, we can consider the same orthogonal basis of Jacobi polynomials with a sweep of p-q parameters corresponding to: $p = [2,\ 3,\ 5,]$ and $q = [0.3,\ 0.5,\ 0.7,\ 0.9,\ 1.1,\ 1.3]$. Although there are 18 possible combinations, some p-q parametrizations produce equal basis. There are only 12 distinct sets of observables, ranging from 6 elements of maximum order 2 to 173 elements of maximum order 5. The result of the reduction gives a sub-optimal basis of 33 elements of maximum order 3 that achieves an empirical error of 0.62, as compared to 1.31 for the traditional EDMD. Note that the reduction provides the possibility to test higher-order polynomial basis than in the traditional form, where a basis of maximum order 5 would count 625 elements. Figure 3.12 shows the performance of the sub-optimal basis of the p-q-EDMD in comparison to the traditional EDMD.

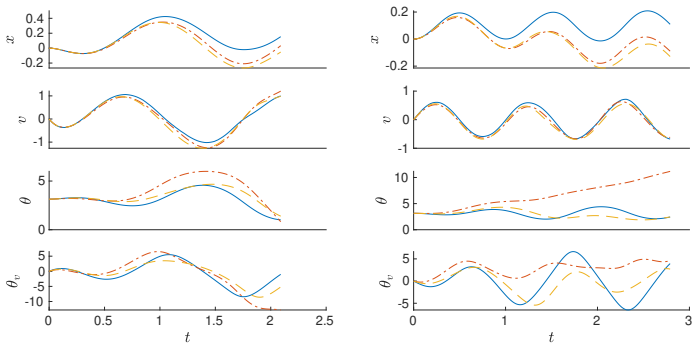

Figure 3.12: Testing trajectories of the traditional EDMD computation against the p-q-EDMD of polynomial elements up to order two. Solid lines are the orbits from the numerical integration of the ODE, dash-dotted lines are the approximation of the EDMD algorithm, and dashes lines are the approximation by the p-q-EDMD algorithm.

Although the use of reduced orthogonal polynomials for the p-q-EDMD provides a method to improve the accuracy of the algorithm

while avoiding computationally heavy high-order and dimensional solutions, the accuracy of the algorithm for systems that have trigonometric components or an arbitrary behavior like exponentials or logarithms is not enough. Therefore, the next section introduces the concept of trigonometric embeddings.

3.5.1 Trigonometric Embeddings

In this section, we consider the problem of representing dynamic systems with oscillatory behavior by polynomial expansions and the possibility to increase the parsimony of the approximation by the inclusion of trigonometric functions as elementary units of the polynomial expansion. Similar embeddings could be used for any particular behavior, using associated functions. Similar to the idea that took the dynamic mode decomposition algorithm to the extended version, where instead of performing a regression on the states, the extended method considers a set of functions of the state (the so-called observables), the trigonometric embeddings, or more generally function embeddings, provide specific functions of the state conveying particular information.

Consider the discrete-time dynamical system (3.86) and assume that a subset of the state $x^{tg} \subseteq x$ has trigonometric components in the difference equation $T(x, u)$. For each of these state variables an extension of the state space is defined including a pair of sine and cosine:

$$x_e = \begin{bmatrix} x_{e_1} \\ \vdots \\ x_{e_{2m+1}} \end{bmatrix} = \begin{bmatrix} x_1 \\ \vdots \\ x_n \\ \sin x_1^{tg} \\ \cos x_1^{tg} \\ \vdots \\ \sin x_m^{tg} \\ \cos x_m^{tg} \end{bmatrix}, \tag{3.94}$$

where $m \leq n$. Using this extended set of variables, the approximation of the dynamics can be achieved via the p-q-EDMD.

Consider for example an arbitrary discrete-time dynamical system

$(\mathcal{M},\mathcal{U},T(x,u),k)$, where $n = 2$, $r = 2$ and $x^{tg} = x_2$, i.e., the system has two state variables where the second one has a trigonometric component and two inputs within the non-linear mapping $T(x,u)$. Moreover a Hermite basis of orthogonal polynomials of univariate elements up to order 2, i.e., $\pi_{\alpha=[0,\,1,\,2]}(x) = [1,\ 2x,\ 4x^2-2]$, is used. For illustration purposes, assume an arbitrary p-q parametrization $p = 3$ and $q = 0.7$. The resulting basis of polynomials for the approximation of the dynamics is

$$\Psi(x) = \begin{bmatrix} 1 \\ 2x_1 \\ 4x_1^2 - 2 \\ 2x_2 \\ 4x_1x_2 \\ 4x_2^2 - 2 \\ 2\cos(x_2) \\ 4x_1\cos(x_2) \\ 4x_2\cos(x_2) \\ 4\cos^2(x2) - 2 \\ 2\sin(x_2) \\ 4x_1\sin(x_2) \\ 4x_2\sin(x_2) \\ 4\cos(x_2)\sin(x_2) \\ 4\sin^2(x_2) - 2 \end{bmatrix}. \tag{3.95}$$

Note that the embeddings are not restricted to trigonometric functions, but could for instance include logarithmic, exponential or hyperbolic functions, if the non-linear mapping $T(x,u)$ has state variables with such a behavior. However, the functional embeddings and particularly the trigonometric embeddings, that add two more variables for each trigonometric state, increases exponentially the dimension of the set of observables and it is necessary to resort to the previous p-q-quasi norm reduction.

The application of trigonometric embeddings to the orbits of the pendulum problem, considering that only the angle θ has trigonometric components, reduces the empirical error of the approximation, from the aforementioned value of 0.62 (provided by p-q-EDMD) to 0.17. To achieve these results, we consider a p-q sweep where $p = [2,\ 3,\ 4,\ 5]$, $q = [0.3,\ 0.5,\ 0.7,\ 0.9,\ 1.1,\ 1.3]$ and the available orthogonal polynomi-

als in Matlab. The sub-optimal solution is a Laguerre polynomial basis with parameters $p = 4$ and $q = 0.7$. Although the approximation error in the test set is reduced, the inclusion of the two extra trigonometric variables, and the increased p value produces a basis of 65 elements. Figure 3.13 depicts the result of the algorithm in comparison with the benchmark EDMD.

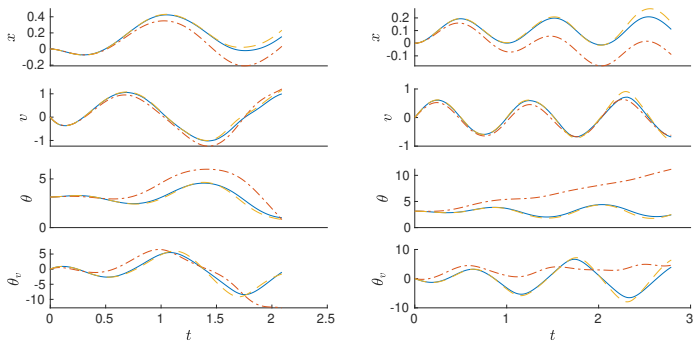

Figure 3.13: Testing Trajectories of the traditional EDMD against the p-q-EDMD with trigonometric embeddings. Solid lines are the orbits from the numerical integration of the ODE, dash-dotted lines are the approximation of the EDMD algorithm, and dashes lines are the approximation by the p-q-Trigonometric EDMD algorithm.

3.5.2 Inverted Pendulum: Experimental Results

For illustration purposes, and to compare numerically various expansions, we consider the real-life application provided by a Feedback Digital Pendulum 33-005-PCI (Figure 3.14).

Figure 3.14: Feedback Digital Pendulum 33-005-PCI

This pendulum is the same as described in the beginning of this Section. A DC motor drives the cart along the rail to which a pendulum is attached. The available experimental set-up provides, through two encoders, the noisy measurements of the cart position and the pendulum angle every 0.01 [s]. Therefore, the output equation is given by:

$$y = \begin{bmatrix} 1 & 0 & 0 & 0 \\ 0 & 0 & 1 & 0 \end{bmatrix} \begin{bmatrix} x \\ v \\ \theta \\ \theta_v \end{bmatrix} + w_n, \tag{3.96}$$

where $w_n \sim \mathcal{N}(0,\, \sigma^2)$.

However, the knowledge of the cart velocity and the angular velocity are necessary to compute an approximation through the EDMD algorithm. A simple differentiation of the displacements gives an amplification of the noise, impeding the possibility of getting accurate approximations of the dynamics. This can be alleviated by the design of two Kalman filters based on simple kinematic expressions. The Kalman filter [Paul Zarchan, 2009] is a model-based technique which allows recovering on-line estimations by blending the prediction of a mathematical model with the available on-line measurements. Here, the idea is to avoid using a full differential equation model such as (3.87), as this would be contradictory with the objective of developing a data-driven EDMD model. Hence, the method relies on basic kinematic relations

$$\begin{aligned} x_{k+1} &= x_k + v_k \cdot \Delta t + a_k \cdot 0.5 \cdot \Delta t^2 \\ v_{k+1} &= v_k + a_k * \Delta t \\ a_{k+1} &= a_k, \end{aligned} \tag{3.97}$$

where the acceleration is assumed constant. These expressions are used as predictor while the state update equation of the Kalman filter is

$$\begin{bmatrix} \hat{x}_k \\ \hat{v}_k \\ \hat{a}_k \end{bmatrix} = \begin{bmatrix} \hat{x}_{k-1} \\ \hat{v}_{k-1} \\ \hat{a}_{k-1} \end{bmatrix} + K_k \begin{bmatrix} x_k - \hat{x}_{k-1} \\ \frac{x_k - \hat{x}_{k-1}}{\Delta t} \\ \frac{x_k - \hat{x}_{k-1}}{0.5\Delta t^2} \end{bmatrix}, \tag{3.98}$$

where $\hat{\cdot}$ is the estimate of the corresponding variable, x_k is the measurement of the cart position or pendulum angle and K_k is the Kalman

gain that gets updated in every time-step of the algorithm according to the estimation covariance matrix (solution to a Ricatti equation), and the measurement uncertainty. Furthermore, each of the position-velocity pairs has an independent filter with their corresponding parametrization.

For generating the experimental data, the pendulum starts at the stable point $\theta(0) = \pi$ and is exited with a sinusoidal signal at various frequencies and amplitudes, i.e.,

$$\begin{bmatrix} x_0 \\ v_0 \\ \theta_0 \\ \theta_{v0} \end{bmatrix} = \begin{bmatrix} 0 \\ 0 \\ \pi \\ 0 \end{bmatrix}, \; u = A \cdot \sin(\omega t + \phi), \tag{3.99}$$

where the ranges of the different parameters of the forcing signal are: $A \in (0.1,\ 1)$, $\omega \in (\pi,\ 3\pi)$, $\phi \in (0,\ 2\pi)$. The selection of these parameters ensures that the cart movement does not exceed the track limits. Figure 3.15 depicts the result of gathering and filtering the experimental data.

The application of the p-q trigonometric EDMD on the experimental data is a linear predictor suitable for controller synthesis. To this end, we consider a $p - q$ sweep where $p = [2,\ 3,\ 4]$,

$$q = [0.1,\ 0.3,\ 0.5,\ 0.7,\ 0.9,\ 1.1,\ 1.3],$$

a trigonometric embedding over the third state θ and an evaluation of all the available orthogonal polynomials in Matlab. Additionally, and for the consistency of the results, the training and testing sets correspond with the ones used in the simulation results. Table 3.4 shows empirical errors of the best sub-optimal solution for each polynomial basis.

The sub-optimal solution is a Chebyshev polynomial of the first type with parameters $p = 4$, $q = 0.9$ and 85 observables that gives an empirical error of 0.57. Figure 3.16 shows the results of the approximation in the test set.

This section deals with extensions and improvements to the EDMD algorithm for special cases where there is an a priori knowledge of the behavior of a subset of state variables in terms of elemental function, such as trigonometric or logarithmic functions, among others. This expansion

Polynomial basis	Empirical error
Hermite	0.8237
Legendre	0.8249
Laguerre	0.8816
ChebyshevT	0.5731
ChebyshevU	0.8245
Gegenbauer	0.8254
Jacobi	0.8231

Table 3.4: Empirical error for each polynomial basis used in the p-q Trigonometric EDMD.

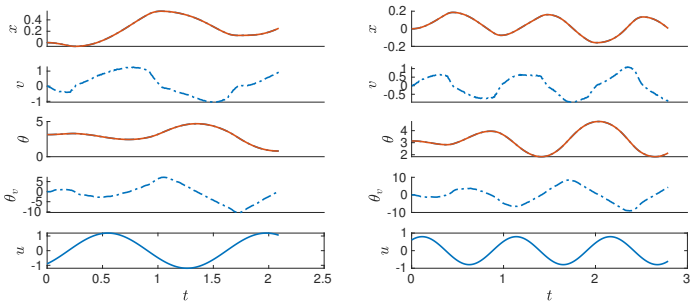

Figure 3.15: Data filtering of the test set for the p-q-Trigonometric EDMD. Solid lines are the orbits from the experimental set-up and dashed lines are the orbits from the Kalman filter.

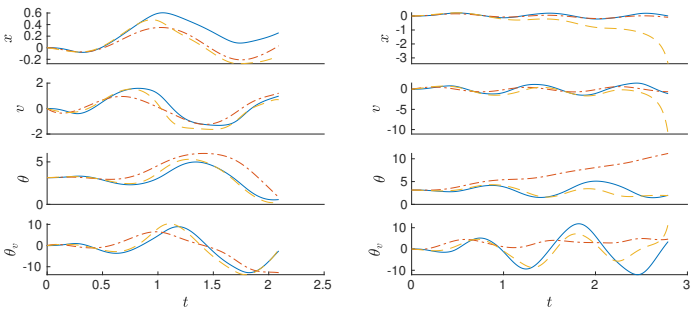

Figure 3.16: Testing trajectories with the p-q-Trigonometric EDMD. Solid lines are the orbits from the filtered experimental set-up, dash-dotted lines are the approximation of the EDMD algorithm, and dashes are the p-q-Trigonometric EDMD approximation.

of the state, coupled with the use of p-q-quasi norms, gives an algorithmic advantage for the approximation of the dynamics of non-linear systems in a data-driven way. Although this approach improves the accuracy of the approximation, the expansion of the state has the risk of increasing the dimension of the set of observables necessary to perform the approximation. As a consequence, the algorithm can fall into the course of the dimensionality problem making solutions computationally unfeasible.

These embeddings represent an additional step for the formulation of observables that better suit a particular system, depending on the ability to select proper embeddings for the state variables. Consequently, they represent a contribution to the open problem of the proper selection of observables for the EDMD algorithm.

On the subject matter of observable selection, there is still the open question of the method to incorporate the knowledge of available models, in a similar fashion as traditional modeling and identification techniques. A combination of the two paradigms, the black box and solely data-driven methods, such as the EDMD, and the traditional identification techniques, has the potential of reducing the necessary set of observables further while also improving the accuracy even further.

3.6 Interconnected Dynamical Systems

An interconnected dynamical system is a collection of dynamical systems, and an interconnection topology that describes the energetic exchange between them, i.e., which output of system A injects energy into which input of system B.

Consider a system $\Sigma = \left(\{\Sigma_i\}_{i=1}^{N}, G_{i,j}\right)$ given as a collection of dynamical systems

$$\Sigma_i : \begin{cases} \dot{x}_i = f_i(x_i) + u_i + G_{i,j} \\ y_i = h_i(x_i) \end{cases}, \tag{3.100}$$

where $x_i \in \mathbb{R}^{n_i}$ $(i = 1, \ldots, M)$ is the state of the i^{th} subsystem, M is the number of subsystems, $u_i \in \mathbb{R}^{r_i}$ is the input of the i^{th} subsystem,

and $y_i \in \mathbb{R}^{m_i}$ is the output of the i^{th} subsystem. The input u_i can be divided into external inputs u_i, and internal inputs $G_{i,j}$, that come from the neighboring subsystems of the network.

Figure 3.17 depicts this situation, where the first subsystem in the network provides energy to its neighbors and vice-versa. This interaction potentially changes the location and stability of the first subsystem fixed points.

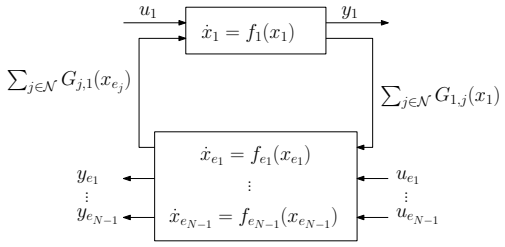

Figure 3.17: Subsystem feedback interconnection with the network.

From a controller synthesis perspective, where the external inputs must drive the system to a desired state, the controller must account for the effect of the interconnection input. Figure 3.18 shows the topology of the controller assuming that it has information of the interconnection states.

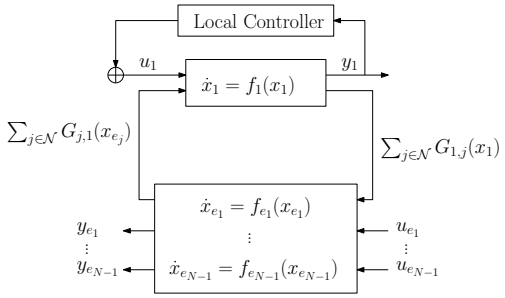

Figure 3.18: Subsystem local controller with measurement of the interconnection state.

The objective is to generate linear predictors that accurately describe the local dynamics of a system without having the complete information of the driving force given by the neighboring systems. Next section in-

troduces the concept of linear predictors with a combination of affine, and non-affine input signals.

3.6.1 A Case Study: Two Duffing Oscillators

For illustration purposes, consider an interconnection of two Duffing oscillators where the parameters yield a dynamic behavior with two basins of attraction (see Figure 3.19). The differential equations that describe this system are

$$\begin{aligned}
\dot{x}_{1,1} &= x_{1,2} \\
\dot{x}_{1,2} &= 0.5x_{1,2} + x_{1,1} - x_{1,1}^3 + 2.2x_{2,1} + u_1 \\
\dot{x}_{2,1} &= x_{2,2} \\
\dot{x}_{2,2} &= 0.5x_{2,2} + x_{2,1} - x_{2,1}^3 + 2.2x_{1,2} + u_2,
\end{aligned} \tag{3.101}$$

where the first state variable of each system drives the second one of its counterpart, e.g., $G_{i,j} = 2.2x_{i,j}$. Figure 3.19 shows the behavior of the two systems where the inputs are randomly selected step signals over $u_1, u_2 \in [-2\ 2]$. The numerical integration with a time step $\Delta t = 0.05$, and six randomly selected initial conditions $x_{i,j}(0) \in [-2\ 2]$, gives a set of orbits that can be exploited as dataset for the EDMD algorithm. The training set consists of four trajectories, while two are kept for testing. All the trajectories are of different lengths because the accuracy of the algorithm decreases with the presence of redundant data at the asymptotically stable points, and the integration is stopped upon convergence. As a consequence, the sample size for the approximation of the linear predictors is 3.324 where 2.150 are available for training and 1.174 for testing.

Recall that it is necessary to have an input-affine EDMD approximation to apply a model predictive control algorithm. Although this is the case for the input space, it is not necessary to have that restriction for the interconnection inputs. Therefore, the suitable approximation for the synthesis algorithms is hybrid. In order to get such a behavior, first consider an approximation where none of the input are affine and the state of the system is expanded to include the inputs similarly to the approach by Korda [Korda and Mezić, 2018b].

3.6.2 Development of the EDMD Algorithm

Consider first a non-affine approximation where the set of state variables is expanded to include the inputs as states, as proposed in [Korda and Mezić, 2018b]. This means that the inputs are state variables of the system with zero dynamics, i.e., $u(k+1) - u(k) = 0$.

With the trajectories of the training and testing sets and the previous rationale for handling the inputs of the system, define the sets of snapshots as

$$XU = \begin{bmatrix} x_1 & x_2 & \cdots & x_N \\ x_{\Sigma,1} & x_{\Sigma,2} & \cdots & x_{\Sigma,N} \\ u_1 & u_2 & \cdots & u_N \end{bmatrix} \quad YU_+ = \begin{bmatrix} y_1 & y_2 & \cdots & y_N \\ y_{\Sigma,1} & y_{\Sigma,2} & \cdots & y_{\Sigma,N} \\ u_{1+} & u_{2+} & \cdots & u_{N+} \end{bmatrix} \tag{3.102}$$

where the $+$ subscript denotes the time shift of the input by one Δt and x_Σ are the interconnection input variables. Generally, this shifted value of the input is not available for the last time instance in the orbits, however, given that numerical integration stops at convergence, the last sample of the simulation is usually not a complete Δt after the penultimate, and keeping this value decreases the accuracy of the algorithm. Additionally, note that this representation includes any number of inputs as state variables, and in turn, it is not limited to single-input systems.

The lifting process consists in evaluating the new state vector with a vector valued function of observables $\Psi = [\psi_1 \cdots \psi_d]^T : \mathcal{M} \times \mathcal{U} \to \mathbb{C}^{1\times d}$, i.e.,

$$\Psi(x,u) = \begin{bmatrix} \Psi_x(x) \\ \Psi_{xu}(x,u) \\ \Psi_u(u) \end{bmatrix} = \begin{bmatrix} \psi_1(x) \\ \vdots \\ \psi_{dx}(x) \\ \psi_{dx+1}(x,u) \\ \vdots \\ \psi_{dxu}(x,u) \\ \psi_{dxu+1}(u) \\ \vdots \\ \psi_{du}(u) \end{bmatrix}. \tag{3.103}$$

For the selection of these functions, we will continue with orthogonal polynomials that have the advantage of improving the accuracy of the approximation. Additionally, benefiting from the aforementioned reduction methods for the dimension and maximum order of the basis achieve an accurate approximation while avoiding computationally expensive basis [Garcia-Tenorio et al., 2020].

The conditions that these observables must satisfy to get the non-affine predictor is

$$\Psi_x(y, u_+) = U_d \Psi(x, u) + r(x, u), \tag{3.104}$$

where $r(x, u) \in \mathcal{F}$ is the residual term to minimize in order to find the regression or linear predictor matrix U_d. Considering that the best approximation minimizes the residual term, the following objective function

$$\|r(x, u)\|^2 = \frac{1}{N} \sum_{i=1}^{N} \frac{1}{2} \left\| \Psi(y_i, u_{i+}) - U_d \Psi(x_i, u_i) \right\|_2^2, \tag{3.105}$$

gives an accurate approximation of U_d, through the ordinary least-squares solution [Williams et al., 2015], that has a closed analytical form given by

$$G = \Psi(XU)\Psi(XU)^\top \qquad A = \Psi(YU^+)\Psi(XU)^\top, \tag{3.106}$$

$$U_d^\top = G \backslash A. \tag{3.107}$$

Even though this approximation is suitable for recovering the spectrum, the evolution of the input space is not important for controller synthesis algorithms. Recall from (3.103) that there is a division of the polynomial basis in subsets that depend on just the state, the input or both. Assume that the dimension of these subsets is: $\dim \Psi_x(x) \in \mathbb{N}^{dx}$, $\dim \Psi_{x,u} \in \mathbb{N}^{dxu}$ and $\dim \Psi_u \in \mathbb{N}^{du}$. To get a linear predictor matrix L from the sets of snapshots, define a A_L matrix as

$$A_L = \Psi_x(Y)\Psi(XU)^\top, \tag{3.108}$$

i.e., from the original definition of matrix A (3.106) slice out the last $dxu + du$ rows from matrix A to get this new matrix A_L.

$$
\begin{aligned}
A &= \begin{bmatrix} A_L \\ \star \end{bmatrix} \\
&= \begin{bmatrix} \Psi_x(Y) \\ \cancel{\Psi_{xu}(YU^+)} \\ \cancel{\Psi_u(U^+)} \end{bmatrix} \begin{bmatrix} \Psi_x(X)^\top & \Psi_{xu}(XU)^\top & \Psi_u(U) \end{bmatrix} \\
&= \begin{bmatrix} \Psi_x(Y)\Psi_x(X)^\top & \Psi_x(Y)\Psi_{xu}(XU)^\top & \Psi_x(Y)\Psi_u(U) \\ \cancel{\Psi_{xu}(YU^+)\Psi_x(X)^\top} & \cancel{\Psi_{xu}(YU^+)\Psi_{xu}(XU)^\top} & \cancel{\Psi_{xu}(YU^+)\Psi_u(U)} \\ \cancel{\Psi_u(U^+)\Psi_x(X)^\top} & \cancel{\Psi_u(U^+)\Psi_{xu}(XU)^\top} & \cancel{\Psi_u(U^+)\Psi_u(U)} \end{bmatrix}.
\end{aligned}
$$

Then, the linear predictor that describes the evolution of state observables is

$$L = A_L G^{-1}, \tag{3.109}$$

or from the original definition of the EDMD matrix for the non-affine forced approximator (3.107), this linear predictor matrix comes from slicing the last $dxu + du$ rows of U_d. Furthermore, slicing the columns of the linear predictor matrix into the matrix bocks that weight each of the observables sets gives the evolution of state observables as

$$\Psi(y) = L_x \Psi_x(x) + L_{xu} \Psi_{xu}(x, u) + L_u \Psi_u(u), \tag{3.110}$$

where $L_x = L(1 : dx)$, $L_{x,u} = L(dx + 1 : dx + dxu)$ and $L_u = L(dx + dxu + 1 : \text{end})$. The order-one observables that capture each of the state variables. Accordingly, the approximation of the state evolution map $T^k(x, u) = x_k$ for a known sequence of inputs and from the initial condition x_0 in terms of the state observables is

$$\hat{x}(k + 1) = \Psi_B^{-1}(B^\top \Psi_x(y(k))). \tag{3.111}$$

Consider Jacobi orthogonal polynomials and a p-q parameter sweep where $p = [3\ 4\ 5]$ and $q = [0.4\ 0.5\ 0.6]$. The result of the non-affine algorithm on each of the subsystems with their corresponding training and testing sets is depicted in Figure 3.20, and the summary of the results is in Table 3.5.

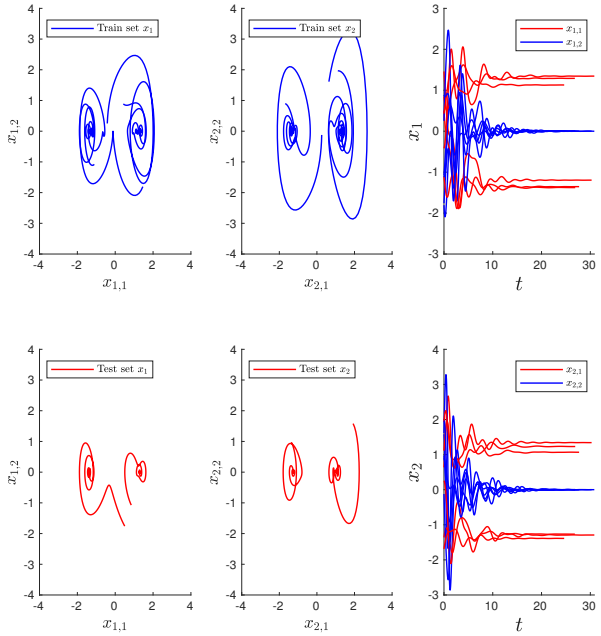

Figure 3.19: Two interconnected Duffing oscillators: 4 trajectories constitute the training set and 2 trajectories are kept for testing purposes.

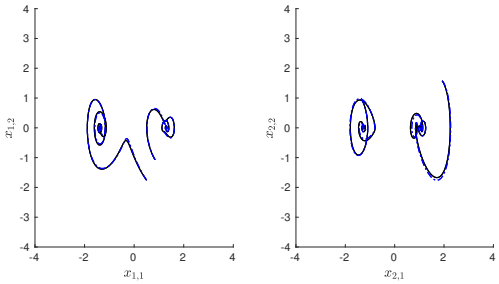

Figure 3.20: Test orbits from the non-affine forced EDMD algorithm. Solid lines are the theoretical trajectories and dashed lines are the approximation by the algorithm

Table 3.5: p, q, dimension, and empirical error for the non-affine approximation of the interconnected duffing equation.

	p	q	dim	ϵ
System 1	4	0.4	13	0.74
System 2	4	0.4	13	0.65

Even though this representation is not suitable for control, it illustrates the advantages of the choice of orthogonal polynomials with p-q-quasi norm reduction. The linear predictors are able to approximate the dynamics of two systems, each with two state variables with the least amount of data, and a substantial reduction in the amount of polynomial elements. Additionally, this approximation is suitable for analysis based on the spectral decomposition of the Koopman operator as shown in Chapter 4. Likewise, the eigenfunctions of the Koopman operator should be useful to analyze forced systems, not only in terms of equilibrium points, their stability and regions of attraction, but also in terms of bifurcations and limit cycles. These extensions are still an open subject for research.

Consider next the restriction of the observables on the input space to be affine, i.e., the set of observables for this input signal is the constant function, i.e., $\Psi_u = u$, while the interconnection inputs remain state variables. This restriction modifies the set of observables that becomes,

$$\Psi(x, x_\Sigma, u) = \begin{bmatrix} \Psi_x(x) \\ \Psi_{xu}(x, x_\Sigma) \\ u \end{bmatrix} = \begin{bmatrix} \psi_1(x) \\ \vdots \\ \psi_{dx}(x) \\ \psi_{dx+1}(x, x_\Sigma) \\ \vdots \\ \psi_{dxu}(x, x_\Sigma) \\ u_1 \\ \vdots \\ u_d \end{bmatrix}. \tag{3.112}$$

The same polynomial basis and p-q parameter sweep is used as in the previous developments, and the result of the input-affine approximation

of each of the subsystems with their corresponding training and testing sets is depicted in Figure 3.21, and the summary of the results is in Table 3.6.

Table 3.6: p, q, dimension, and empirical error for the input-affine approximation of the interconnected duffing equation.

	p	q	dim	ϵ
System 1	4	0.5	10	1.14
System 2	4	0.5	10	1.73

Notice that the suboptimal q value for the input-affine approximation is larger than in the non-affine case, and, as a consequence, the dimension of the polynomial basis should be larger, which is not the case. Indeed, all the polynomials on the input space are eliminated leaving only the constant terms. As a consequence, the empirical error increases, but the approximation is suitable for controller synthesis, and depending on the case, the accuracy could be enough for control.

In addition, this approximation requires the value of the interconnection input, which is a drawback of the algorithm, which is not suitable for decentralized controllers where the available information is the local state. The solution to this issue goes along the line of the statistical, geometric and observability properties of the interconnection inputs.

For illustrative purpose, consider the input-affine approximation without the knowledge of the interconnection signal, i.e., this variable enters the linear predictor as another state variable of the system where the only information provided to the predictor is the initial condition. Figure 3.22 depicts how the linear predictors give an approximation of their own state, and the interconnection input. For this particular case, all the states, including the interconnection, converge to the vicinity of their corresponding asymptotically stable equilibrium point, and are accurate for the first time steps of the trajectory, meaning that an MPC controller synthesis with short control horizon should be suitable for driving the system.

Although this contribution is a step further into the possibility of controlling such systems, the algorithm still relies on the partial knowledge of the energy injected by neighboring subsystems. Consequently,

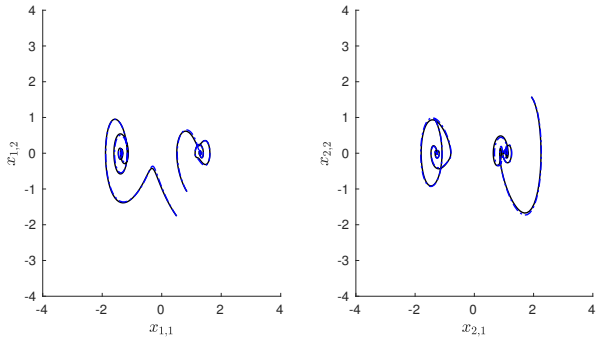

Figure 3.21: Test orbits from the input-affine forced EDMD algorithm. Solid lines are the theoretical trajectories and dashed lines are the approximation by the algorithm

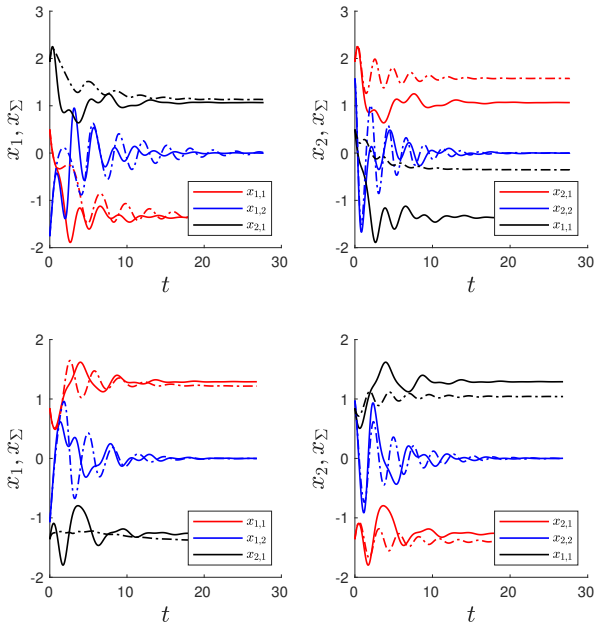

Figure 3.22: Test orbits from the input-affine forced EDMD algorithm, where the interconnection input is unknown. Solid lines are the theoretical trajectories and dashed lines are the approximation by the algorithm.

the method is not suitable yet for decentralized control, where there is only information of the local state.

3.6.3 Controlling the Interconnection

Coupled with the extensions to the formulation of the EDMD based linear predictors for interconnected systems, the controller synthesis will be the traditional multiple-input multiple-output model predictive control (MPC) with integral action [Di Ruscio, 2013].

Consider a non-autonomous linear discrete time system

$$\begin{aligned} x(k+1) &= A_L x(k) + B_L u(k) \\ y(k) &= C_L x(k), \end{aligned} \tag{3.113}$$

with state variables $x \in \mathcal{M} \subseteq \mathbb{R}^n$, input space $u(k) \in \mathcal{U} \subseteq \mathbb{R}^l$, output space $y \in \mathcal{M}_y \subseteq \mathbb{R}^m$, discrete-time $k \in \mathbb{N}_0^+$, and system matrices A_L, B_L and C_L, that describe the evolution of the system from an arbitrary initial condition $x_0 = x(0) \in \mathcal{M}$ for a sequence of inputs $u \triangleq (u_i)_{i=0}^k$.

The classical formulation of the MPC with integral action solves for the rate of change of the input signal $\Delta u_k = u_k - u_{k-1}$ for each time instance according to the evolution of the system on a prediction and control horizon N_{pc}. The control sequence that drives the system to the desired output state comes from the minimization cost function

$$\begin{aligned} J_k = &\left(y_{k+1|N_{pc}} - r_{k+1|N_{pc}}\right)^\top Q \left(y_{k+1|N_{pc}} - r_{k+1|N_{pc}}\right) \\ &+ \Delta u_{k|N_{pc}}^\top P \Delta u_{k|N_{pc}}^\top, \end{aligned} \tag{3.114}$$

where $r_k \triangleq (r_i)_{i=k}^{k+N_{pc}}$ is the reference signal on the prediction horizon, the matrix $Q \in \mathbb{R}^{N_{pc}m \times N_{pc}m}$ is block diagonal with N_{pc} symmetric positive semi-definite matrices and $P \in \mathbb{R}^{N_{pc}r \times N_{pc}r}$ is also a block diagonal matrix of N_{pc} symmetric positive semi-definite matrices.

The solution is equivalent to a quadratic problem with objective function (3.114) subject to (3.113) and accepts constraints on the maximum and minimum values of the inputs or their rate of change.

With some matrix manipulations, and considering a smaller control horizon than the prediction horizon for computational efficiency, the

problem in standard quadratic programming form is

$$\begin{aligned} &\min_{u} u^\top H u + h^\top u \\ &\text{s.t. } L_c u \leq b, \end{aligned} \tag{3.115}$$

where H, h, are the constant matrix and vector of the problem, and L_c and b are the matrix and vector for the linear inequality constraints.

The application of the controller to the input-affine and interconnection non-affine predictor for the coupled Duffing equation problem, where the prediction horizon is ten steps and the control horizon is four steps drives both systems to the origin. Figure 3.23 shows the result of applying the algorithm to all the initial conditions from the training and test sets.

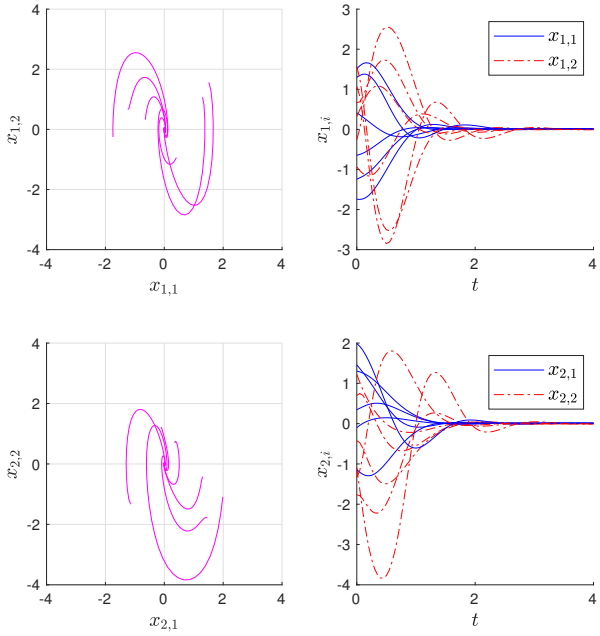

Figure 3.23: MPC synthesis for the interconnected Duffing equation.

Although there are only two systems for the control of interconnections, the possibility of controlling different network topologies depends on the ability to capture the behavior of the interconnection inputs, a

problem related to the observability of the different contributions of the neighboring systems based on the measurement of their sum.

A potential improvement to the methodology is the achievement of a decentralized controller, where individual subsystems operate on local information, without the need of a costly information exchange layer or a centralized information gathering. Given the fact that it is possible to approximate the interconnection free response of each system, the difference between these two models is a potential solution to the approximation of the interconnection effect.

3.7 Summary

This section presents the traditional theory regarding regions of attraction, the Koopman operator and the approximation of its discrete-time truncation via the EDMD algorithm, one of the contributions is a basis reduction method based on p-q-quasi norms that reduces the dimension and order of the approximation, and in turn, increases the accuracy of the algorithm. A basis reduction method based on polynomial accuracy is also proposed, that can be combined with the p-q-quasi norm reduction to give lower dimensional approximations suitable for subsequent analysis and synthesis algorithms that benefit computationally from the use of smaller approximations.

Additionally, and contrary to traditional algorithms, using the inverse of order-one polynomial elements to recover the state does not break the orthogonality of the basis when the single state variable observables are included in the vector valued function of observables. Moreover, there is no need to include additional optimization algorithms in the process to recover the state.

Another improvement of the EDMD algorithm is the incorporation of a priori knowledge such that the set of observables includes embeddings of elementary functions that increase the accuracy of the approximation. This method is a step further into the inclusion of information regarding the differential equation for the approximation of the linear predictors. Further research will probably show how to include the knowledge from a mass and energy balance modeling process or empirical knowledge re-

garding the dynamics to further improve the approximation.

Finally, this section presents linear and expanded approximations of interconnected dynamical systems for control. From these approximations, it is possible to set-up linear MPC algorithms that rely on the knowledge of the state and the partial knowledge of the interconnection input.

Chapter 4

Approximating the ROA via EDMD & Koopman operator

This section describes our main results for the characterization of the asymptotically stable points region of attraction in the multi-stability scenario with the Koopman operator. In order to achieve this goal in a data-driven approach, we show how our method can be used to find the fixed points of the system, determine their stability and finally, analyze the spectrum of the operator to get the ROA. There are three assumptions that must hold for the approximation of the Koopman operator and the application of the algorithm. First, the EDMD algorithm has enough trajectories from the dynamical system to have a proper estimate of the operator. Second, Assumptions 1-3 from Section 3.2 hold. Third, the system is ergodic [Eisner et al., 2015] or in terms of polynomial chaos, it has finite variance [Marelli and Sudret, 2018]. For our particular case, this means that every initial condition in the state space converges to a specific asymptotically stable fixed point.

4.1 Fixed Points

The first step of the analysis consists of locating the fixed points to assess their stability. Recall from Definition 3.1.1 in Section 3.1 that a fixed point of the discrete time nonlinear system (3.1) is an invariant

subspace that has the property that whenever the state starts in it, it will remain in it for all future time.

Consider the forward and backward state evolution map of the system given by the Koopman operator in (3.54) and (3.55). If the evolution of these mappings is invariant then the system is at a fixed point. The solution of the minimization of the squared norm of the difference between the state and its evolution map from different initial conditions in the state space gives the location of the fixed points [Garcia-Tenorio et al., 2019].

Lemma 4.1.1 (Fixed points)**.** *Let $(\mathcal{M}; T(x); k)$ be a dynamical system that admits a Koopman operator approximation $(\mathcal{F}_d; U_d; k)$, and x^* is a fixed point of $T(x)$. Then*

$$x^* = \underset{x}{\operatorname{argmin}} \left\| \Psi_B^{-1} \left(B^\top \Xi M^k \Phi(x_0) \right) - x \right\|_2^2. \tag{4.1}$$

Proof. Let $T^k(x) = \Psi_B^{-1}(B^\top \Xi M^k \Phi(x_0))$ the flow map of $(\mathcal{M}; T(x); k)$, assume $k = K$ finite, and define $b(x) = \Psi_B^{-1}(B^\top \Xi M \Phi(x))$, using Definition 3.1.1 and $b(x)$, the least squares problem

$$J(x) = \frac{1}{2} \left\| b(x) - x \right\|^2, \tag{4.2}$$

with solution

$$x^* = \underset{x}{\operatorname{argmin}} \left(J(x) \right), \tag{4.3}$$

gives the location of the fixed points. □

Remark 5. *Note that this procedure is possible under the portion of the state space from where the data snapshots lie, and corresponds to the fixed points of the nonlinear underlying hyperbolic dynamical system. If the system is not hyperbolic, this condition does not hold.*

Remark 6. *This lemma is only accountable for the location of the fixed points in the state space; it does not give information about their stability.*

Remark 7. *Equation* (3.54) *is a nonlinear, discrete-time evolution mapping, and under the definition of fixed point, i.e., $\bar{T}^k(x^*) = x^*$ it is possible to get the approximation of the hyperbolic fixed points by solving*

$$\bar{x}^* \subseteq \{x \in \mathbb{R}^n \colon \bar{T}^k(x) - x = 0\}. \tag{4.4}$$

In practice, this procedure poses two problems. First, as the nonlinear mapping (3.54) *comes from a set of observables, the dimension and complexity of these functions affect the possibility of getting a solution in polynomial type. In high order polynomial expansions, even if it is possible to find a solution, the computational time is high. Second, when there is a solution, it is not clear which elements of the subset represent an actual fixed point of the system, solving a non-linear set of equations gives a number of solutions in the complex plane where some of which correspond to the real-valued solutions of the system, i.e., not all the points of the subset are fixed points of the system, while the converse is true. Considering the data driven case, the fixed points of the system are not known a priori and therefore using this definition to approximate the fixed points is not feasible.*

With the location of the fixed points, it is necessary to establish their stability.

4.1.1 Example

For illustration purposes, consider the ongoing example of the Duffing equation with damping and two basins of attraction. Recall that this system has a saddle at the origin and two asymptotically stable equilibrium points.

For the approximation of the equilibrium points in Lemma 4.1.1 the initial conditions from the test set are not enough to identify all of the fixed points from a multi-start algorithm. Consequently, a new set of points in the original portion of the state space is generated to start the optimization. Additionally, recall that the evolution of the system based on eigenfunctions according to (3.54) has an additional computational step than the system evolution based on observables in (3.72), which is the spectral decomposition of the Koopman matrix. Therefore, the use of the evolution based on observables improves the accuracy of the location of the fixed points. Table 4.1 shows the numerical result and Figure 4.1 depicts the location of the initial conditions and the result of the method.

Table 4.1: Duffing equation fixed points location.

	Theoretical	Algorithmic
x_A^*	(-1,0)	(-1.002,0.001)
x_B^*	(0,0)	(0.003,0.001)
x_C^*	(1,0)	(1.003,0)

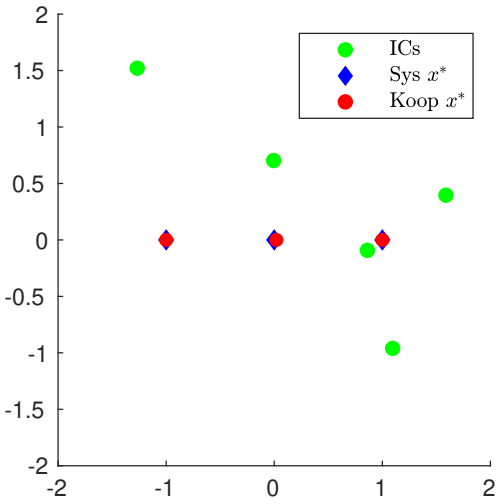

Figure 4.1: Initial conditions and location of the fixed points for the Duffing equation.

4.2 Stability of Fixed Points

The traditional way of establishing the local stability of a hyperbolic fixed point is through the analysis of the Jacobian matrix of the system (3.1) evaluated at the fixed point. Our proposed approach is to analyze the state evolution map from the approximation of the Koopman operator in the same way.

Definition 4.2.1 (Stability)**.** *Let* $(\mathcal{M}; T(x); k)$ *be a dynamical system that admits a Koopman operator approximation* $(\mathcal{F}_d; U_d; k)$*. Define a non-linear state evolution map* $b(x) = \Psi_B^{-1}(B^\top \Xi M^k \Phi(x))$ *from the state*

evolution map (3.54)*, the local linearization* $b(x)$ *at a given point* x^* *is*

$$\begin{aligned} x(k+1) &= \left[\frac{\partial T(x)}{\partial x_1} \cdots \frac{\partial T(x)}{\partial x_n}\right]\Bigg|_{x^*} x(k) \\ &= \left[\frac{\partial b(x)}{\partial x_1} \cdots \frac{\partial b(x)}{\partial x_n}\right]\Bigg|_{x^*} x(k) \\ &= Hx(k). \end{aligned} \tag{4.5}$$

The local stability of a fixed point x^* *with respect to the eigenvalues* $\{\mu_i\}_{i=1}^n$ *from the spectral decomposition of the matrix* H *are given by,*

- *if* $|\mu_i| < 1$ *for all* $i = 1, \ldots, n$ *then* x^* *is asymptotically stable.*
- *if* $|\mu_i| > 1$ *for all* $i = 1, \ldots, n$ *then* x^* *is unstable.*
- *if* $|\mu_i| > 1$ *for some* $i = 1, \ldots, n_k$ *and* $|\mu_i| < 1$ *for some* $i = n_k + 1, \ldots, n$*, then* x^* *is also unstable but has modal components that converge to it, making it a saddle point.*

Remark 8. *Note that the inequalities are strictly greater-than or less-than, this is in accordance with the hyperbolicity assumption.*

4.2.1 Stability Example

Continuing the Duffing equation example, recall that the fixed points of the system are: asymptotically stable for x_A^*4, unstable saddle for the origin x_B^*, and asymptotically stable for x_C^*. The first step to get the stability of fixed points is to calculate the Jacobian matrix of (3.54). However, given that (3.72) is more accurate, the Jacobian matrix according to the evolution of observables is

$$J = \begin{bmatrix} -0.0147x_1^2 + 1.32 \times 10^{-4}x_1 + 1.0 & 0.0967 \\ -0.292x_1^2 + 3.81 \times 10^{-3}x_1 + 0.0976 & 0.9407 \end{bmatrix} \tag{4.6}$$

Notice that this matrix is only function of x_1 because all of the fixed points are in $x_2 = 0$. Next, the evaluation of the Jacobian matrix for the

three different values of x_1 and their corresponding eigenvalues are:

$$J|_{x_A^*} = \begin{bmatrix} 0.9901 & 0.0967 \\ -0.1986 & 0.9407 \end{bmatrix} \qquad \lambda_A = \begin{Bmatrix} 0.9654 + 0.1364i \\ 0.9654 - 0.1364i \end{Bmatrix} \tag{4.7}$$

$$J|_{x_B^*} = \begin{bmatrix} 1.0049 & 0.0967 \\ 0.0976 & 0.9407 \end{bmatrix} \qquad \lambda_B = \begin{Bmatrix} 0.8705 + 0.0000i \\ 1.0751 + 0.0000i \end{Bmatrix} \tag{4.8}$$

$$J|_{x_C^*} = \begin{bmatrix} 0.9901 & 0.0967 \\ -0.1986 & 0.9407 \end{bmatrix} \qquad \lambda_C = \begin{Bmatrix} 0.9655 + 0.1336i \\ 0.9655 - 0.1336i \end{Bmatrix} \tag{4.9}$$

Table 4.2 shows the norm of the respective eigenvalues for each case, and the corresponding stability according to the classical linear theory analysis. With the information about the location and stability of fixed points, the main result of this Chapter is formulated, i.e., the approximation of the boundary of the ROA via eigenfunctions of the Koopman operator.

Table 4.2: Fixed point stability for the Duffing equation.

	$\lvert\lambda_1\rvert$	$\lvert\lambda_2\rvert$	Stability
x_A^*	0.97	0.97	AS
x_B^*	0.88	1.08	Saddle
x_C^*	0.97	0.97	AS

4.3 Approximation of the ROA boundary

This section describes our results for the approximation of the ROA for asymptotically stable fixed points in a data-driven approach using the discrete-time approximation of the Koopman operator. The claim of the main result of the paper is: If there is a system with multiple stable equilibrium points that admits a Koopman operator approximation, then, the level sets of Koopman eigenfunctions with unitary associated eigenvalue give the approximation of the ROA of those stable points. The constant value of the level sets comes from evaluating the Koopman eigenfunctions on the saddle points in the boundary.

To state the theorem and provide its proof, recall and consider the following properties of dynamical systems and the ROA of stable points from Section 3.2.

1. The boundary of the ROA is the union of the stable manifolds of the *type-one* fixed points in the boundary.

2. The stable manifold of a *type-one* fixed point in an n-dimensional system is a $(n-1)$-diemensional hyper surface.

If it is possible to capture the $(n-1)$-dimensional hyper surface that converges to the *type-one* saddle points in the boundary of the ROA via the Koopman operator, then, it is possible to get the boundary of the ROA.

The proposed method to get the $(n-1)$-dimensional hyper surface is to generate invariant eigenfunctions that are constant along the trajectories of the system. If there are eigenfunctions that are invariant along the trajectories of the system, then, evaluating these eigenfunctions on the *type-one* saddle points of the system gives the constant values for which the invariant eigenfunctions capture the stable manifold of the saddle points, i.e., the level sets of the invariant eigenfunction. A level set of an arbitrary function $h(x)\colon \mathbb{R}^n \to \mathbb{C}$ for any constant $c \in \mathbb{C}$ is $\Gamma_c(h(x)) = \{x \in \mathbb{R}^n \colon h(x) = c\}$.

To guarantee the existence of invariant eigenfunctions, consider the following property of the eigenfunctions of the Koopman operator (see property 1 in Mauroy and Mezic [2016] for its analogous in continuous time).

Property 4.4. *Suppose $\phi_1, \phi_2 \in \mathcal{F}_d$ are Koopman eigenfunctions of an arbitrary system with associated eigenvalue μ_1 and μ_2. If $\bar{\phi}(x) = \phi_1^{k_1}(x)\phi_2^{k_2}(x) \in \mathcal{F}_d$, for constants $k_1, k_2 \in \mathbb{C}$, then, $\bar{\phi}(x)$ is an eigenfunction constructed upon the product of two arbitrary eigenfunctions with associated eigenvalue $\bar{\mu} = \mu_1^{k_1}\mu_2^{k_2}$.*

Proof. It follows from condition (3.26) that

$$\left[U_d\bar{\phi}\right](x) = \left[U_d(\phi_1^{k_1}\phi_2^{k_2})\right](x) \tag{4.10}$$

$$= \left([U_d\phi_1](x)\right)^{k_1}\left([U_d\phi_2](x)\right)^{k_2} \tag{4.11}$$

$$= \mu_1^{k_1}\phi_1^{k_1}(x)\mu_2^{k_2}\phi_2^{k_2}(x). \tag{4.12}$$

□

Meaning that from a finite approximation of the Koopman operator, there is an infinity of possibly dependent eigenfunctions. Moreover, from the previous construction, it is possible to find the complex constants k_1 and k_2 for eigenvalues μ_1 and μ_2 such that $\bar{\mu} = 1$. Meaning that $\bar{\phi}(x) = \phi_+(x)$, where ϕ_+ denotes an eigenfunction with a unitary associated eigenvalue. From (3.26) it follows that $\phi_+(x)$ is an eigenfunction invariant along the trajectories of the system because

$$[U_d^k \phi_+](x) = \phi_+(x) \tag{4.13}$$
$$= c \tag{4.14}$$

With the previous properties and developments, the main theorem that describes our main results is:

Theorem 4.4.1. *If there exists a dynamical system $(\mathcal{M}; T(x); k)$ with multiple stable points that admits a Koopman operator approximation $(\mathcal{F}_d; U_d; k)$. Then, the approximation of the stable manifold of the type-one saddle points $\hat{x}^*$ in the boundary of the ROA is the level set of an invariant eigenfunction $\phi_+(x)$ where the constant value comes from the evaluation of the invariant eigenfunction on the saddle point in the boundary, i.e.,*

$$W^s(\hat{x}^*) = \Gamma_{c_{\phi_+(\hat{x}^*)}} \phi_+(x) \tag{4.15}$$
$$\subseteq \{x \in \mathbb{R}^n \colon \phi_+(x) = c_{\phi_+(\hat{x}^*)}\}. \tag{4.16}$$

Proof. From the definition of stable manifold of a *type-one* saddle point (3.15) in Section 3.2

$$W^s(\hat{x}^*) = \{x \in \mathbb{R}^n \colon \lim_{k\to\infty} T^k(x) = \hat{x}^*\}, \tag{4.17}$$

evaluating this manifold with an arbitrary eigenfunction $\phi(x)$, and using the condition of the Koopman operator in (3.25) gives

$$\phi(W^s(\hat{x}^*)) \approx \{x \in \mathbb{R}^n \colon \lim_{k\to\infty} \phi(T^k(x)) = \phi(\hat{x}^*)\} \tag{4.18}$$
$$\approx \{x \in \mathbb{R}^n \colon \lim_{k\to\infty} [U_d^k \phi](x) = \phi(\hat{x}^*)\} \tag{4.19}$$

Recall from (3.26) that the eigenvalue determines the dynamics of the associated eigenfunction, meaning that for this arbitrary eigenfunction,

the associated eigenvalue must be unitary for the equality to hold. Also, from (4.14) we get that the time evolution of an eigenfunction with a unitary associated eigenvalue is constant, or invariant along the trajectories of the system, meaning that it is independent on time evolution. These two developments imply that

$$\phi(W^s(\hat{x}^*)) = \{x \in \mathbb{R}^n \colon \phi_+(x) = c_{\phi_+(\hat{x}^*)}\}. \tag{4.20}$$

Notice that the right-hand part of (4.20) is the definition of level set for an eigenfunction with unitary associated eigenvalue $\phi_+(x)$. Additionally, the trivial eigenfunction $\phi_{\mu=1} = 1$ belongs to the set of eigenfunctions with unitary associated eigenvalue, consequently, the left-hand holds for a subset of the invariant eigenfunctions $\phi_+(x)$. Therefore, the stable manifold of a *type-one* saddle point in the boundary of the ROA is

$$\Gamma_{c_{\phi_+(\hat{x}^*)}}\phi_+(x) \subseteq \{x \in \mathbb{R}^n \colon \phi_+(x) = c_{\phi_+(\hat{x}^*)}\}. \tag{4.21}$$

□

In summary, the discrete approximation of the Koopman operator serves to find the nontrivial unitary eigenfunction that characterizes the ROA of asymptotically stable points.

The level set (4.16) gives the ROA boundary, and therefore, it is possible to find a classification rule of the different initial conditions in the state space that converge to any of the asymptotically stable equilibrium points. A geometrical approach to the classification problem is identifying the hyperplane that represents the boundary. This is a common approach when using the backwards integration of the dynamical system to find the set of points that compose the hyperplane. Although this is a possible approach, classifying an initial condition based on the geometry of the manifold is often difficult, especially when the hyperplane describing the boundary is not a function, or the system is of higher than three dimensions.

The approximation of the discrete-time Koopman operator from the EDMD algorithm using orthogonal polynomials as observables gives a set of eigenfunctions whose eigenvalue is unitary or close to unitary. Considering the difficulties of classifying the initial conditions based on the geometry of the stable manifold of saddles points, we propose two different

methods based on this set of eigenfunctions to determine the convergence of an arbitrary initial condition.

Definition 4.4.1 (Saddle classifier)**.** *Let* $\{\phi_+^i \colon \mu_i = 1\}_{i=1}^{\infty}$ *be a set of nontrivial eigenfunctions of a dynamical system* $(\mathcal{M}; T(x); k)$ *that accepts an approximation of the discrete-time Koopman operator* $(\mathcal{F}_d; U_d; k)$ *based on EDMD, and let* $\hat{x}^*$ *be a type-one saddle point in the boundary of the ROA separating the asymptotically stable points* x_A^* *and* x_B^**. The convergence of an arbitrary initial condition* x_0 *to either asymptotically stable equilibrium points* x_A^* *or* x_C^* *is*

$$\begin{aligned} x_A &\subseteq \{x_0 \in \mathbb{R}^n \colon \Re[\phi_+(x_0)] \geq \Re[\phi_+(\hat{x}^*)]\} \\ x_C &\subseteq \{x_0 \in \mathbb{R}^n \colon \Re[\phi_+(x_0)] < \Re[\phi_+(\hat{x}^*)]\}, \end{aligned} \tag{4.22}$$

where $\Re[\cdot]$ *denotes the real part of the evaluation of the eigenfunction.*

Remark 9. *The points that converge to either asymptotically of the stable fixed points* x_A^* *or* x_C^* *is a subset and not an equality because not all eigenfunctions with associated eigenvalue equal to one capture this phenomenon. The particular characteristics that an eigenfunction must have to satisfy this criterion is still open.*

Remark 10. *Recall from Section 3.1 that a hyperbolic fixed point is of type-k if k eigenvalues of the Jacobian matrix have modulus greater than one. If only one eigenvalue has modulus greater than one,* x^* *is a type-one fixed point.*

This criterion is closely related to the geometric one, especially because there is the need for a clear separatrix given by the real part eigenfunction evaluation in the boundary saddle point. This implies that for every pair of asymptotically stable fixed points to be classified there must be an eigenfunction that separates the two. When the dimension of the problem starts to grow, especially in the amount of asymptotically stable fixed points, the rule given by Definition 4.4.1 becomes a combination of the evaluations of the initial condition, compared to the evaluation of the different saddle points in the boundaries. Although is similar to the geometric approach, this is an algebraic comparison, not geometrical.

Because of the invariant nature of the eigenfunction with associated eigenvalue equal to one along the trajectories of the system, we propose

a second criterion to classify the initial conditions that is independent on the aforementioned boundary of the ROA given by the level set. Theorem 3.2.1 states that the stable manifold of *type-one* saddle points can be captured with an eigenfunction with associated eigenvalue equal to one. Extrapolating this concept to the asymptotically stable fixed points, it is possible to find a unitary eigenfunction that is invariant along its ROA.

Definition 4.4.2 (AS classifier)**.** *Let* $\{\phi_+^i \colon \mu_i = 1\}_{i=1}^{\infty}$ *be a set of non-trivial eigenfunctions of a dynamical system* $(\mathcal{M}; T(x); k)$ *that accepts an approximation of the discrete-time Koopman operator* $(\mathcal{F}_d; U_d; k)$ *based on EDMD. Let* $\{x_I^*\}_{I=1}^{L}$ *be a set of* L *asymptotically stable fixed points in the space state, and define* $C_l(\phi) \colon \mathbb{C} \to \mathbb{C}$ *as an arbitrary function of the observations. The set of points* x_I *that converge from an arbitrary initial condition* x_0 *to the fixed points* x_I^* *is*

$$x_I \subseteq \{x \in \mathbb{R}^n \colon C_l(\phi_+(x_0)) = C_l(\phi_+(x_I^*))\} \tag{4.23}$$

Remark 11. *The ideal case is to have a real valued constant eigenfunction where* $C_l(\phi(x)) = \phi(x)$*. Although this is theoretically possible, i.e., to find an eigenfunction invariant along the ROA of the asymptotically stable fixed point, the necessary conditions for this to happen is still an open question. For* $C_l(\phi(x)) = \angle(\phi(x))$*,* $C_l(\phi(x)) = |\phi(x)|$ *and* $C_l(\phi(x)) = \Re R(\phi(x))$ *there is a chance of getting an accurate classification based on the natural eigenfunction from the EDMD approximation or by constructing the eigenfunction that satisfies* (4.23)*. Nevertheless, the current method to find an eigenfunction that accurately classifies according to either of these functions of* ϕ *is by checking the necessary conditions for the eigenfunction to be accurate under each rule. As well as the constant case, the conditions that guarantee an accurate behavior is still an open question.*

Remark 12. *Although the eigenfunction that satisfies conditions* (4.23) *is suitable for the classification of all the approximated state space into its respective point of convergence, note that the equality is replaced by a subset because not all eigenfunctions with an associated eigenvalue equal to one satisfy this criterion. To the best of the author knowledge, the criteria to make it an equality are still unknown.*

Section 5.2 exemplifies the different results of performing the analysis with the different classification schemes. In general, the available eigen-

functions with a unitary eigenvalue that come directly from the EDMD algorithm or a constructed one from (4.12) give an accurate result by using Definition 4.4.1. For the classification based on the asymptotically stable equilibrium points from Definition 4.4.2, finding an eigenfunction that satisfies this criterion is not trivial.

In summary, the approximation of the Koopman operator serves to find the unitary eigenfunction that characterizes the ROA of asymptotically stable fixed points.

4.4.1 ROA Example

For illustration purposes, consider the example of the Duffing equation with damping and two asymptotically stable equilibrium points. This system satisfies Assumptions 1-3 from section 3.2 because there is only one fixed point in the stability boundary of the two asymptotically stable points, which is the saddle point at the origin. Given that it is unique, it cannot violate the transversality condition.

Theorem 3.2.1 states that the stable manifold of the saddle point at the origin is the boundary of the region of attraction of the two asymptotically stable points. Furthermore, theorem 4.4.1 states that a nontrivial eigenfunction with a unitary associated eigenvalue captures this stable manifold. Consider the level plot of fig. 4.2 that shows a unitary eigenfunction of the discrete-time approximation of the Koopman operator. In contrast with to the previous example of eigenfunctions for the duffing oscillator in Section 3.4.5, this eigenfunction does not come from the approximation using only one trajectory for each of the asymptotically stable points. Instead, the set of eigenfunctions comes from a full basis, i.e., $q = \infty$ for a value of $p = 4$ that for two state variables, gives a set of 25 observables and therefore, the same amount of eigenfunctions. The training and testing sets come from 400 uniformly distributed initial conditions over $x_1, x_2 \in \begin{bmatrix} -2 & 2 \end{bmatrix}$ with a $\Delta t = 0.1$ and contrary to the previous cases, there are only 11 points per trajectory, not a full numeric integration until convergence. Again, the division between the training and testing set is $50 - 50$.

Notice that the amount of points for the accurate approximation of

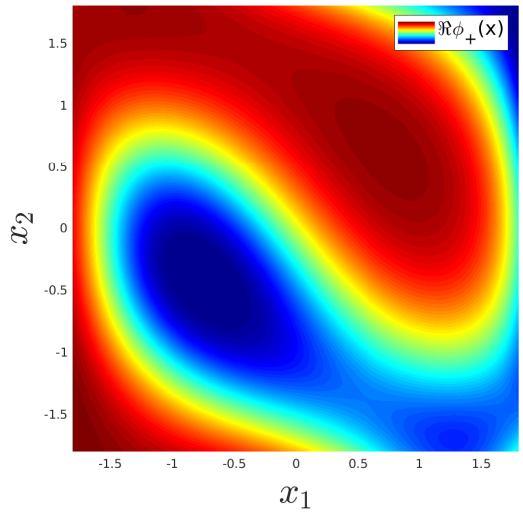

Figure 4.2: Level plot of the real part of the unitary eigenfunction of the discrete-time approximation of the Koopman operator for the Duffing equation problem.

eigenfunctions is five times greater than the necessary points for the approximation of the dynamics. Furthermore, the dimension and order of the basis is greater, and given that for this case there are more initial conditions and less points per trajectory, as a result, the available points for the approximation cover uniformly the portion of the space state under evaluation. The reason for this different approach is that the method for building accurate unitary eigenfunctions is still an open question.

Evaluating the unitary eigenfunction at the identified saddle point near the origin gives the constant value of the level set that describes the stable manifold. Identifying this line and classifying according to it is not the best numerical approach. Notice that the ROA of each of the points corresponds to a subset of the space state that is either above or below the stable manifold when evaluated by the unitary eigenfunction. Therefore, the classification rule does not rely on the interpolation of points in the manifold to check if a point in the state space is above or below the line. The classification rule is according to the evaluation of an individual point with the unitary eigenfunction and the comparison

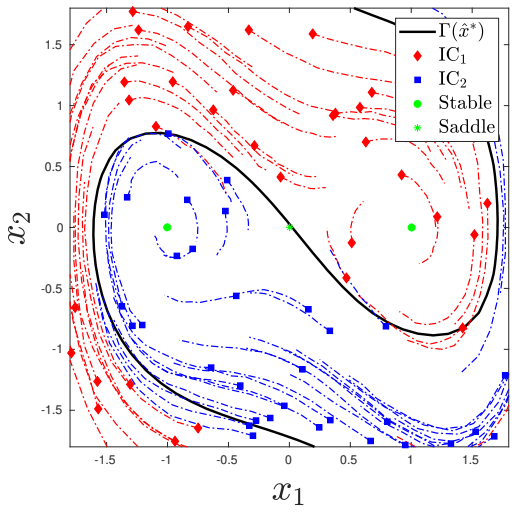

Figure 4.3: Stable manifold approximation and initial condition classification based on the evaluation of the unitary eigenfunction in the saddle point.

of the real part of this value to the constant value of the level set as in definition 4.4.1.

Figure 4.3 depicts the approximation of the stable manifold of the saddle point, and the correct classification of the test set of initial conditions, where the application of the classification criterion gives an error of 2.5%. In this figure it is clear that the stable manifold cannot be represented as a function and therefore, its geometry in not a convenient classification rule. If the system under study has more than two state variables, the problem of classifying according to the geometry of the stable hyperplane is worse.

4.5 Algorithm

The approach presented in section 3.4 and 4.1-4.3 for obtaining the attraction regions of asymptotically stable fixed points is summarized in Algorithm 1, for which the following assumptions hold.

Assumption 4. *The system under consideration has multiple hyperbolic fixed points.*

Assumption 5. *At least one of the fixed points is asymptotically stable.*

Assumption 6. *There is enough snapshot data either from measurements of the real system or a numerical simulation for constructing an approximation of the Koopman operator.*

4.6 Additional Examples

To test further the reliability of the method, we first apply it to a model of competitive exclusion with two state variables to graphically show the effect of the eigenfunction with unitary eigenvalue. Then, a five-state variable mass action kinetics (MAK) model that allows displaying the effectiveness of the algorithm for higher dimensional systems. The Lotka-Volterra and the MAK systems are suitable for the analysis because of their geometrical properties. They are nonnegative compartmental systems that, depending on the parameterization, have hyperbolic fixed points that satisfy the Hartman-Grobman theorem [Chellaboina et al., 2009]. The hyperbolicity of the fixed points implies that their stable and unstable manifolds intersect transversely at the saddle points. Therefore, Assumptions 1-3 are satisfied in this kind of systems under the right parameterization.

The numerical integration of the systems from a random set of initial conditions gives the dataset of trajectories for the algorithm. A subset is used to calculate the Koopman operator approximation via the EDMD algorithm, and another subset is used for testing the algorithm accuracy according to the empirical error (3.56), where this error serves to determine the best $p - q$ parameters from a sweep over the different values.

4.6.1 Biochemical System Models

Kinetic reaction networks describe the dynamical behavior in chemical and biochemical systems, and the most commonly used method

Algorithm 1: Approximation of the ROA boundary via the eigenfunctions of the Koopman operator. A data-driven calculation that approximates the fixed points and their stability and the eigenfunction of the Koopman operator, generates the unitary eigenfunction, and analyzes the saddle points in the ROA to get its boundary.

For a dynamical system that satisfies Assumptions 4-6;
Data: $\{x_i, y_i\}_{i=1}^{N}$
Result: $\partial R_A(x_s^*)$
initialization;
$[\Phi(x), M] \longleftarrow \text{EDMD}\left(\{x_i, y_i\}_{i=1}^{N}, q, p\right)$;
$b(x) \longleftarrow \Psi_B^{-1}(B^\top \Xi M^k \Phi(x))$;
$x^* \longleftarrow \text{argmin}_x \|b(x) - x\|_2^2$;
$E_q \longleftarrow \text{size}(x^*)$;
for $i \leftarrow 1$ **to** E_q **do**
  $H_i \longleftarrow \left[\frac{\partial b(x)}{\partial x_1} \cdots \frac{\partial b(x)}{\partial x_n}\right]\Big|_{x_i^*}$;
  $\{\mu_{i,j}\}_{j=1}^{n} \longleftarrow \text{eig}(H_i)$;
  if $|\mu_{i,j}| < 1$ for all $j = 1, \ldots, n$ **then**
    $x_i^* \leftarrow x_s^*$
  else if $|\mu_{i,j}| < 1$ for some $j = 1, \ldots, n$ **then**
    $x_i^* \leftarrow \hat{x}^*$
  else
    $x^* \leftarrow x_u^*$
  end
end
$\hat{E}_q \longleftarrow \text{size}(\hat{x}^*)$;
$E_s \longleftarrow \text{size}(x_s^*)$;
$\phi_+(x) \longleftarrow \{\phi_1^{k_1}(x)\phi_2^{k_2}(x) \colon \mu_1^{k_1}\mu_2^{k_2} = 1\}$;
for $i \leftarrow 1$ **to** E_s **do**
  for $j \leftarrow 1$ **to** $\hat{E}_q$ **do**
    $W_j^s(\hat{x}_j^*) \longleftarrow \{x \in \mathbb{R}^n \colon \phi_+(x) = \phi_+(\hat{x}_j^*)\}$;
  end
  $\partial R_A(x_i^*) = \cup W^s(\hat{x}_j^*)$
end

to model their behavior are polynomial ordinary differential equations. These sets of equations are mathematically well-established, and they have a broad range of numerical solution techniques and solvers. Additionally, they model the systems in a deterministic way, according to the average behavior of the state variables [Feinberg, 1987]. The advantages of using these systems is their non-negativity and compartmental characteristics, coupled with the fact that depending on the parametrization, the fixed points of the system are hyperbolic [Chellaboina et al., 2009]. Hence, they satisfy the Assumptions (1-3) to perform the analysis presented in this thesis.

Each biochemical reaction network gives rise to a dynamical system, which describes the evolution of the species concentrations in the network over time. Each biochemical reaction has three sets associated to it: the set of chemical species $\mathcal{S}$, the set of complexes of the network $\mathcal{C}$, and the set of reactions in the network $\mathcal{R}$. The following set of reactions constitute a network of 6 reactions between 5 complexes composed by 5 chemical species.

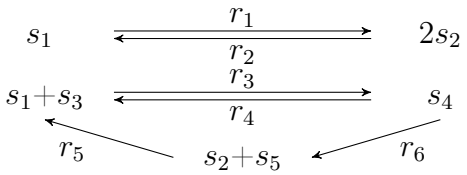

(4.24)

For an arbitrary Network, consider m to be the number of chemical species, n the number of complexes and a r the number of reactions in the network. We can write the set $\mathcal{S} = \{s_1, s_2, s_3, s_4, s_5\}$, which has an associated composition vector x of nonnegative molar concentrations per species, $x \in \mathbb{R}^n_+$, the set of complexes, $\mathcal{C} = \{s_1, s_2, s_1 + s_3, s_4, s_2 + s_5\}$, the set,

$$\mathcal{R} = \left\{ \begin{array}{c} s_1 \to 2s_2 \\ 2s_2 \to s_1 \\ s_1 + s_3 \to s_4 \\ s_4 \to s_1 + s_3 \\ s_2 + s_5 \to s_1 + s_3 \\ s_4 \to s_2 + s_5 \end{array} \right\}, \tag{4.25}$$

with the associated reactions rate vector function $\rho : \mathcal{R} \to \mathbb{R}^r_+$ that

associates a positive rate constant to each reaction. Having these sets, the definition of a reaction kinetics network is:

Definition 4.6.1 (Reaction Network)**.** *A biochemical reaction network consists in a quadruple* $\{\mathcal{S}, \mathcal{C}, \mathcal{R}, \rho\}$ *such that:*

i. the finite set $\mathcal{S}$ *is the set of species,*

ii. the finite set $\mathcal{C}$ *is the finite set of complexes,* $\mathcal{C} \subset \mathbb{R}^{\mathcal{S}}$*, where each element of the set is the sum of species*

$$\sum_{s \in \mathcal{S}} \alpha_s s_s \tag{4.26}$$

where α_s *is the stoichiometric coefficient of the* s^{th} *species.*

iii. The finite set $\mathcal{R}$ *is the set of reactions,* $\mathcal{R} \subset \mathcal{C} \times \mathcal{C}$ *such that,*

a. $y \to y \notin \mathcal{R}, \quad \forall y \in \mathcal{C}$*.*

b. For each $y \in \mathcal{C}$ *there exists* $y' \in \mathcal{C}$ *such that* $y' \to y \in \mathcal{R}$ *or such that* $y \to y' \in \mathcal{R}$*.*

iv. And the vector function ρ *that associates a positive rate constant to each reaction.*

Given an initial concentration $x(0) \in \mathbb{R}^n_+$ of the interacting species, kinetic rates, and the topology of the biochemical network, such as (4.24), the mass-balance ODEs describe how the concentration $x(t)$ of each species evolves with time.

Definition 4.6.2 (Species ODE)**.** *For a reaction network* $\{\mathcal{S}, \mathcal{C}, \mathcal{R}, \rho\}$ *the formation rate function* $f_s(x) : \mathbb{R}^n_+ \to \mathbb{R}$ *is*

$$f_s(x) = \sum_{y \to y' \in \mathcal{R}} (\alpha'_s - \alpha_s) \rho_{y \to y'} \prod_{s \in \mathcal{S}} x_s^{\alpha_s}. \tag{4.27}$$

This formation rate function is the time derivative of species concentration, i.e., $\dot{x} = f(x)$*.*

Consider for example the first species of network (4.24), according to the species differential equation ODE, its formation rate is

$$\begin{aligned} f_1(x) &= (0-1)r_1(x_1^1 x_2^0 x_3^0 x_4^0 x_5^0) \\ &\quad + (1-0)r_2(x_1^0 x_2^2 x_3^0 x_4^0 x_5^0) \\ &\quad + (0-1)r_3(x_1^1 x_2^0 x_3^1 x_4^0 x_5^0) \\ &\quad + (1-0)r_4(x_1^0 x_2^0 x_3^0 x_4^1 x_5^0) \\ &\quad + (1-0)r_5(x_1^0 x_2^1 x_3^0 x_4^0 x_5^1) \\ &= -r_1 x_1 + r_2 x_2^2 - r_3 x_1 x_3 + r_4 x_4 + r_5 x_2 x_5 \end{aligned} \tag{4.28}$$

To extend the per-species definition of the ODE to a complete reaction network in matrix notation. First, define the matrix exponentiation of $x \in \mathbb{R}^n$ by a matrix $\alpha = [\alpha_{i,j}] \in \mathbb{R}^{r \times n}$ as $x^\alpha \in \mathbb{R}^r$ such that its *i-th* component is the product $x_1^{\alpha_{i,1}} x_2^{\alpha_{i,2}} \cdots x_n^{\alpha_{i,n}}$. Then, define $\circ$ as the element-wise Hadamard product, and finally, the MAK ODE is

$$f(x) = (\alpha' - \alpha)^\top (x^\alpha \circ \rho), \tag{4.29}$$

where α and α' are the stoichiometric coefficient for the reactants and the products respectively in the network. For the reaction network (4.24) the stoichimetric matrices are

$$\alpha = \begin{bmatrix} 1 & 0 & 0 & 0 & 0 \\ 0 & 2 & 0 & 0 & 0 \\ 1 & 0 & 1 & 0 & 0 \\ 0 & 0 & 0 & 1 & 0 \\ 0 & 1 & 0 & 0 & 1 \\ 0 & 0 & 0 & 1 & 0 \end{bmatrix} \qquad \alpha' = \begin{bmatrix} 0 & 2 & 0 & 0 & 0 \\ 1 & 0 & 0 & 0 & 0 \\ 0 & 0 & 0 & 1 & 0 \\ 1 & 0 & 1 & 0 & 0 \\ 1 & 0 & 1 & 0 & 0 \\ 0 & 1 & 0 & 0 & 1 \end{bmatrix}, \tag{4.30}$$

The system of ODEs that represent the dynamics of the average species

concentration is

$$\dot{x} = \begin{bmatrix} -1 & 1 & -1 & 1 & 1 & 0 \\ 2 & -2 & 0 & 0 & -1 & 1 \\ 0 & 0 & -1 & 1 & 1 & 0 \\ 0 & 0 & 1 & -1 & 0 & -1 \\ 0 & 0 & 0 & 0 & -1 & 1 \end{bmatrix} \left(\begin{bmatrix} x1 \\ x2^2 \\ x1x3 \\ x4 \\ x2x5 \\ x4 \end{bmatrix} \circ \begin{bmatrix} r_1 \\ r_2 \\ r_3 \\ r_4 \\ r_5 \\ r_6 \end{bmatrix} \right) \tag{4.31}$$

$$\begin{aligned} & -r_1x_1 + r_2x_2^2 - r_3x_1x_3 + r_4x_4 + r_5x_2x_5 \\ & 2r_1x_1 - 2r_2x_2^2 - r_5x_2x_5 + r_6x_4 \\ = & -r_3x_1x_3 + r_4x_4 + r_5x_2x_5 \\ & r_3x_1x_3 - r_4x_4 - r_6x_4 \\ & -r_5x_2x_5 + 5r_6x_4 \end{aligned} \tag{4.32}$$

4.6.2 Lotka-Volterra Model

Consider a Lotka-Volterra model where two species compete for the same resource described by the following network:

$$\begin{aligned} s_1 &\underset{r_2}{\overset{r_1}{\rightleftarrows}} 2s_1 \\ s_2 &\underset{r_4}{\overset{r_3}{\rightleftarrows}} 2s_2 \\ s_1{+}s_2 &\xrightarrow{r_5} s_1 \\ s_1{+}s_2 &\xrightarrow{r_6} s_2 \end{aligned} \tag{4.33}$$

where s_1 and s_2 are the competing species, r_1 and r_3 describe the growth rates of the species respectively, r_2 and r_4 are the constants that describe competition between members of the same species, and the constants r_5 and r_6 describe the competition between species. The values of these constants predicts the potential outcome of the competition. Depending on the parameterization there can be a co-existence or an exclusion of one of the species against the other. The case of interest is the exclusion one, and the objective is to find the set of initial conditions within the state space that lead the model to one of the stable points where one species completely takes over the other.

The ordinary differential equation that describes the dynamics of the

model comes from the matrices

$$\alpha = \begin{bmatrix} 1 & 0 \\ 2 & 0 \\ 0 & 1 \\ 0 & 2 \\ 1 & 1 \\ 1 & 1 \end{bmatrix} \qquad \alpha' = \begin{bmatrix} 2 & 0 \\ 1 & 0 \\ 0 & 2 \\ 0 & 1 \\ 0 & 1 \\ 1 & 0 \end{bmatrix}, \tag{4.34}$$

The differential equation that describes the network (4.33) according to the matrices (4.34) and (4.29) is

$$\dot{x}_1 = r_1 x_1 - r_2 x_1^2 - r_5 x_1 x_2 \tag{4.35}$$
$$\dot{x}_2 = r_3 x_2 - r_4 x_2^2 - r_6 x_1 x_2, \tag{4.36}$$

where the parameterization for the species to have two particular asymptotically stable fixed points is $r = [2\ 1\ 2\ 1\ 3\ 3]^\top$. With this choice, the system has four fixed points: an unstable point at the origin defined as x_A^*, a saddle point at $(0.5, 0.5)$ defined as x_D^* and two asymptotically stable at $(0, 2)$ and $(2, 0)$ defined as x_B^* and x_C^* respectively. The geometry of this problem provides a simple representation of the stable manifold of the saddle point which is the line $x_1 = x_2$, therefore, giving a closed formulation for the comparison with the stable manifold provided by the operator by the construction of the eigenfunction with an associated eigenvalue equal to one.

The integration of the system from 200 uniformly distributed random initial conditions over $x_1, x_2 \in [0\ 2]$ give the datasets for approximating the operator via the EDMD algorithm and the dataset to test the accuracy of the algorithm; both sets, the training and test ones are 50% of the trajectories from the original set. We apply the EDMD algorithm for the training set with a Laguerre polynomial basis where a sweep over the $p - q$ values gives the best performance when $q = 1.1$ and $p = 3$ for the truncation scheme. This selection produces a polynomial basis with 13 elements of an order less than 3 and a Koopman operator of order 13. Figure 4.4 shows the retained indices after implementing the truncation scheme.

The identification of the fixed points via Lemma (4.1.1) gives an absolute error of 0.15%, and the linearization of the state evolution map

from (3.54) evaluated at the fixed points accurately provides their stability according to the norm of the eigenvalues λ; these are the eigenvalues of the linearization of the state evolution map (where $\Psi_B^{-1}(x) = [1-x_1,\, 1-x_2]^\top$ for this particular case) evaluated at the identified fixed points. Table 4.3 summarizes these results.

Table 4.3: Lotka-Volterra equation fixed points, location and stability.

	Theoretical	Algorithmic	$\lvert\lambda_1\rvert$	$\lvert\lambda_2\rvert$	Stability
x_A^*	(0,0)	(-0.006,-0.006)	1.21	1.22	Unstable
x_B^*	(0,2)	(0,2)	0.66	0.82	AS
x_C^*	(2,0)	(2,0)	0.82	0.66	AS
x_D^*	(0.5,0.5)	(0.5,0.5)	0.81	1.10	Saddle

Figure 4.5 depicts the comparison between the theoretical trajectories given by the integration of the differential equations and the state evolution map (3.54) from the same initial conditions. It also depicts the comparison between the theoretical boundary of the attraction regions $x_1 = x_2$ and the boundary given by the level set of the constructed eigenfunction with unitary associated eigenvalue from (4.16). The error in the classification of the initial conditions is of 2%, while the mean absolute error between the boundaries of the regions of attraction is 3%.

Figure 4.6 shows four eigenfunctions of the Koopman operator, where the problem of the determination of the invariant unitary eigenfunction is apparent. The approximation methods such as the EDMD can yield $\phi_{\mu=1} = 1$, which is a trivial constant eigenfunction that does not provide information about the system. Therefore, it is necessary to get a nontrivial invariant eigenfunction. Recall from (4.12) the relationship that the set of eigenfunctions satisfies, where $\phi_+(x) = \phi_1^{k_1}(x)\phi_2^{k_2}(x)$ is an eigenfunction of the Koopman operator with associated eigenvalue $\mu_+ = \mu_1^{k_1}\mu_2^{k_2}$ for a set of complex constants k_1 and k_2. Therefore, setting $\mu_1^{k_1}\mu_2^{k_2} = 1$ and computing a solution for k_1 and k_2 gives the desired invariant eigenfunction.

Figure 4.6 also depicts the resulting invariant eigenfunction that captures the stable manifold of the saddle point, and the two eigenfunctions with real-valued eigenvalues close to one used for the construction. The eigenvalues of these eigenfunctions are $\mu_1 = 1.07$ and $\mu_2 = 0.83$. It is still not clear how to properly select these eigenfunctions, the best

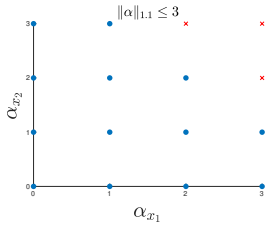

Figure 4.4: Retained indices for the approximation of the Koopman operator for the Lotka-Volterra model with a choice of $q = 1.1$ and $p = 3$.

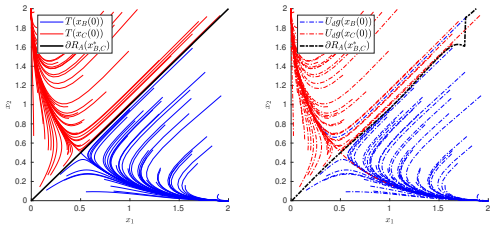

Figure 4.5: Trajectories and boundary of the asymptotically stable points of: a) The system differential equation, and b) The Koopman operator and the eigenfunction with unitary associated eigenvalue.

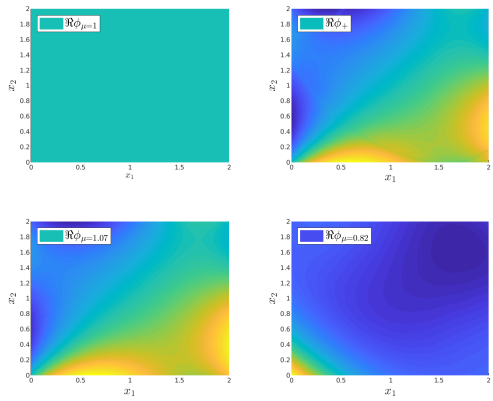

Figure 4.6: Eigenfunctions of the Koopman operator. a) Trivial eigenfunction with $\mu = 1$, b) Constructed eigenfunction ϕ_+, c) First eigenfunction for constructing ϕ_+, and d) Second eigenfunction for constructing ϕ_+.

performance happens when the construction is upon real-valued eigenfunctions, and not having them does hinder the accuracy, constructing the unitary eigenfunction with non real-valued eigenfunctions also gives a good estimate of the approximation.

4.6.3 Mass Action Kinetics

Consider the simple network of an auto-catalytic replicator on a continuous flow stirred tank reactor described by the network

$$\begin{aligned} s_1{+}2s_3 &\xrightarrow{r_1} s_2{+}3s_3 \\ s_2{+}2s_4 &\xrightarrow{r_2} 3s_4 \\ s_3 &\xrightarrow{r_3} s_5 \\ s_4 &\xrightarrow{r_4} s_5 \end{aligned} \tag{4.37}$$

where s_1 is the resource the species s_3 consumes to replicate and produce substrate s_2, which is consumed by species s_4 to replicate, and s_5 is the dead species from both groups. $r_1 > r_3$, and $r_2 > r_4$ are the pairs of replication rate constants and the species death constants. The dynamics of the network (4.37) come from matrices

$$\alpha = \begin{bmatrix} 1 & 0 & 2 & 0 & 0 \\ 0 & 1 & 0 & 2 & 0 \\ 0 & 0 & 1 & 0 & 0 \\ 0 & 0 & 0 & 1 & 0 \end{bmatrix} \qquad \alpha' = \begin{bmatrix} 0 & 1 & 3 & 0 & 0 \\ 0 & 0 & 0 & 3 & 0 \\ 0 & 0 & 0 & 0 & 1 \\ 0 & 0 & 0 & 0 & 1 \end{bmatrix}, \tag{4.38}$$

The differential equation that describes the network (4.37) according to the matrices (4.38) and (4.29), and considering the material exchange with the environment is

$$\begin{aligned} \dot{x}_1 &= -r_1 x_1 x_3^2 + d - dx_1 \\ \dot{x}_2 &= +r_1 x_1 x_3^2 - r_2 x_2 x_4^2 - dx_2 \\ \dot{x}_3 &= +r_1 x_1 x_3^2 - r_3 x_3 - dx_3 \\ \dot{x}_4 &= +r_2 x_2 x_4^2 - r_4 x_4 - dx_4 \\ \dot{x}_5 &= +r_3 x_3 + r_4 x_4 - dx_5, \end{aligned} \tag{4.39}$$

where d is the in/out-flow (dilution rate) of the system, and the substrate s_1 is the only component in the input flow. The value for the reaction rates vector $k = [7\ 5\ 0.3\ 0.05]^\top$ yields five fixed points: three asymptotically stable ones, i.e., the working point defined as x_A^*, a point where species s_3 thrives and species s_4 washes-out defined as x_C^*, and a wash-out point where the concentration of both species is zero defined as x_E^*, and two saddle points defined as x_B^* and x_D^*. The objective is to find the attraction region of the working point using the eigenfunctions with unitary associated eigenvalue. For this particular case, as the system is not a two-dimensional one, the geometry of the stable manifold is not evident. Therefore, the criteria for classifying the test set of initial conditions is not trivial.

A set of 360 random initial conditions is generated to integrate the system with a $\Delta t = 0.1$ and get the snapshot data for the approximation of the Koopman operator via the EDMD algorithm. From this set of snapshots, 50% is used to approximate the operator, and the other 50% to test the accuracy of the state evolution map, the eigenfunctions, and the results of the classification scheme based on the unitary eigenfunction. A sweep over the $p-q$ values gives the best performance for the truncation scheme when $q = 0.8$ and $p = 4$ which leads to an order of 163 by 163 elements of the approximation of the Koopman operator, and thus, a set of 163 eigenfunctions, eigenvalues and modes. From the set of eigenfunctions, the two eigenfunctions with real eigenvalue closest to one are $\mu_1 = 1.00008$, and $\mu_2 = 0.99983$ are selected to analyze the system. The eigenvalue associated with these eigenfunctions is close enough to one to provide an accurate analysis.

The identification of the fixed points via Lemma 4.1.1 gives an absolute error of 0.15%, and the linearization of the state evolution map from (3.54) evaluated at the fixed points provides an accurate description of their stability according to the norm of the eigenvalues λ. Table 4.4 shows the results from the theoretical and algorithmic location of the fixed points, Table 4.5 shows the results of taking the norm of the eigenvalues λ of the linearization of the state evolution map (3.54), evaluated at each of the fixed points.

Figure 4.7 depicts the results of evaluating the initial conditions, indexing over the whole training set, of the test set on the eigenfunctions

Table 4.4: Location of fixed points.

	Theoretical	Algorithmic	Error %
x_A^*	(0.23,0.09,0.30,0.54,0.59)	(0.23,0.09,0.30,0.54,0.59)	0.08
x_B^*	(0.21,0.67,0.30,0.07,0.47)	(0.23,0.62,0.30,0.11,0.49)	0.00
x_C^*	(0.23,0.76,0.30,0.00,0.46)	(0.23,0.76,0.30,0.00,0.46)	0.00
x_D^*	(0.76,0.23,0.09,0.00,0.14)	(0.70,0.3,0.11,0.00,0.17)	0.54
x_E^*	(1.00,0.00,0.00,0.00,0.00)	(1.00,0.00,0.00,0.00,0.00)	0.00

Table 4.5: Stability of fixed points.

	$\lvert\lambda_1\rvert$	$\lvert\lambda_2\rvert$	$\lvert\lambda_3\rvert$	$\lvert\lambda_4\rvert$	$\lvert\lambda_5\rvert$	Stability	
x_A^*	0.89	0.98	0.98	0.97	0.98	AS	Working Point
x_B^*	1.04	0.98	0.98	0.98	0.98	Saddle	
x_C^*	0.98	0.98	0.93	0.98	0.98	AS	x_4 Wash-out
x_D^*	1.05	0.96	0.98	0.98	0.97	Saddle	
x_E^*	0.90	0.98	0.98	0.97	0.97	AS	Wash-out

with an associated eigenvalue equal to one. The evaluation of the selected eigenfunction with $\mu = 1.00008$ (denoted ϕ_{+_1}) at the initial conditions of the test set and the saddle fixed points x_B and x_D shows that the evaluation at the former gives an accurate classification of the initial conditions that converge to the asymptotically stable fixed point x_A. The evaluation of the selected eigenfunction with $\mu = 0.99983$ (denoted ϕ_{+_2}) at the initial conditions of the test set and the saddle fixed points x_B and x_D shows that the evaluation at the latter gives an accurate classification of the initial conditions that converge to the asymptotically stable fixed point x_E. The combination of these two conditions specifies the criterion to classify the initial conditions that converge to the different asymptotically stable fixed points. Figure 4.8 shows the result of the classification criterion, where the correct classification surrounds the miss-classified initial conditions, with an error of 12%.

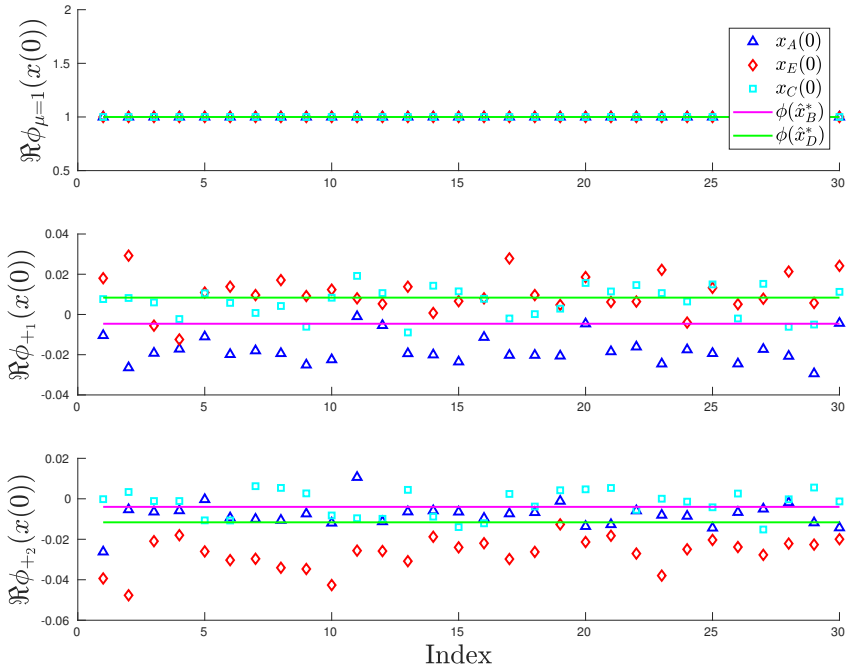

Figure 4.7: Eigenfunctions with unitary associated eigenvalue a) Trivial b) $\mu > 1$ c) $\mu < 1$.

4.7 Discussion and Summary

Even if we had the tools for extracting all kinds of information regarding the system, there are limitations for the deduction of the eigenfunctions. The right choice of the polynomial basis based on the known structure of the differential equation, the optimal truncation scheme, the choice of eigenfunctions to construct the one with unitary associated eigenvalue are open questions for improving the algorithm and the analysis.

Also, there is the problem of the required data to train the Koopman operator properly. For the two exemplified cases, the amount of data is sufficient to produce an accurate nonlinear model of the systems. Considering the proposed method over traditional identification techniques

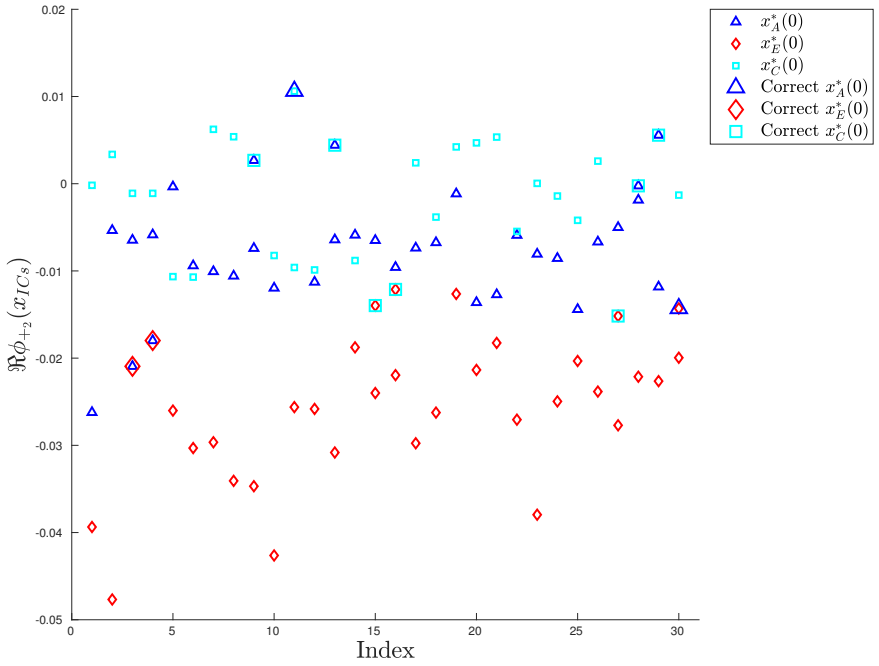

Figure 4.8: Classification of the initial conditions with respect to the evaluation of the eigenfunctions on the saddle points.

would be necessary to develop experimental design techniques specifically for the calculation of the Koopman operator to reduce the necessary data.

Furthermore, the relation between the eigenfunctions and their associated eigenvalues is still open. There are other dynamical characteristics to be analyzed from this association, as the dynamic behavior of eigenfunctions whose associated eigenvalue matches the local spectra of the fixed points is a potential source of information of the underlying dynamical system.

A possible improvement would be for the choice or construction of eigenfunctions. All eigenfunctions are able to capture different information and properties (relevant or not, accurate or not), and the analysis is limited to the invariant sets of these eigenfunctions. An analysis based on the spectral and geometric characteristics of real-valued and complex-

valued eigenfunctions could give more information about the system for control purposes.

This Section presents the theoretical and algorithmic contributions that allow the approximation of regions of attraction for asymptotically stable fixed points. Regarding the analysis, it is restricted to hyperbolic systems because of the impossibility to determine the location of limit cycles based only on snapshot data of the system.

The main component of the method is an accurate calculation of the systems' EDMD. From this decomposition it is possible to locate the hyperbolic fixed points of the system and give their stability along with their *type*. Additionally, an accurate decomposition with a suitable set of observables gives an accurate approximation of the Koopman operator, which, in turn, provides the basis for producing a non-trivial eigenfunction with eigenvalue equal to one. By combining these two results from the EDMD, it is possible to analyze the *type-one* fixed points in order to get an approximation of the ROA for the asymptotically stable fixed points.

Chapter 5

Anaerobic Digestion Process

The biological process through which multiple organisms break down organic matter in the absence of oxygen is called Anaerobic Digestion (AD). The benefits of the AD process include both the production of energy and the production of low sludge. What motivates the use of the AD process on an industrial scale is its capacity of degrading strong and resilient substrates, the low sludge production, and the possibility of making a profit out of the production of methane gas [Mailleret et al., 2003].

5.1 Problem Statement

The model of the anaerobic digestion system under study considers two reactions: acidogenesis and methanogenesis. The following reaction network describes the biological transformations:

$$\begin{aligned} a\xi_1 &\xrightarrow{r_1(\xi)} c\xi_2 + \xi_3, \\ d\xi_2 &\xrightarrow{r_2(\xi)} \mathrm{CH}_4 + \xi_4. \end{aligned} \tag{5.1}$$

In the first reaction, the acidogenic bacteria ξ_3 consumes the organic substrate ξ_1 for growth and produces volatile fatty acids ξ_2. In the second

reaction, the methanogenic bacteria ξ_4 uses the volatile fatty acids as a substrate for growth and produces methane. It is necessary to maintain the balance between the acidogenesis and the methanogenesis states in the operation of the AD process to avoid acidification, which is the state of accumulation of volatile fatty acids in the reactor that produces the washout of methanogenic bacteria.

For an ideal continuously stirred tank reactor, the following differential equations describe the system dynamics of the reaction network (5.1):

$$\begin{aligned}
\dot{\xi}_1 &= u(\xi_{\text{in}_1} - \xi_1) - ar_1(\xi), \\
\dot{\xi}_2 &= u(\xi_{\text{in}_2} - \xi_2) + cr_1(\xi) - dr_2(\xi), \\
\dot{\xi}_3 &= -u\xi_3 + r_1(\xi), \\
\dot{\xi}_4 &= -u\xi_4 + r_2(\xi),
\end{aligned} \tag{5.2}$$

with a methane outflow rate

$$Q(\xi) = qr_2(\xi), \tag{5.3}$$

where $\xi = [\xi_1 \ \xi_2 \ \xi_3 \ \xi_4]^T \in \mathbb{R}^4_+$ is the state vector, $u \in \mathbb{R}_+$ is the dilution rate, $\xi_{\text{in}_1}, \xi_{\text{in}_2} \in \mathbb{R}_+$ are the concentrations of organic substrate and volatile fatty acids in the influent, $a, b, c \in \mathbb{R}_+$ are the stoichiometric coefficients, $q > 0$ is the yield for the methane production, and $r_1(\xi), r_2(\xi)$ are the reaction rates defined as

$$r_1(\xi) = f_1(\xi_1)\xi_3, \tag{5.4}$$

$$r_2(\xi) = f_2(\xi_2)\xi_4, \tag{5.5}$$

where the growth functions, $f_1(\xi_1)$ and $f_2(\xi_2)$ are based on Monod and Haldane kinetics respectively as

$$\begin{aligned}
f_1(\xi_1) &= \mu_{m_1} \frac{\xi_1}{K_{s_1} + \xi_1}, \\
f_2(\xi_2) &= \mu_{m_2} \frac{\xi_2}{K_{s_2} + \xi_2 + \frac{\xi_2^2}{K_{i_2}}}.
\end{aligned} \tag{5.6}$$

A canonical state space transformation of the AD system can be obtained by considering the partition $\xi = [\xi_a \ \xi_b]^T$, where $\xi_a = [\xi_3 \ \xi_4]^T$

and $\xi_b = [\xi_1\ \xi_2]^T$, and a linear transformation of the states $x_a = \xi_a$ and $x_b = \xi_b - C_b C_a^{-1}\xi_a$ [Bastin and Dochain, 1990, Bastin and Van Impe, 1995] as

$$\begin{aligned} \dot{x}_a &= u(w_a - x_a) + C_a\rho(x), \\ \dot{x}_b &= u(w_b - x_b), \end{aligned} \tag{5.7}$$

where $x_a \triangleq [x_3\ x_4]^\top$ are the state variables that represent the acidogenic and methanogenic bacteria respectively, $x_b \triangleq [x_1\ x_2]^\top$, are the state variables that represent a linear combination of the four state variables, $C_a = I_2$, $\rho(x) \triangleq [\rho_1(x)\ \rho_2(x)]$ are the reaction rates, $w_a \triangleq [w_3\ w_4]^\top = [0\ 0]^\top$ are the concentrations of species in the input flow, $w_b \triangleq [w_1\ w_2]^\top = [\xi_{\text{in}_1}\ \xi_{\text{in}_2}]$ are the concentrations of substrates in the input flow,

$$C_b = \begin{bmatrix} -a & 0 \\ c & -d \end{bmatrix},$$

is the stoichiometric matrix, and the reaction rates in the canonical state space are

$$\rho_i(x) = r_i(\xi)|_{\xi_a = x_a;\ \xi_b = x_b + C_b C_a^{-1} x_a}\ ,\ i = 1, 2.$$

Unlike the four-state representation (5.2), the canonical state representation is a two-state variable nonlinear differential equation system in the bacterial populations x_a and a two-state linear differential equation where the state is a linear combination of species and substrates. This linear part is assumed to be fast in comparison with the nonlinear part and therefore its dynamics can be neglected for the analysis of the behavior of the system in the species concentration. As a consequence the problem reduces to a two-state system for which the analysis is easier and can be illustrated in 2D figures of the bacterial concentrations.

In general, the species measurements are not available. They often come from computer sensors from models such as [Bernard et al., 2001] whose identification comes from the available data such as gas flow-rate (sum of all gas compounds), the content of volatile suspended solids, volatile fatty acids, total organic carbon or chemical oxygen demand among others.

Table 5.1: Model parameters

a	42.14		K_{s_1}	7.1	g/l
c	116.15	mmol/g	K_{s_2}	9.28	mmol/g
d	268	mmol/g	K_{i_2}	256	mmol/g
μ_{m_1}	1.2	day^{-1}	ξ_{in_1}	[60 - 90]	g/l
μ_{m_2}	0.74	day^{-1}	ξ_{in_2}	[160 - 245]	mmol/l
q	453		u	[0.42 - 0.5]	day^{-1}

Depending on the magnitude of the dilution rate and substrate concentration at the inflow, the system may possess up to six equilibrium points. In [Sbarciog et al., 2010a] and [Shen et al., 2007], the authors present the regions in the input space for which various numbers of equilibria occur, and their stability. This analysis example will consider the multi-stability case, where there are two asymptotically stable equilibrium points, one representing the desired working point of the system, where the acidogenic and methanogenic bacteria coexist, and the other, the acidification point.

Consider the benchmark presented in [Sbarciog et al., 2010b] with system parameters as in Table 5.1, where the authors present the stability boundaries for the problem using backward integration. For the analysis, the value of the dilution rate is fixed at $u = 0.45$ [day^{-1}], and the concentration of substrates at the input are set in a grid, where $40 \leq w_1 \leq 70$ [g/l] and $170 \leq w_2 \leq 225$ [mmol/l]. This paper will not consider a unique dilution rate, instead, it considers a three dimensional grid of dilution rate, and input concentrations to perform the analysis.

Figure 5.1 depicts the phase plane orbits of bacteria population for different values of the inlet for the dilution rate and substrate concentration. The system has six equilibrium points: two asymptotically stable, the working point x_A^* in which the species coexist and the acidification point x_B^* of methanogenic wash-out. Additionally, the unstable saddle points are: the point that separates the two asymptotically stable x_C^*, the two acidogenic wash-out points x_D^*, x_E^*, and the total wash-out of the system x_F^*. Each of these points is of *type-k*, where k is the number of unstable modes of the equilibrium point.

The objective is to get the separation of the state space for the dif-

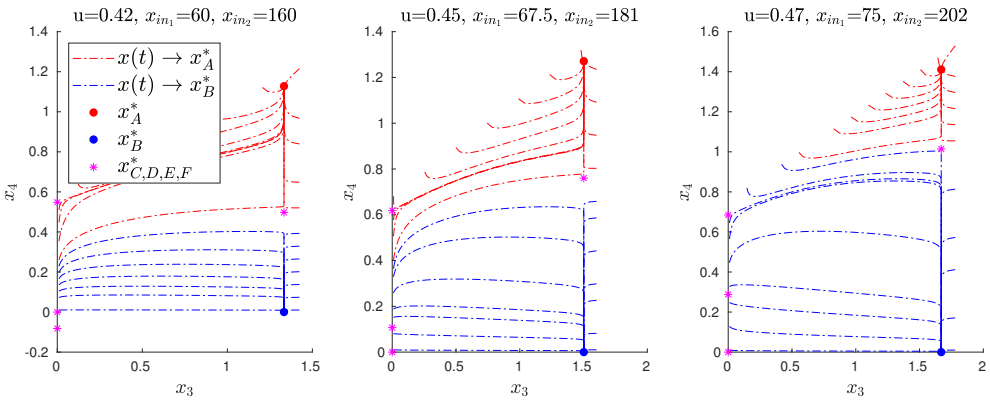

Figure 5.1: Phase plane, three different realizations of the anaerobic digestion process.

ferent parameterizations that specifies if an initial condition converges to either one of the asymptotically stable equilibrium points. Depending on the magnitude of the dilution rate and substrate concentration at the inflow, the system may possess up to six equilibrium points. In [Sbarciog et al., 2010a], the authors present the regions in the input space for which various numbers of equilibria occur and their stability.

5.2 Anaerobic Digestion Analysis

The Chapters sections present the necessary tools to perform the analysis, a methodology to get an approximation of the discrete-time Koopman operator based on orthogonal polynomials, and a couple of degree and dimension reduction methods. This representation gives the possibility to approximate the location of the fixed points of the system, provides their stability, and use the set of eigenfunctions with an associated eigenvalue equal to one in conjunction with the *type-one* saddle points in the boundary of the ROA to determine the convergence of an arbitrary point in the state space. In summary, the required steps to perform the analysis are:

1 From a set of system trajectories, and with the EDMD algorithm of Section 3.4, calculate the discrete-time approximation of the Koop-

man operator.

2 From the discrete-time representation, use (4.1) to find the fixed points of the system.

3 Calculate the Jacobian of (3.54), and evaluate it on the fixed points to get their local stability according to the spectral decomposition of the matrix. It is important to remark that these eigenvalues come from the classical stability analysis of linear systems, and are not related to the eigenvalues of the Koopman operator.

4 Analyze the ROA of the system. This includes finding an eigenfunction with associated eigenvalue equal to one for the case where the EDMD algorithm fails to provide an accurate one. This eigenfunction comes from (4.12).

Given that the anaerobic digestion system in its reduced form (5.2) is bistable under some operating conditions, where the separatrix between the stability regions is the stable manifold of a unique *type-one* saddle point, we can show the accuracy of the method analyzing this system.

Consider 100 different operating conditions of system (5.2) in a 3D grid of four different dilution rates u, five different values for the organic substrate ξ_{in_1} and five different values for the volatile fatty acids ξ_{in_2} with values given in Table 5.2.

5.2.1 Training and Testing Data

The EDMD algorithm captures the dynamics of the portion of the state space where the data for the calculation lies. For the case of the eigenfunctions that approximate the ROA of the process, it is especially important to have an even distribution of data on the portion of the state space subject to evaluation.

There are some geometrical properties that hold for the reduced Anaerobic Digestion System [Sbarciog et al., 2010a]. Specifically, it is important to note that the reduced system (5.2) is nonnegative by definition; concentrations cannot be negative, and the canonical representation

Table 5.2: Algorithm Parameters.

u	[0.42, 0.44, 0.44, 0.5]		
ξ_{in_1}	[60 67.5 75 82.5 90]		
ξ_{in_2}	[160.0 181.25 202.5 223.75 245.0]		
Polynomials	Hermite Legendre Laguerre Chebyshev first Chebyshev second Jacobi (1, 1) Jacobi (0.5, 1)		
p	[8 9 10 11]		
q	[0.6 0.7 0.8 0.9 1.0 1.1]		
	Min	Max	Average
Train points	2,943	5,237	3,811
Test points	3,253	5,877	4,199
Δt	0.1 [s]		

is also compartmental, where all the trajectories lie inside an invariant set S_x given by

$$S_x = \left\{ x \in \mathbb{R}^4 : \begin{array}{c} \xi_1 = x_1 - ax_3 \geq 0 \\ \xi_2 = x_2 + cx_3 \geq 0 \\ \xi_3 = x_3 \geq 0 \\ \xi_4 = x_4 \geq 0 \end{array} \right\}. \tag{5.8}$$

From the boundary given by this subspace of $\mathbb{R}^4$ we define a set of initial conditions for every one of the cases. Figure 5.2 depicts the selection of such initial conditions and their respective orbits for an arbitrary realization, specifically, for $u = 0.44$, $\xi_{in_1} = 90$, and $\xi_{in_2} = 245$. The uniform distribution of these initial conditions on the boundary gives enough snapshot data for the approximation and testing of the discrete-time Koopman operator.

Given that these trajectories come from the numerical integration of (5.7), an important consideration is the final integration time. The

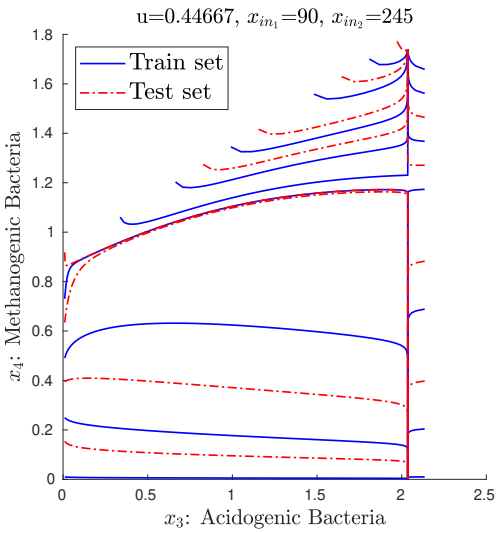

Figure 5.2: Training and testing sets of snapshots for the approximation of the discrete-time Koopman operator. Initial conditions are uniformly distributed in the boundary of S_x

integration algorithm[1] stops when a specific orbit is inside an ϵ-ball of the steady state because repeated data in the asymptotically stable fixed points affects the condition number of G in (3.39), and as a consequence it affects the accuracy of the approximation of the Koopman operator from (3.38). When the integration stops, the final Δt of the integration is inconsistent with the fixed time-step of the integration, therefore, affecting also the accuracy of the approximation. The solution to this problem is to discard the last value of every trajectory.

5.2.2 Approximating the Koopman operator

The first step to approximate the discrete-time Koopman operator is to define a set of orthogonal polynomials that act as observables for the system. Consider for example a set of Jacobi polynomials $\pi_\alpha^{(\eta,\nu)}(x)$ of

[1]MATLAB(R) ode23s

degree α with parameters η and ν that satisfy the differential equation

$$\begin{aligned} 0 =&(1-x^2)\frac{\mathrm{d}^2}{\mathrm{d}x^2}y(x) \\ &+(\eta-\nu-(\eta+\nu+2)x)\frac{\mathrm{d}}{\mathrm{d}x}y(x) \\ &+\alpha(\alpha+\eta+\nu+1)y(x). \end{aligned} \tag{5.9}$$

The solution of this differential equation for a set of nonnegative integers $\alpha_1 = \{0,\ 1,\ 2,\ 3\}$, and parameters $\eta = 0.5$ and $\nu = 1$ is summarized in Table 5.3, where the subscript on α indicates the univariate solutions for the first component of the state vector.

Table 5.3: Basis for the first state variable x_1. Solution to the Jacobi ODE with parameters $\eta = 0.5$ and $\nu = 1$.

$J(\alpha_1)$	$\pi_{\alpha_1}^{0.5,1}(x_1) = y(x_1)$
$J(0_1)$	1
$J(1_1)$	$7x_1/4 - 1/4$
$J(2_1)$	$99x_1^2/32 - 9x_1/16 - 21/32$
$J(3_1)$	$715x_1^3/128 - 143x_1^2/128 - 319x_1/128 + 27/128$

Every element of the polynomial basis comes from (3.58), which gives a total of 16 polynomial elements for the full basis without truncation that correspond to all the available combinations of the products between two univariate polynomials, i.e., the whole basis is

$$\Psi(x) = \begin{bmatrix} J(0_1)J(0_2) \\ J(1_1)J(0_2) \\ J(2_1)J(0_2) \\ \vdots \\ J(0_1)J(1_2) \\ J(1_1)J(1_2) \\ \vdots \\ J(3_1)J(3_2) \end{bmatrix} = \begin{bmatrix} 1 \\ 7x_1/4 - 1/4 \\ 99x_1^2/32 - 9x_1/16 - 21/32 \\ \vdots \\ 7x_2/4 - 1/4 \\ (7x_1/4 - 1/4)(7x_2/4 - 1/4) \\ \vdots \\ (715x_1^3/128 + \cdots + 27/128)(715x_2^3/128 + \cdots + 27/128) \end{bmatrix} \tag{5.10}$$

The first reduction method is to apply a truncation scheme on this basis. From the definition of the q-quasi norm in (3.60), and the p-q-quasi

norm truncation scheme in (3.61), take for example the values of $p = 3$ and $q = 0.5$ to reduce the degree and dimension of the basis. Figure 5.3 depicts the result of applying the truncation scheme, where the resulting number of polynomial elements is 8, effectively reducing the maximum degree from 6 to 3 and the dimension by half. The redefined basis for the observables is

$$\Psi(x) = \begin{bmatrix} J(0_1)J(0_2) \\ J(1_1)J(0_2) \\ J(2_1)J(0_2) \\ J(3_1)J(0_2) \\ J(0_1)J(1_2) \\ J(1_1)J(1_2) \\ J(0_1)J(2_2) \\ J(0_1)J(3_2) \end{bmatrix} = \begin{bmatrix} 1 \\ 7x_1/4 - 1/4 \\ 99x_1^2/32 - 9x_1/16 - 21/32 \\ 715x_1^3/128 - 143x_1^2/128 - 319x_1/128 + 27/128 \\ 7x_2/4 - 1/4 \\ (7x_1/4 - 1/4)(7x_2/4 - 1/4) \\ 99x_2^2/32 - 9x_2/16 - 21/32 \\ 715x_2^3/128 - 143x_2^2/128 - 319x_2/128 + 27/128 \end{bmatrix} \tag{5.11}$$

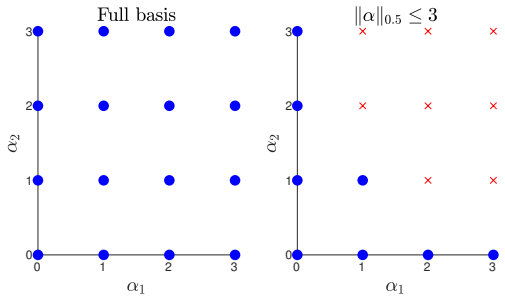

Figure 5.3: Full basis vs. truncated basis

With the definition of the train, test and observables set, the discrete-time approximation of the Koopman operator comes from the calculation of matrices A from (3.40), G from (3.39), and finally U_d from (3.38).

Recall that for the state evolution map of the approximation of the Koopman operator (3.54), and the error threshold (3.67) for the second reduction method, an elemental matrix B with l rows, and n columns where there is a single unitary element per column in the index of an injective observable needs to be defined to recover the state and set the error threshold for the elimination of polynomial elements. A simple

solution to this problem is to select the univariate polynomial elements of degree one as stated in (3.69) from the basis. This type of selection also gives the advantage that the inverse of the selected function by B is linear. By applying this criterion, in the application example,

$$B = \begin{bmatrix} 0 & 1 & 0 & 0 & 0 & 0 & 0 & 0 \\ 0 & 0 & 0 & 0 & 1 & 0 & 0 & 0 \end{bmatrix}^\top, \tag{5.12}$$

that selects the second and fifth element of the polynomial basis which are the univariate, order-one, and injective linear functions of the set of observables that define the set $\Psi_B(x) = [\psi_2(x),\ \psi_5(x)]$, and whose inverse gives the linear function of observations that recover the state as

$$\Psi_B^{-1} = \begin{bmatrix} \frac{1}{7}(4x_1 + 1) & \frac{1}{7}(4x_2 + 1) \end{bmatrix}. \tag{5.13}$$

With the definition of B, the approximation is further reduced via the second method, where the threshold for the elimination of polynomial elements from the basis comes from (3.66), and (3.67) as

$$\bar{\epsilon} = \max \left(\sum_{i=1}^{N} \|\psi_2(y_i) - U_{d_2}\Psi(x_i)\|_2^2, \tag{5.14}$$

$$\sum_{i=1}^{N} \|\psi_5(y_i) - U_{d_5}\Psi(x_i)\|_2^2 \right), \tag{5.15}$$

giving a lower degree, and reduced order approximation of the discrete-time Koopman operator that accurately satisfies condition (3.36) for the set of observables.

With the reduced discrete-time Koopman operator matrix U_d, the set of observables $\Psi(x)$, the set $\Psi_B(x)$, and its corresponding inverse, the linear predictor that approximates the dynamics of the system from an arbitrary initial condition comes from (3.54). Although it is useful to have this linear approximation of the evolution of the states according to the spectral decomposition of the discrete-time approximation of the Koopman operator, in practice, it is enough to use a linear predictor based on the original set of observables as in (3.36). Considering again that $y = T^k(x)$,

$$\Psi_B(x_k) = (U_d^k \Psi(x_0))^\top B \tag{5.16}$$

$$y = \Psi_B^{-1}(\Psi_B(x_k)). \tag{5.17}$$

Equation (5.16) is linear, and describes the linear evolution of observations of the state space. Along with matrix B, it only describes the linear evolution of a set of injective functions whose inverse recovers the state. Given that B selects the order-one observables, (5.17) is also a linear function. The benefit of having the evolution according to the polynomial basis of observables instead of the eigenfunctions of the discrete-time approximation of the Koopman operator is in terms of accuracy. Equation (3.54) needs the left eigenvectors W^* of matrix U_d to get the eigenfunctions as in (3.50), and the right eigenvectors Ξ to recover the value of the evolved observations. To have this full representation it is necessary to calculate the inverse of Ξ, adding additional error because of the numerical approximation of the higher order inverse. As a consequence, the set of eigenfunctions also suffer accuracy issues. For eliminating this induced numerical error, the solution is to get matrix W^* as the right eigenvectors of $U_d^\top$, and apply (3.50) to get the eigenfunctions.

Using the linear evolution of observables (5.16) and (5.17) instead of eigenfunctions, the linear predictor for the case of Jacobi polynomials (5.11) is

$$\begin{aligned}\Psi_B(x_k) =&(U_d^k\Psi(x_0))^\top B\\ =&\begin{bmatrix}U_{d_2}\Psi(x_0) & U_{d_5}\Psi(x_0)\end{bmatrix} &(5.18)\\ y =&\begin{bmatrix}\frac{1}{7}(4U_{d_2}\Psi(x_0)+1) & \frac{1}{7}(4U_{d_5}\Psi(x_0)+1)\end{bmatrix}. &(5.19)\end{aligned}$$

In conclusion, these changes in the computation of the approximation give a linear predictor and a set of eigenfunctions that do not have an additional inverse numerical error.

There are still some open problems to solve in the approximation of the discrete-time Koopman operator. For our particular case, in which we select a type of orthogonal polynomial and then apply a p-q-quasi norm truncation scheme, there is no current solution to determine the type of polynomial, and the values of the p-q parameters that give the best performance. Therefore, we perform the approximation of the discrete-time Koopman operator for different types of polynomials with different values for the p-q parameters and evaluate their performance using the empirical error (3.56) to select the suboptimal polynomial type and parameter values. Table 5.2 shows the different type of polynomials, the values

for the p-q sweep, and the minimum, maximum, and average number of training and testing points.

Table 5.4 shows the result of averaging the empirical error given by every one of the polynomials, and the total time required to perform the calculation[2]. Despite the fact that a Legendre polynomial has the lowest average empirical error within the set, there are some cases where the accuracy of the Legendre polynomial basis does not hold well enough to determine an accurate classifier.

Table 5.4: Grid optimization results for different types of polynomials.

Polynomial	**Av. error**	**Time [m]**
Hermite	0.89	31
Legendre	0.64	31
Laguerre	2.75	44
Chebyshev first	0.77	29
Chebyshev second	0.76	30
Jacobi (1, 1)	0.71	31
Jacobi (0.5, 1)	0.67	42

Figure 5.4 shows the empirical error for each of the parameterizations in the grid, for the case, $u = 44$, $\xi_{in_1} = 82.5$, and $\xi_{in_2} = 223.75$, the Legendre polynomial has an error of 1.65, that is high enough for the EDMD algorithm not to give an accurate approximation of the discrete-time Koopman operator. Therefore, the selection of the type of basis for the whole analysis is Jacobi with parameters $\eta = 0.5$, and $\nu = 1$. Note that some of the cases have a greater empirical error in which the approximation is not ideal. The reason to have these inconsistencies in the results will be covered in the next section.

5.2.3 Discrete-Time Approximation Result

Recall from Theorem 3.2.1, and Definitions 4.4.1 and 4.4.2 that it is necessary to have an accurate location and stability of the fixed points of the system. Either to determine the stable manifold of the *type-one*

[2]Intel(R) Core(TM) i7-7567U CPU @ 3.50GHz, 16GB DDR4 RAM @ 2400MHz

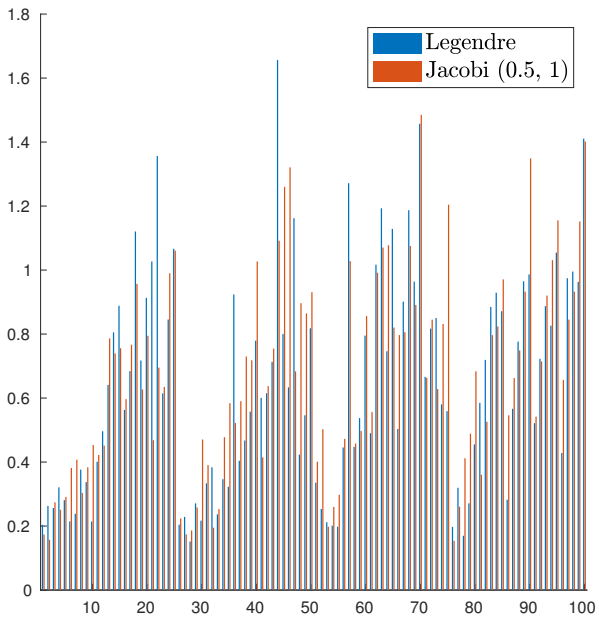

Figure 5.4: Empirical error for every test of the 3D grid of parameterizations.

saddle points in the boundary of the ROA for the classification criterion 4.4.1, or to apply the classification criterion 4.4.2 on the asymptotically stable ones.

For either of the classification criteria to perform correctly it is only necessary to get the location and stability of the working point x_A^*, the acidification point x_B^*, and the point that separates these two x_C^*. Recall from Section 4.1 that the fixed points are given by the solution of (4.1), and in practice, the solution to this equation from different start points gives the whole set of fixed points according to the discrete-time approximation of the Koopman operator. The starting points for the identification of the fixed points come from the trajectories of the test set, where the initial condition of every trajectory is a starting point for the solution. In addition to these points, and for this particular case it was necessary to select a random point along these trajectories because counting only with the initial conditions, there was no available starting point that gave an identification of the acidification wash-out point. Table 5.5 shows the results of applying (4.1) to the selected initial conditions.

Table 5.5: Anaerobic digestion fixed points for $u = 0.47$, $x_{in_1} = 75$, and $x_{in_2} = 160$.

	Theoretical	Algorithmic	
x_A^*	(1.67, 1.25)	(1.67, 1.25)	Working point
x_B^*	(1.67, 0.00)	(1.67, 0.00)	Acidification
x_C^*	(1.67, 0.86)	(1.67, 0.86)	Separation saddle
x_D^*	(0.00, 0.13)	(0.00, 0.19)	Acidogenic wash-out
x_E^*	(0.00, 0.53)	(0.00, 0.53)	Acidogenic wash-out
x_F^*	(0.00, 0.00)	(0.00, 0.02)	Wash-out

For the stability of the fixed points, consider the linear evolution of observations (5.19) and definition 4.2.1. The application of (4.5) on (5.19), and with $U_d = (U_{i,j})$, the Jacobian matrix $J = (J_{i,j})$ for the nonlinear evolution operator on the states is

$$J_{1,1} = U_{2,2} + \frac{1}{4}U_{2,6}\left(7x_2 - 1\right) + \frac{4}{7}\left(U_{2,3}\left(\frac{99x_1}{16} - \frac{9}{16}\right) - U_{2,4}\left(-\frac{2145{x_1}^2}{128} + \frac{143x_1}{64} + \frac{319}{128}\right)\right) \tag{5.20}$$

$$J_{1,2} = U_{2,5} + \frac{1}{4}U_{2,6}\left(7x_1 - 1\right) + \frac{4}{7}\left(U_{2,7}\left(\frac{99x_2}{16} - \frac{9}{16}\right) - U_{2,8}\left(-\frac{2145{x_2}^2}{128} + \frac{143x_2}{64} + \frac{319}{128}\right)\right) \tag{5.21}$$

$$J_{2,1} = U_{5,2} + \frac{1}{4}U_{5,6}\left(7x_1 - 1\right) + \frac{4}{7}\left(U_{5,3}\left(\frac{99x_2}{16} - \frac{9}{16}\right) - U_{5,4}\left(-\frac{2145{x_2}^2}{128} + \frac{143x_2}{64} + \frac{319}{128}\right)\right) \tag{5.22}$$

$$J_{2,2} = U_{5,5} + \frac{1}{4}U_{5,6}\left(7x_1 - 1\right) + \frac{4}{7}\left(U_{5,7}\left(\frac{99x_2}{16} - \frac{9}{16}\right) - U_{5,8}\left(-\frac{2145{x_2}^2}{128} + \frac{143x_2}{64} + \frac{319}{128}\right)\right). \tag{5.23}$$

Evaluating the identified fixed points in the Jacobian matrix and getting the respective eigenvalues give their local stability. Table 5.6 shows the result of this process for the same arbitrary case of the anaerobic digestion system. These results come from a Jacobi polynomial basis with $\eta = 0.5$, $\nu = 1$, $p = 9$, and $q = 0.7$.

Figure 5.5 shows the theoretical and approximated fixed points of an arbitrary realization of the anaerobic digestion system from the solution of (5.5) from 24 initial conditions. These come from the orbits of the train set, one for every starting point of the train set, and one from an arbitrary point along those trajectories. The error of the working point,

Table 5.6: Anaerobic digestion fixed points stability for $u = 0.47$, $x_{in_1} = 75$, and $x_{in_2} = 160$.

	$\lvert\lambda_1\rvert$	$\lvert\lambda_2\rvert$	Stability
x_A^*	0.6448	0.8210	AS
x_B^*	0.6444	0.9834	AS
x_C^*	0.6443	1.0212	Saddle
x_D^*	1.0160	1.0596	Unstable
x_E^*	0.9318	1.0597	Saddle
x_F^*	0.9554	1.0589	Saddle

the separating saddle and the acidification point is low enough for every realization of the system for an accurate analysis of the ROA.

The results of approximating the discrete-time Koopman operator are summarized in Figure 5.6 that shows in the first row the most accurate realizations of the anaerobic digestion system, and in the second row, the realizations with the highest empirical error. Although the trajectories for the training set of each of the cases come from the same parameterization for the process with a different value for the dilution rate and input concentrations, not all of the orbits for the training set give the same amount of information. The reduced, nonlinear canonical model for the anaerobic digestion system (5.7) has a bifurcation phenomenon for the fixed points depending on the input parameters [Sbarciog et al., 2010a]. For the bi-stability case, the displacement of the separating saddle x_C^* is directly proportional to the values of input concentrations, especially for the volatile fatty acids concentration ξ_{in_2} (see Figure 5.1). As a consequence, the size of the ROA for the asymptotically stable fixed points changes. The fact that the selection of initial conditions for all the realizations is uniform along the boundary of the state space, makes the available data for the acidification ROA scarce, and reduces the accuracy of the algorithm. A solution to this problem is to generate the data with an experimental design that gives enough information on both regions. The reason to avoid that approach is because for our particular case, it defeats the purpose of analyzing the system without prior knowledge of the system, otherwise we would have to know the ROA to find the ROA.

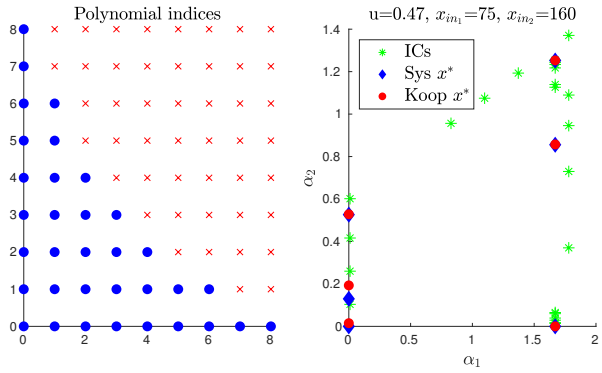

Figure 5.5: Location of fixed points in the state space from the solution of the minimization problem (4.1) from different initial conditions.

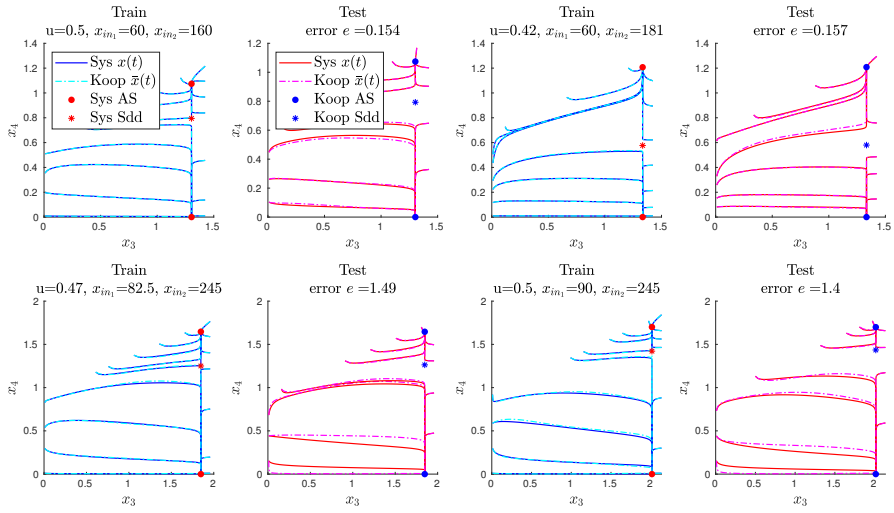

Figure 5.6: Training orbits, testing orbits, and fixed points with their respective approximations based on Koopman linear predictor and analysis algorithms.

5.2.4 Approximating the ROA

The spectral decomposition of the discrete-time approximation of the Koopman operator gives a set of eigenvalues with their respective eigenfunctions. In the approximation from a Jacobi-type polynomial basis, and under the selected p-q sweep, each of the system gets a subset of the eigenfunctions with a unitary or near unitary eigenvalue. For the reduced-order anaerobic digestion system, and under the selected set of orbits for the approximation of the Koopman operator, the set of eigenfunctions is rich enough so that it contains at least one unitary eigenfunction that characterizes the stable manifold of the separating saddle point for the classification of an arbitrary initial condition. If that was not the case, the eigenfunction with unitary associated eigenvalue comes from (4.12). Several tests over the construction of unitary eigenfunctions suggest that selecting the eigenfunctions with a real valued eigenvalue closest to one improves the performance of the algorithm. Also note that (4.12) has an infinity solutions, and as a consequence not all eigenfunctions constructed this way give an accurate result. The selection of the base eigenfunctions and the solutions to the construction to guarantee an accurate approximation for either of the selection criteria is still an open question.

Also, it is important to note that the constant eigenfunction is also part of the unitary eigenfunctions set, i.e., $\phi_+(x) = 1$. In particular, because of the presence of the constant observable when approximating the discrete-time Koopman operator, this trivial eigenfunction is often present in the approximation. As a result, the eigenfunction that gives an accurate classification is a near unitary, or a constructed one.

In this case, and for the 100 different parameterizations, the approximation of the discrete-time Koopman operator gives a set of eigenfunctions whose unitary or near unitary eigenvalue give an accurate classification by the saddle selection rule (4.4.1). This result is depicted in Figure 5.7, where the associated eigenvalue is real, exactly one, and whose associated eigenfunction is nontrivial. The accuracy of this eigenfunction and the application of the saddle classification rule is the comparison of an additional test set of 900 initial conditions of the state space against the algorithm. For the realization under consideration, the error is 3 misclassified initial conditions out of the 900.

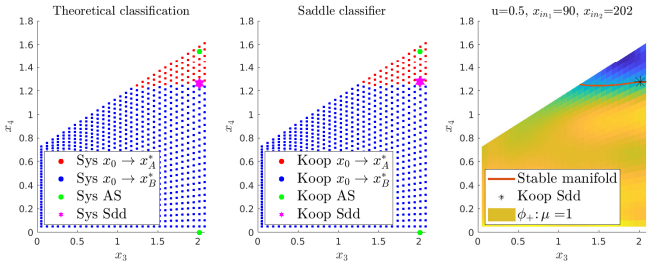

Figure 5.7: Saddle based classification for $u = 0.5$, $\xi_{in_1} = 90$ and $\xi_{in_2} = 202$.

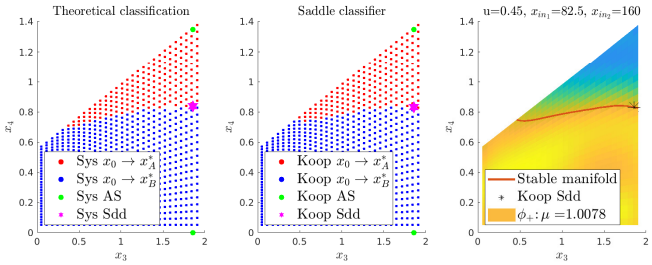

Figure 5.8: Saddle based classification for $u = 0.45$, $\xi_{in_1} = 82.5$ and $\xi_{in_2} = 160$.

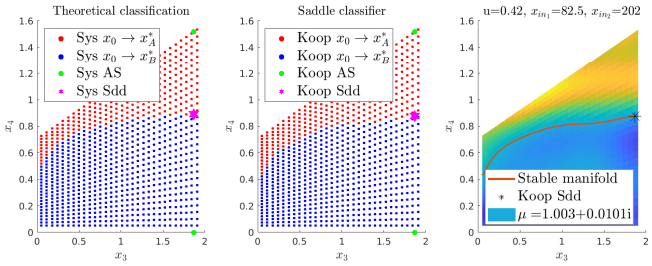

Figure 5.9: Saddle based classification for $u = 0.42$, $\xi_{in_1} = 82.5$ and $\xi_{in_2} = 202$.

Consider next a realization where the approximation of the discrete-time Koopman operator gives a real valued nontrivial eigenfunction that has an associated eigenvalue near unitary, i.e., $\mu = 1.0078$. Figure 5.8 that although the accuracy decreases, the number of misclassified initial conditions is seven out of 900, it is still a good approximation of the stable manifold and the convergence of an arbitrary initial condition in the state space.

For illustration purposes, consider now a case where the associated eigenvalue is not real valued or unitary, where $\mu = 1.003 + 0.0101i$. The eigenfunction along with the saddle classification algorithm gives an error of 35 misclassified initial conditions out of 900 where the result is given in Figure 5.9. It shows that the eigenfunction is not monotonic with respect to x_4, and although the approximation of the stable manifold is accurate, and the non-monotonic portion is completely below the threshold given by the real part of the eigenfunction evaluated at the saddle point. If that was not the case the eigenfunction would give a classification error in the ROA of x_A^*.

Recall from Section 5.1 that the driving forces in the reduced anaerobic digestion process are the dilution rate, which is the controlled input of the process, and the uncontrolled fluctuations of inlet organic matter and volatile fatty acids concentration. These driving forces produce a displacement of the fixed points, and consequently a displacement of the stable manifold of the separating saddle point in the boundary of the ROA [Shen et al., 2007]. Additionally, consider the canonical system representation as it allows for graphical representations of the bacterial dynamics in a 2D plane. As a consequence the movement of the separating saddle stability boundary can be illustrated in $x_3 - x_4 - x_i$ 3D plots where $x_i = \{u, \xi_{in_1}, \xi_{in_2}\}$ that sweep over one of the parameters while the other two are constant.

Figure 5.10 illustrates two different cases for the $x_3 - x_4 - u$ case, varying the dilution rate between $0.42 \leq u \leq 0.54$ as shown in Table 5.2 and keeping constant values of $\xi_{in_1} = \{90, 82.5\}$, and $\xi_{in_2} = \{160, 224\}$. The plot shows the displacement of the fixed points, especially how the stable manifold and the working point x_A^* move toward each other in the x_4 axis, decreasing the methane production rate according to (5.3), and reducing the portion of the state space that converges to the working

point.

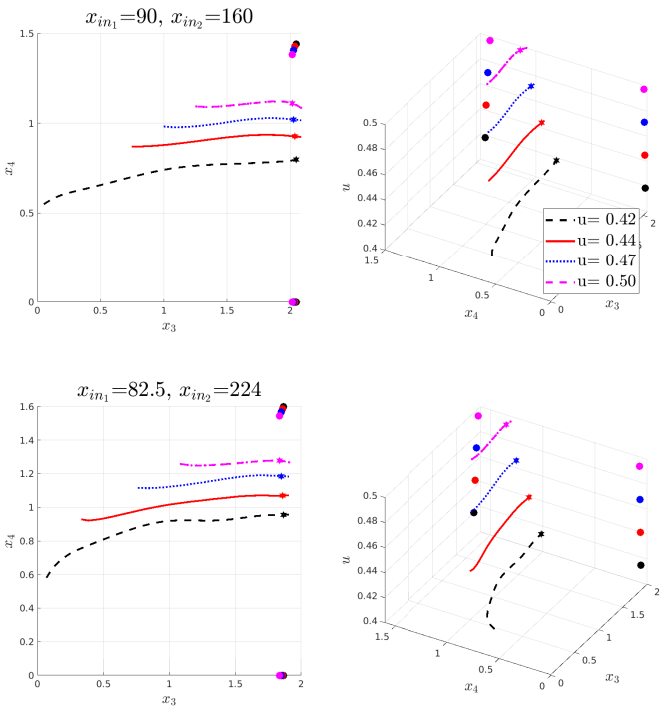

Figure 5.10: Intersection of the stable manifold for different realization with different concentrations ξ_{in_1}, constant dilution rant and concentration ξ_{in_2} at the input.

Consider now the $x_3 - x_4 - \xi_{in_1}$ that describes an increase in the organic matter input concentration as $60 \leq \xi_{in_1} \leq 90$ for the values given in Table 5.2 for two different constant values of dilution rate and volatile fatty acid concentration of $u = \{0.447, 0.473\}$, and $\xi_{in_2} = \{160, 224\}$, using the same fixed values for the input concentration as the previous case. Figure 5.11 depicts the approximation of the stable manifold of the dividing saddle, and shows that the relation between the organic matter and the dividing saddle is directly proportional in both axis. As a consequence, an increase in the organic matter concentration at the input has the potential of increasing the methane production with the drawback of having a reduction of the working point ROA.

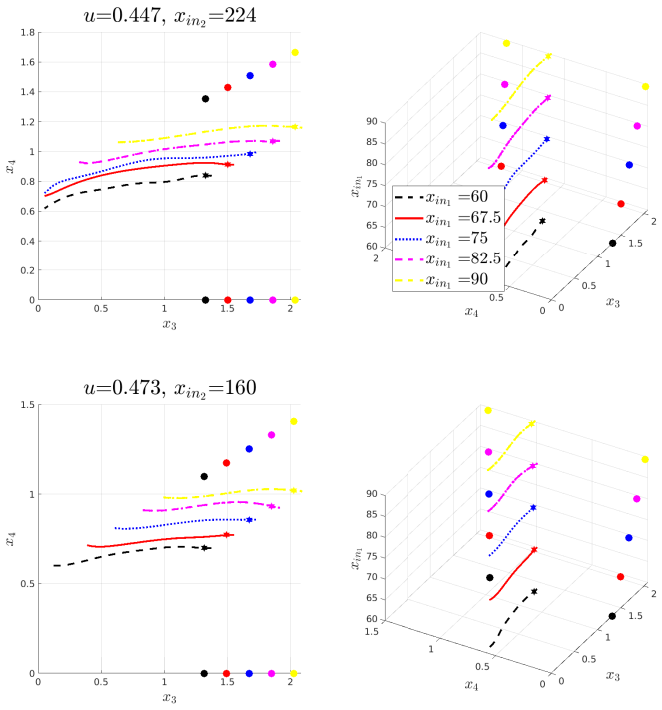

Figure 5.11: Intersection of the stable manifold for different realization with different u, and constant concentrations at the input.

The final case considers the same constant values for the organic matter concentration at the input feed of $\xi_{in_1} = \{90, 82.5\}$ as in the first case, and evaluates two different values of the dilution rate $u = \{0.447, 0.5\}$ while varying the values of volatile fatty acids concentration in the input feed given by Table 5.2, i.e., $160 \leq \xi_{in_2} \leq 245$. Figure 5.12 shows the approximation of the dividing saddle stable manifold that gives the boundary of the ROA for the asymptotically stable fixed points. In this case, the movement of the stable manifold and the working point are on the x_4 axis and is directly proportional to the volatile fatty acids concentration at the input. As a consequence, there is an increase in the methane production and a reduction of the effective state space that converges to the working point.

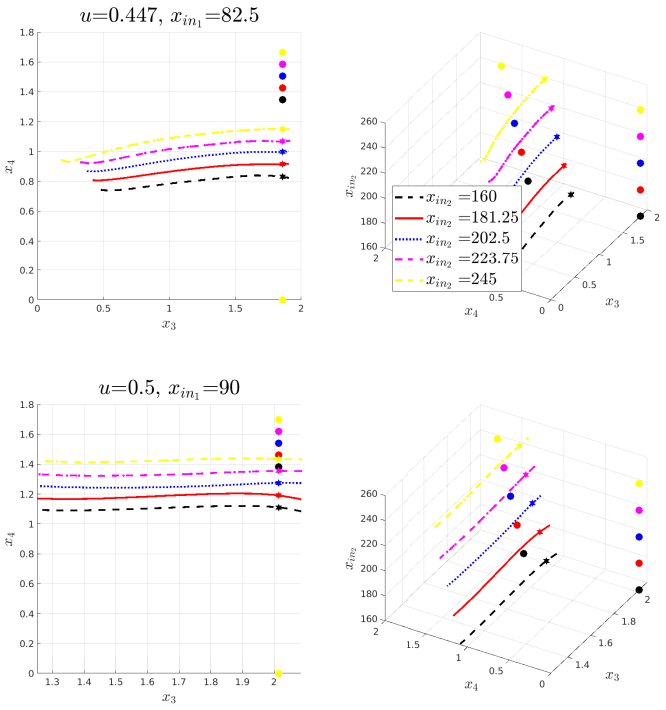

Figure 5.12: Intersection of the stable manifold for different realizations with different x_{in_2}, constant dilution rate and x_{in_1} concentration at the input.

5.3 Discussion

In general, not only for the case of the anaerobic digestion system, the analysis of the ROA is static, that is, it comes from a fixed value of the input. For the process at hand these are the input concentrations of substrates and the dilution rate. The rationale behind this approach is the movement and bifurcation phenomena present in the equilibrium points of nonlinear systems. For example, consider the movement of the fixed points with respect to the input concentrations and dilution rate as depicted in Figures 5.10 to 5.12. The working point ROA size is inversely proportional to all the variations in the input, while the converse applies for the movement of the working point. Meaning that

a transient and steady state optimization of biogas production benefits from a dynamical analysis instead of a static one, which can reduce the computational burden for this type of optimizations, and can improve the current heuristic approach [Sbarciog et al., 2011].

Under the Koopman operator approach and the discrete-time approximation given by the EDMD algorithm, it is possible to formulate an expansion of the state space defined as the product of the original space and the input space, which is equivalent to setting the inputs as state variables without specific dynamics. Using a polynomial expansion on the input space rather than considering the approximation given by Korda [Korda and Mezić, 2018b] as an input affine system gives the possibility to handle it as a closed one, and as a consequence, analyze the movement of the equilibrium points and the stability boundary in a dynamic way.

The approximation of the discrete-time Koopman operator, either in static or dynamic ways via the EDMD algorithm still has some important problems to be resolved. The first one is the amount of necessary data to have an accurate representation. For the anaerobic digestion process at hand, the analysis is possible based on a process model that can be numerically integrated from a set of initial conditions. Even though the reduction methods and the possibility to test with different polynomials gives an accurate representation with a reasonable amount of data, the analysis would be unfeasible if the solely available trajectories come from a real digester.

Additionally, the type of data available also poses a problem for the analysis given that the species concentrations are not commonly available, whereas the biogas outflow is. Meaning that the algorithm needs to be extended so that the eigenfunctions from an approximation with partial information are still able to capture the dynamic behavior of the system to approximate all the necessary information: fixed points, stability, unitary eigenfunctions, and classification criteria. Furthermore, for the dynamical analysis, it is necessary to get a classification criterion that not only depends on the current state but also depends on the input concentrations and dilution rate of the system.

The analysis provides a clear criterion that does not depend on the specific geometry of a manifold or the ability to calculate level sets and interpolate between data-points for the classification of an arbitrary point

in the state space. As a result, the analysis can be extended to models with more than two reactions and state variables while preserving a clear and simple criterion for the classification.

Given that it is difficult and costly to acquire data from a reactor, this approach also opens up the possibility of developing an analysis based on the commonly available measurements such as the flow of biogas at the output. To make that possible, it is necessary that the approximation and reduction techniques presented here are extended so that they achieve an accurate approximation of the discrete-time Koopman operator for a reduced set of forced system trajectories.

Chapter 6

Conclusions & Perspectives

The development of the thesis began with an exploratory process of the available literature to analyze and control interconnected dynamical systems. Part of this inquiry were the traditional techniques for model-based and input-output analysis. Dissipativity, passivity, population dynamics and Lyapunov based techniques for the model-based analysis, and techniques for the solution of the Lur'e problem, from the circle criterion up to integral quadratic constraints for the input-output analysis. In addition to the model based techniques, and in the search for a data-driven alternative able to provide analysis tools for the non-linear dynamical systems, this exploration led to the finding of the Koopman operator and its approximation via the EDMD algorithm. Upon further research, and considering the potential that the Koopman operator has to analyze the associated spectrum of the discrete-time operator, its eigenvalues and eigenfunctions, and the potential that the linear predictors from the EDMD have to synthesize controllers, the thesis took upon this path as the selected method to achieve the objectives.

The theory regarding the Koopman operator is a powerful tool that is still in its infancy with a lot of potential to tackle on the plethora of problems regarding the subject matter of control systems analysis and synthesis. However, the closed and analytical Koopman operator representation is only available for a small family of polynomial systems, making it a must, the development of tools to accurately approximate it.

Currently, the best tool for the task of approximating the Koopman

operator is the EDMD algorithm, that is at a similar stage of development as the operator, i.e., in its early stages. There are still several problems to solve within the method, where the main one is the selection of observables. Due to this problem, this work focused on the available tools to improve the selection of observables where it achieved results in the reduction of the dimension of the bases, and a reduction of their maximum order using orthogonal polynomials. Even though the incorporation of these methods results in accurate approximations of the EDMD and Koopman operator, where there is a substantial reduction in the necessary amount of data, there are still some open problems regarding this selection. Currently, the best approximation comes from a p-q-quasi norm parametrization of a particular orthogonal polynomial, where the suboptimal p-q parameters come from a sweep over different values, meaning that there is no systematic approach based on the characteristics of the system or from the analysis of the available data that can give an optimal results for this method. In addition to the parameter sweep, there is also a one for the available families of polynomials (Hermite, Laguerre, etc.), meaning that the problem of the relation between the dynamic of the system and a particular polynomial is still an open question, i.e., which is the best family for a particular problem?

Another of the EDMD problems is the numerical stability of the algorithm, where the problem is in the inverse of matrix G, arguably, the foundation of the algorithm. As a consequence, the inversion of this matrix has to rely on a Moore-Penrose pseudo-inverse, instead of an inverse. The reason for this phenomena is the poor condition number that the matrix has after the selection of the observables and the evaluation of the available data for training the algorithm. Again, a partial solution of this problem comes from the use of orthogonal polynomials and their reduction methods, with the caveat that is not a complete solution because the problem is present even with these polynomials. Another approach to work on this problem was to track its origin, leading to the proposition that the data samples must be devoid of redundant data, this gave the solution of truncating the samples once they reach a stable point. This solution led to another numerical inconsistency: this truncation meant that the last sample of the series is not one whole time-step away from the penultimate, where the solution is to eliminate the last sample. In relation to these sample-data problems, the selection of initial conditions

for the case where the samples come from a numerical integration, or the experimental design when they come from a real system is also important to consider. This work deals with the numerical integration in most of the illustrations (except in the approximation of the dynamics of the pendulum), where the solution is to randomly select initial conditions with a uniform distribution. Although the algorithm shows good results with this method, there is still an open question regarding a systematic approach to select a set of initial conditions that can give more information to the algorithm, as well as reducing the necessary amount of data to have an accurate approximation.

Having an accurate approximation of the dynamics of the system via the EDMD algorithm does not guarantee an accurate approximation of the point spectrum of the Koopman operator. As a consequence of this discrepancy, and given the fact that in the dimensional limit of the set of observables there is a better approximation of the point spectrum of the operator, there is a compromise between basis dimension and operator accuracy. For the most part, the improvements of the EDMD algorithm developed in this work focus on basis reduction methods that uses an error related to the accuracy of the linear predictors, consequently, the algorithm reduces the accuracy of the approximation to the operator. Therefore, there is an open field of research regarding methods to have better approximations of the operator with the EDMD algorithm.

Given all of the aforementioned drawbacks, the focus of the thesis turned into the improvement of the EDMD algorithm to circumvent them. Giving rise to the use of p-q-quasi norms, the reduction by polynomial accuracy, the inverse of order one univariate polynomial elements to recover the state, trigonometric embeddings and data management. With these developments the accuracy of the predictors and the approximation of the Koopman operator had significant improvements, both in the error metrics that determine their effectiveness, and in the reduction of the necessary amount of trajectories, and therefore the amount of data-points for the approximations. Without the developments proposed by the thesis, the method to approximate the boundary of the ROA in the multi-stability analysis problem, would be just a theoretical possibility instead of a thoroughly tested algorithm. Among the most important achievements of the process to approximate the ROA is the fact that it can handle complex systems with more than a couple of state

variables and with several asymptotically stable fixed points. Additionally, it shows potential for the solution of real problems like the static analysis of the anaerobic digestion process.

In conclusion, there is still a long way to consider the EDMD algorithm and the theoretical concepts of the Koopman operator mature tools. Although the recent contributions for the analysis of dynamical systems are growing and becoming widespread, the forecast for these tools, that are expected to bring some of the numerous methods of linear systems into these linear transformations is still not yet fulfilled. Moreover, while synthesis tools are limited to MPC, the availability of the point spectrum of the Koopman operator is not yet exploited, in contrast with the linear systems tools that heavily rely on the spectral decomposition of the state transition matrix. As a consequence, the research to close this gap offers endless possibilities. In that regard, the main contribution of this thesis is grounding the algorithmic methods such that they become widespread in the control systems community and hopefully get more attention and traction for their further development.

Bibliography

Amir Ali Ahmadi and Pablo A. Parrilo. Converse results on existence of sum of squares Lyapunov functions. In *IEEE Conference on Decision and Control and European Control Conference*, pages 6516–6521, Orlando FL, USA, dec 2011. IEEE. ISBN 978-1-61284-801-3.

James Anderson and Antonis Papachristodoulou. Dynamical system decomposition for efficient, sparse analysis. In *49th IEEE Conference on Decision and Control (CDC)*, pages 6565–6570, Atlanta GA, USA, dec 2010. IEEE. ISBN 978-1-4244-7745-6.

Jacqueline Augusiak, Paul J. Van den Brink, and Volker Grimm. Merging validation and evaluation of ecological models to 'evaludation': A review of terminology and a practical approach. *Ecological Modelling*, 280:117–128, 2014.

G. Bastin and D. Dochain. *On-line Estimation and Adaptive Control of Bioreactors*. Elsevier, Amsterdam, 1990.

G. Bastin and J.F. F. Van Impe. Nonlinear and Adaptive Control in Biotechnology: A Tutorial. *European Journal of Control*, 1(1):37–53, jan 1995.

Richard Bellman. Vector Lyanpunov Functions. *Journal of the Society for Industrial and Applied Mathematics Series A Control*, 1(1):32–34, jan 1962. ISSN 0887-4603.

Olivier Bernard, Zakaria Hadj-Sadok, Denis Dochain, Antoine Genovesi, and Jean Philippe Steyer. Dynamical model development and

parameter identification for an anaerobic wastewater treatment process. *Biotechnology and Bioengineering*, 75(4):424–438, 2001. ISSN 00063592.

Steven L. Brunton, Bingni W. Brunton, Joshua L. Proctor, and J. Nathan Kutz. Koopman invariant subspaces and finite linear representations of nonlinear dynamical systems for control. *PLoS ONE*, 11(2):1–19, 2016a.

Steven L. Brunton, Joshua L. Proctor, and J. Nathan Kutz. Discovering governing equations from data by sparse identification of nonlinear dynamical systems. *Proceedings of the National Academy of Sciences*, 113(15):3932–3937, apr 2016b.

Marko Budišić, Ryan Mohr, and Igor Mezić. Applied koopmanism. *Chaos: An Interdisciplinary Journal of Nonlinear Science*, 22(4): 47510, 2012.

Vijaysekhar Chellaboina, Sanjay Bhat, Wassim Haddad, and Dennis Bernstein. Modeling and analysis of mass-action kinetics. *IEEE Control Systems Magazine*, 29(4):60–78, aug 2009.

H D Chiang and L F C Alberto. *Stability Regions of Nonlinear Dynamical Systems: Theory, Estimation, and Applications*. Cambridge University Press, 2015. ISBN 9781316374320.

Edson A. Coayla-Teran, S. E A Mohammed, and P. R C Ruffino. Hartman-Grobman theorems along hyperbolic stationary trajectories. *Discrete and Continuous Dynamical Systems*, 17(2):281–292, 2007.

Federico Cuesta, Francisco Gordillo, Javier Aracil, and Anibal Ollero. Stability analysis of nonlinear multivariable Takagi-Sugeno fuzzy control systems. *IEEE Transactions on Fuzzy Systems*, 7(5):508–520, 1999.

David Di Ruscio. Model Predictive Control with Integral Action: A simple MPC algorithm. *Modeling, Identification and Control*, 34(3): 119–129, 2013.

Georgi M Dimirovski. *Complex Systems: Relationships between Control, Communications and Computing*, volume 55. Springer, 2016.

Tanja Eisner, Bálint Farkas, Markus Haase, and Rainer Nagel. *Operator Theoretic Aspects of Ergodic Theory*, volume 272 of *Graduate Texts in Mathematics*. Springer International Publishing, Cham, 2015.

Nesma ElKalaawy and Amr Wassal. Methodologies for the modeling and simulation of biochemical networks, illustrated for signal transduction pathways: A primer. *BioSystems*, 129:1–18, 2015.

Martin Feinberg. Chemical reaction network structure and the stability of complex isothermal reactors-I. The deficiency zero and deficiency one theorems. *Chemical Engineering Science*, 42(10):2229–2268, 1987. ISSN 00092509.

C. Garcia-Tenorio, D. Tellez-Castro, E. Mojica-Nava, and A. Vande Wouwer. Analysis of hyperbolic systems via data-driven koopman operator. *Submitted to Applied Mathematics and Computation*, 2020.

Camilo Garcia-Tenorio, Nicanor Quijano, Eduardo Mojica-Nava, and Jorge Sofrony. Bond graph model-based for IDA-PBC. In *2016 IEEE Conference on Control Applications (CCA)*, pages 1098–1103. IEEE, sep 2016. ISBN 978-1-5090-0755-4.

Camilo Garcia-Tenorio, Duvan Tellez-Castro, Eduardo Mojica-Nava, and Alain Vande Wouwer. Analysis of a Class of Hyperbolic Systems via Data-Driven Koopman Operator. In *International Conference on System Theory, Control and Computing (ICSTCC)*, pages 566–571, 2019.

Hugues Garnier and Liuping Wang, editors. *Identification of Continuous-time Models from Sampled Data*. Advances in Industrial Control. Springer-Verlag London, London, 1 edition, 2008.

Peter Giesl and Sigurdur Hafstein. Review on computational methods for Lyapunov functions. *Discrete and Continuous Dynamical Systems-Series B*, 20(8):2291–2331, 2015.

L. Grujic and D. Siljak. Asymptotic stability and instability of large-scale systems. *IEEE Transactions on Automatic Control*, 18(6):636–645, dec 1973. ISSN 0018-9286. URL `http://ieeexplore.ieee.org/document/1100422/`.

Wassim M Haddad and VijaySekhar Chellaboina. *Nonlinear dynamical systems and control : a Lyapunov-based approach*. Princeton University Press, 2008. ISBN ISBN-13: 978-0-6911-3329-4.

P. Ioannou. Decentralized adaptive control of interconnected systems. *IEEE Transactions on Automatic Control*, 31(4):291–298, apr 1986. ISSN 0018-9286. URL `http://ieeexplore.ieee.org/document/1104282/`.

E. Kaiser, J. N. Kutz, and S. L. Brunton. Sparse identification of nonlinear dynamics for model predictive control in the low-data limit. *Proceedings of the Royal Society A: Mathematical, Physical and Engineering Sciences*, 474(2219), 2018.

Hassan K Khalil. *Nonlinear systems*. Prentice Hall, 3rd edition, 2002. ISBN 0130673897,9780130673893,0131227408,9780131227408.

Stefan Klus, Péter Koltai, and Christof Schütte. On the numerical approximation of the Perron-Frobenius and Koopman operator. *Journal of Computational Dynamics*, 3(1):51–79, 2016.

Roelof Koekoek, Peter A. Lesky, and René F. Swarttouw. *Hypergeometric Orthogonal Polynomials and Their q-Analogues*. Springer Monographs in Mathematics. Springer Berlin Heidelberg, Berlin, Heidelberg, 2010.

Katerina Konakli and Bruno Sudret. Polynomial meta-models with canonical low-rank approximations: Numerical insights and comparison to sparse polynomial chaos expansions. *Journal of Computational Physics*, 321:1144–1169, sep 2016a.

Katerina Konakli and Bruno Sudret. Reliability analysis of high-dimensional models using low-rank tensor approximations. *Probabilistic Engineering Mechanics*, 46:18–36, 2016b.

Bernard O. Koopman. Hamiltonian Systems and Transformation in Hilbert Space. *Proceedings of the National Academy of Sciences*, 17 (5):315–318, may 1931.

Milan Korda and Igor Mezić. On Convergence of Extended Dynamic Mode Decomposition to the Koopman Operator. *Journal of Nonlinear Science*, 28(2):687–710, apr 2018a.

Milan Korda and Igor Mezić. Linear predictors for nonlinear dynamical systems: Koopman operator meets model predictive control. *Automatica*, 93:149–160, 2018b. URL `http://arxiv.org/abs/1611.03537`.

Yueheng Lan and Igor Mezić. Linearization in the large of nonlinear systems and Koopman operator spectrum. *Physica D: Nonlinear Phenomena*, 242(1):42–53, 2013.

A Lasota and James A. Yorke. Exact dynamical systems and the frobenius-perron operator. *TRANSACTIONS OF THE AMERICAN MATHEMATICAL SOCIETY*, 273(1):375–384, 1982.

Qianxiao Li, Felix Dietrich, Erik M. Bollt, and Ioannis G. Kevrekidis. Extended dynamic mode decomposition with dictionary learning: A data-driven adaptive spectral decomposition of the koopman operator. *Chaos: An Interdisciplinary Journal of Nonlinear Science*, 27 (10):103111, 2017.

A. Linnemann. Decentralized control of dynamically interconnected systems. *IEEE Transactions on Automatic Control*, 29(11):1052–1054, nov 1984. ISSN 0018-9286. URL `http://ieeexplore.ieee.org/document/1103423/`.

Ludovic Mailleret, Olivier Bernard, and J. P. Steyer. Robust regulation of anaerobic digestion processes. *Water Science and Technology*, 48(6): 87–94, 2003. ISSN 02731223.

Anirudha Majumdar, Amir Ali Ahmadi, and Russ Tedrake. Control and verification of high-dimensional systems with dsos and sdsos programming. In *53rd IEEE Conference on Decision and Control*, pages 394–401, 2014.

Stefano Marelli and Bruno Sudret. An active-learning algorithm that combines sparse polynomial chaos expansions and bootstrap for structural reliability analysis. *Structural Safety*, 75(August 2017):67–74, 2018.

B. M. Maschke and A.J. J van der Schaft. Interconnection of systems: the network paradigm. In *35th Conference on Decision and Control*, volume 1, pages 207–212. IEEE, 1996.

A. Mauroy and J. Hendrickx. Spectral identification of networks using sparse measurements. *SIAM Journal on Applied Dynamical Systems*, 16(1):479–513, 2017a. ISSN 15360040.

A. Mauroy, I. Mezić, and J. Moehlis. Isostables, isochrons, and koopman spectrum for the action–angle representation of stable fixed point dynamics. *Physica D: Nonlinear Phenomena*, 261:19 – 30, 2013. ISSN 0167-2789. URL `http://www.sciencedirect.com/science/article/pii/S0167278913001620`.

Alexandre Mauroy and Julien M. Hendrickx. Spectral identification of networks with inputs. In *2017 IEEE 56th Annual Conference on Decision and Control, CDC 2017*, volume 2018-Janua, pages 469–474, sep 2017b. ISBN 9781509028733.

Alexandre Mauroy and Igor Mezic. Global Stability Analysis Using the Eigenfunctions of the Koopman Operator. *IEEE Transactions on Automatic Control*, 61(11):3356–3369, nov 2016.

Igor Mezić. Spectral Properties of Dynamical Systems , Model Reduction and Decompositions. *Nonlinear Dynamics*, 41(1):309–325, 2005. ISSN 0924-090X.

Igor Mezić. Koopman operator spectrum and data analysis, feb 2017.

Arnold Neumaier. Solving Ill-Conditioned and Singular Linear Systems: A Tutorial on Regularization. *SIAM Review*, 40(3):636–666, 2003.

Frank K. Lu Paul Zarchan, Howard Musoff. *Fundamentals of Kalman Filtering:: A Practical Approach*, volume 232 of *Progress in Astronautics and Aeronautics (Volume 232)*. AIAA (American Institute of Aeronautics & Astronautics), 3 edition, 2009.

Sigurdur Hafstein Peter Giesl. Review on computational methods for lyapunov functions. *Discrete & Continuous Dynamical Systems - B*, 20:2291, 2015.

Joshua L. Proctor, Steven L. Brunton, and J. Nathan Kutz. Dynamic mode decomposition with control. *SIAM Journal on Applied Dynamical Systems*, 15(1):142–161, 2016.

Nicanor Quijano, Carlos Ocampo-Martinez, Julian Barreiro-Gomez, German Obando, Andres Pantoja, and Eduardo Mojica-Nava. The Role of Population Games and Evolutionary Dynamics in Distributed Control Systems: The Advantages of Evolutionary Game Theory. *IEEE Control Systems*, 37(1):70–97, feb 2017. ISSN 1066-033X. URL `http://ieeexplore.ieee.org/document/7823106/`.

Lorenzo Rosasco, Ernesto De Vito, Andrea Caponnetto, Michele Piana, and Alessandro Verri. Are Loss Functions All the Same? *Neural Computation*, 16(5):1063–1076, 2004. ISSN 08997667.

M. Sbarciog, M. Loccufier, and E. Noldus. Determination of appropriate operating strategies for anaerobic digestion systems. *Biochemical Engineering Journal*, 51(3):180–188, 2010a.

Mihaela Sbarciog, Mia Loccufier, and Erik Noldus. The estimation of stability boundaries for an anaerobic digestion system. *IFAC Proceedings Volumes*, 43(6):359 – 364, 2010b. ISSN 1474-6670. 11th IFAC Symposium on Computer Applications in Biotechnology.

Mihaela Sbarciog, Mia Loccufier, and Alain Vande Wouwer. On the optimization of biogas production in anaerobic digestion systems*. *IFAC Proceedings Volumes*, 44(1):7150 – 7155, 2011. ISSN 1474-6670. 18th IFAC World Congress.

Peter J. Schmid. Dynamic mode decomposition of numerical and experimental data. *Journal of Fluid Mechanics*, 656:5–28, aug 2010.

M. Erol Sezer and Özay Hüseyin. Stabilization of Linear Time-Invariant Interconnected Systems Using Local State Feedback. *IEEE Transactions on Systems, Man, and Cybernetics*, 8(10):751–756, 1978. ISSN 0018-9472. URL `http://ieeexplore.ieee.org/document/4309846/`.

Shuiwen Shen, Giuliano C Premier, Alan Guwy, and Richard Dinsdale. Bifurcation and stability analysis of an anaerobic digestion model. *Nonlinear Dynamics*, 48(4):391–408, 2007. ISSN 1573-269X.

Shih-Ho Wang and E. Davison. On the stabilization of decentralized control systems. *IEEE Transactions on Automatic Control*, 18(5):473–

478, oct 1973. ISSN 0018-9286. URL `http://ieeexplore.ieee.org/document/1100362/`.

Dragoslav D. Siljak. Stability of Large-Scale Systems under Structural Perturbations. *IEEE Transactions on Systems, Man, and Cybernetics*, 2(5):657–663, 1972. ISSN 0018-9472. URL `http://ieeexplore.ieee.org/document/4309194/`.

Dragoslav D Siljak. *Decentralized Control of Complex Systems*. Mathematics in science and engineering. Academic Press, 1991.

S. J. Skar, R. K. Miller, and A. N. Michel. On Nonexistence of Limit Cycles in Interconnected Systems. *IEEE Transactions on Automatic Control*, 26(3):669–676, 1981. ISSN 15582523.

Bruno Sudret. Global sensitivity analysis using polynomial chaos expansions. *Reliability Engineering and System Safety*, 93(7):964–979, 2008. ISSN 09518320.

Eric Walter and Luc Pronzato. *Identification of parametric models from experimental data*. Springer-Verlag London, London, 1 edition, 1997. ISBN 978-3-540-76119-8.

Jan C. Willems. Dissipative dynamical systems Part II: Linear systems with quadratic supply rates. *Archive for Rational Mechanics and Analysis*, 45(5):352–393, 1972a. ISSN 0003-9527. URL `http://link.springer.com/10.1007/BF00276494`.

JanC. Willems. Dissipative dynamical systems part I: General theory. *Archive for Rational Mechanics and Analysis*, 45(5):321–351, 1972b.

Matthew O. Williams, Ioannis G Kevrekidis, and Clarence W Rowley. A Data-Driven Approximation of the Koopman Operator: Extending Dynamic Mode Decomposition. *Journal of Nonlinear Science*, 25(6): 1307–1346, dec 2015.

Matthew O. Williams, Clarence W. Rowley, and Ioannis G. Kevrekidis. A kernel-based method for data-driven koopman spectral analysis. *Journal of Computational Dynamics*, 2(2):247–265, may 2016. ISSN 2158-2491.